Author(s): Mahajan, Shreya; Lahtinen, Manu

Title: Recent Progress in Metal-organic Frameworks (MOFs) for CO2 Capture At Different Pressures

Year: 2022

Version: Published version

Please cite the original version:

Mahajan, S., & Lahtinen, M. (2022). Recent Progress in Metal-organic Frameworks (MOFs) for
CO2 Capture At Different Pressures. Journal of Environmental Chemical Engineering, 10(6),
Article 108930. https://doi.org/10.1016/j.jece.2022.108930

Check for updates

# Recent progress in metal-organic frameworks (MOFs) for CO$_2$ capture at different pressures

Shreya Mahajan, Manu Lahtinen[*]

*Department of Chemistry, University of Jyväskylä, P.O. Box 35, FI-40014 JY, Finland*

ABSTRACT

Global climate change ensued by the rise in atmospheric CO$_2$ levels is one of the greatest challenges our planet is facing today. This worldwide distress demands technologies that can contribute to our society toward "negative carbon emissions". Carbon capture and storage (CCS) technologies are in important role for capturing CO$_2$ from existing emission sources, such as industrial and energy production point sources, before new more prominent modifications to the energy infrastructure can be implemented. Recently, alongside point source capture, direct air capture (DAC) processes have emerged as highly sought-after technologies that are able to capture CO$_2$ from the ambient air. Alongside the traditional inorganic adsorbents, a new class of solid porous adsorbents, called as metal-organic frameworks (MOFs) have emerged in recent years also, as a group of potentially very efficient materials to capture CO$_2$. The promising results of MOF-based adsorbents have already achieved great interest and have contributed to their ever-accelerating research to develop new and even better adsorbents for both point source and DAC recovery technologies. This review highlights the research that has been focused on utilizing MOFs in the carbon capture processes, particularly targeting materials applicable to low CO$_2$ partial pressures but also capturing processes in pure CO$_2$ (1 bar) will be reviewed, because it is a widely used test condition for characterizing sorption properties of MOF adsorbents. Herein, we outline four major approaches, through which the CO$_2$ adsorption capacity and selectivity can be boosted, including targeted modifications of the metal centers, pore size control, proper selection and substitution of linker units, and functionalization of MOFs by amines. The mechanisms of the sorption event are also reviewed from the perspective of both physisorption and chemisorption phenomena. At the end of the review, we briefly examine the variables related to the coordination of technical-economical, process-technical, and physicochemical properties of adsorbents, which both researchers and engineers should consider when developing new adsorbents and recovery processes, with emphasis on material processing, capture capacity, selectivity, regeneration cyclicity, and cost.

## 1. Introduction

According to the International Energy Agency report "World Energy Outlook 2021" (IEA, 2021, Paris, https://www.iea.org/reports/world-energy-outlook-2021), the worldwide energy demand has witnessed significant 2.3 % growth in the years 2018 and 2019 with an estimate of 1.3 % annual growth until 2040 [1]. The Covid pandemic is estimated to have caused a temporary reduction in energy demand of around 5 % by 2020 but it has already been caught up quickly in following years, as the Covid situation has somewhat eased globally. However, considering the overall picture in the intervening years, comprehensive demands of mankind are mostly being adhered by the consumption of accessible fossil fuels, such as natural gas, petroleum and coal, to produce energy.

The main by-product of this combustion is carbon dioxide (CO$_2$), lined as a major greenhouse gas [1,2]. Wherefore, the augmented quantity of CO$_2$ emissions over the years has led to extensive adverse effects on the natural environment, such as global warming, climate change, ocean acidification, rising sea levels, melting of the glaciers, species extinction and ozone depletion, to mention few. Thus, not only threatening humankind and the environment but also the synergy among them [3,4]. Ever since the 19th century, the abrupt and continual increase is witnessed in atmospheric CO$_2$ concentrations from thereabout 280 ppm (the early 1800 s) to ~ 417 ppm (2022), thus representing an increase of about 50 % compared to the average of 1750–1800. According to the Intergovernmental Panel on Climate Change (IPCC)[5,6] it is predicted that 980 ppm atmospheric CO$_2$ concentration could be reached by 2100

[7–9]. As the carbon dioxide content increases, so will the earth's temperature [10]. It is estimated that an increase of 1.4 °C observed in the 1990 s will reach an average temperature increase of 6.1 °C in 2100 if no globally significant actions are taken to mitigate climate change [11].

To address the challenges associated with increased atmospheric $CO_2$ concentrations it is indispensable that significant and drastic measures are taken promptly, to tackle this inevitably growing problem, by mitigating greenhouse gas concentrations and thereby limiting global warming. To remedy worldwide threats, IPCC has contemplated carbon capture as a simple and important strategy for constraining anthropogenic $CO_2$ emissions [12]. In addition to limiting global warming to 1.5 °C, IPCC prompted expeditious, consequential, and innovative amendments in the energy sector, transport, buildings and their energy management, industrial field and cities to reduce emission levels by 45 % till 2030 [13]. To achieve these objectives, IEA has launched various projects to attain an annual $CO_2$ emission cap of fourteen gigatons to limit the augmentation of global temperature to 2 °C. Also, the IEA regards carbon capture as one of the promising measures to reduce $CO_2$ emissions, of which these technologies may alone contribute up to eight gigatons of the annual aim of 14 gigatons [14–16].

$CO_2$ capture is prominently a "negative carbon technology". In general, $CO_2$ capture techniques focus on $CO_2$ emissions from the industrial origins, for instance, cement production plants, power plants, metallurgical industries, and petroleum refineries and can be classified into three main categories: pre-combustion, capture during combustion and post-combustion. Of the above, post-combustion capture is one of the most mature and favorable methods [17]. Typically, depending on the source, the temperature of flue gas is around 40–90 °C and the pressure is close to atmospheric pressure (1 bar), the $CO_2$ concentration of which can range from 4 % (natural gas combined cycle processes) to $13 - 15$ % (coal-fired combustion plant). Main impurities include $H_2O$ (~5 %), and acid gases, such as $SO_x$ and $NO_x$, in lower amounts [4]. Existing technologies include membrane separation [18,19], amine scrubbing [20–23] and adsorption with solid adsorbents [4,24,25]. Of the above, the aqueous amine-based absorption (e.g. ethanolamine-water solutions) has been the prevailing technique for the post-combustion based $CO_2$ separation despite its well-known drawbacks, like unavoidable loss of amine in course of the ongoing operation, corrosive properties of the solutions and high power consumption over regeneration process due to the heating of large volumes of water with a known high heat capacity [26]. However, adsorption-based alternatives are becoming progressively more competitive.

The adsorption of $CO_2$ from ambient air by direct air capture (DAC) is a method that has emerged in recent years as an alternative "negative carbon technology". It has already proved to be a promising method to limit global warming. Even though our atmosphere contains already hundreds of gigatons of $CO_2$ its very dilute concentration (~417 ppm, 0.04 %) is a serious obstacle to the development of successful and efficient $CO_2$ capturing techniques due to e.g., low diffusion and uptake rates, chemical inertness and targeting selectivity towards $CO_2$. Adsorption under very dilute $CO_2$ causes considerable loss of entropy making a high heat of adsorption as an essential parameter to render adsorption process sufficiently spontaneous [26–29]. Despite the challenge of the adsorption process, alongside with point-source $CO_2$ capturing, the reachability of $CO_2$ from ambient air has encouraged researchers increasingly to develop new applications based on DAC [30,31]. However, significantly more development is needed on the separation techniques used to capture $CO_2$ from different low-concentration feeds [32,33].

Research groups of Lackner et al. and Keith et. al, can be considered as significant pioneers of DAC research as they were the first to study carbon capturing properties of ion exchange resins and alkali solutions, respectively [34–37]. Up to date studies have shown how versatile and innovative DAC systems could be, capturing techniques potentially ranging from flexibility of location, being anywhere in the world, to usability both for point and distributed $CO_2$ sources, albeit so far only on a small scale. Importantly DAC conditions aid in sustaining the chemical stability of the adsorbent as no exposure to $SO_x$ and $NO_x$ impurities is evident due to their very low concentration in the ambient air, which in contrary is not the case in industrial flue gas emissions [4,38]. Moreover, the atmosphere comprises water vapor, $N_2$ and $O_2$ which should be taken also into account as they may induce both positive and adverse effects to the sorption process itself, to target molecule selectivity, as well as to the stability of an adsorbent itself.

Despite the measures already taken the need for efficient $CO_2$ capture technology is growing rapidly as global warming keeps accelerating. In recent years aqueous amine solutions are being substituted gradually by solid adsorbents that generally have lower heat capacities in contrast to amine-based solvents, as discussed above [39,40]. Due to the many shortcomings accompanied by amine scrubbing techniques, alternative approaches have been made to develop novel amine-functionalized solid materials both for point source and DAC conditions. Typically for DAC conditions, amine-functionalized solid materials are based on chemisorption which is the prime requirement for DAC adsorbents as it is indicated that with chemisorption stronger $CO_2$ binding and higher selectivity (e.g. $CO_2\backslash H_2O$) could be obtained due to the covalent interactions between amino groups and $CO_2$, in contrast to the physisorption that relies on physical less selective weak interactions. The early stage development of amine-appended (tethered/impregnated) $CO_2$ adsorbents originated primarily from old-fashion solid adsorbents that were designed for purification of air indoors, such as in submarines and space crafts [41,42]. In the mid 90 s Leal *et al.* [43] reported a new $CO_2$ adsorbing amine-appended silica gel adsorbent. In their work the $CO_2$ capturing capacities were still rather modest, nonetheless, in the coming years, this new concept drew profound interest [44–50], and thereafter vide variety of amine-functionalized adsorbents have reached an immense growth in their utilizations, in all kinds of areas of carbon capture research. The constantly growing number of new materials have exhibited both improved and unprecedented combinations of properties such as high thermal and chemical stability, remarkable capture efficiency, low sorption heat, good diffusion property, low corrosion affinity, low active component leakage likelihood, and simple packaging and storing requisites [25,39,51–54].

For an exemplary good $CO_2$-binding adsorbent, the following properties can generally be expected: high capacity (>2 mmol $CO_2$ per g of adsorbent), fast sorption kinetics, selectivity (>100; $CO_2$/other gases), recyclability (>1000 cycles), thermal stability, ease of handling and storage, as well as low production cost [55]. Of the above, the high affinity that relates to selectivity is an important criterion for adsorbent efficiency, which in part can be amplified by proper structural design of the adsorbent, as well as modification of amine type and content. Entrapment of the $CO_2$ molecules can further be promoted by the fabrication of exclusive geometric channels which encompasses pore size modification and active site allocation. In this context certain traditional inorganic porous materials such as silica gels exhibit amorphous, microporous characteristics but lack periodic uniform porous structures, thus demonstrating low diffusion performance. Also, few Si-based mesoporous materials, like SBA-15 [56,57], MCM-41[58,59], and KIT-6[60,61] possess uniform meso-sized channel structure but the number and exact locations of amine groups remain ambiguous. Explicitly, the incorporation of strong alkaline amines in large enough pores is ideal for the chemical and reversible sorption of $CO_2$ molecules. In short, the optimized example system works in our body, in our lungs wherein the complex network of channels with varying dimensions engenders diffusive paths for efficient gas exchange in terms of $O_2$ absorption and $CO_2$ desorption. Similarly, an ideal porous adsorbent should render a lung-akin network of pores. For improving the distribution of amines alongside with optimized pore properties, crystalline porous materials can be utilized, of which metal-organic frameworks (MOFs) are the most studied substances.

MOFs are a group of crystalline materials having periodic one-, two-,

or three-dimensional coordination networks constructed by metal-based nodes (single cations or clusters) bonded (coordinate covalent bond; dative bond) with bridging organic ligands. The nearly endless possibilities to combine different metal and ligand components have currently resulted in over 100,000 MOF structures in the Cambridge Structural Database (CSD) [62]. Many of them comprise exceptional characteristics for instance ultralow densities (lowest so far 0.13 g/ cm$^3$) [63], pore volumes with 90 % of free volume[64] and extremely large Brunauer-Emmett-Teller (BET) surface areas up to 10,000 m$^2$/g[65–67]. With the exemplified wide range of characteristics alongside with possibilities in their preparation designs, MOFs have already been developed for number of applications, such as gas separation and storage[25, 68], photo catalysis[69], heterogeneous catalysis[70,71], drug delivery [72,73] and medicinal fields[74,75], electrical energy storage and energy conversion[76,77], ion exchange[78], electrochemical applications[79], deterioration of chemical warfare agents[80,81], the extraction of hazardous substances from air and aquatic environments [82,83], stimuli-responsive and energetic materials[84,85], as well as for carbon capture.[11,86] Some recent achievements on carbon capture by MOF adsorbents are highlighted in Fig. 1.

As an example of the utilization of the phenomenal properties of MOFs in gas sorption, the study of Prof. Yaghi *et al.* [87] in 2005 can be highlighted, wherein MOF-177 was prepared with an excellent high surface area (4500 m$^2$\g) and remarkable CO$_2$ uptake of 33.5 mmol g$^{-1}$ (at 35 bar and 25 °C) corresponding to about two times better CO$_2$ loading capacity at high pressures than compared to much-used zeolites of its time; although at atmospheric pressure (1 bar and 25 °C) only 0.8 mmol g$^{-1}$ of adsorption capacity was observed. As suggested by Li et al. in their perspective, generally at higher pressures large surface areas seem to lead to better adsorption in contrast to lower pressures, wherein chemical properties of the adsorbent are in more dominant role in defining the CO$_2$ adsorption performance [88]. As exemplified by the comparative studies of Yaghi [87] and many others[89–91], one of the major benefits of MOF materials is their structural modularity, which allows accurate crystal design of the structures, aiming to consider the structural and geometrical needs on an application-by-application basis [92–94]. The distinct incorporation of appropriate metal nodes and organic linkers eventually lead to a usable structural libraries, which on

other hand has not been materialized for previously known conventional porous materials [88,95–98].

The arena of MOF research is exceptionally diverse, and a significant number of studies have already been published, particularly for CO$_2$ capture and conversion techniques on a general level as well as also focusing specifically on individual methods [11,98,112–114]. In contrast to the previous reviews, this review focuses on recent studies on the development of amine-doped MOFs, especially for chemisorption carbon capture, mainly at CO$_2$ pressures of one bar and below. In addition, the suitability of physisorption mechanisms for the recovery of dilute CO$_2$ concentrations will also be reviewed. The scope of this review is to endow researchers with a detailed layout of the state of the art, areas to probe and ongoing impediments in the field of carbon capture at different CO$_2$ feeds, thus varying from dilute DAC (417 ppm) to flue gas concentrations (up to 15 % of CO$_2$), while also viewing the adsorption at 1 bar of CO$_2$, which is widely used as a condition for comparative testing of MOF adsorbents, mainly in dry conditions but more recently under moist conditions as well. We also go through ways to improve the carbon dioxide capture capacity, such as via targeted modifications of the metal sites, by pore size control, elongation or substitution of organic linker, and by amination of MOFs, also including amine-impregnation of MOFs. For completeness, the consideration of the water effect is also discussed, albeit briefly. The review is centered on the evolution of the MOF-74 family, though parts of the discussion also apply to other benchmarks MOFs. It does not aim to be a full account of all the MOFs reported for CO$_2$ adsorption and separations but rather to highlight specific strategies and trends in the field of point source and DAC conditions. At the end of the review, we briefly examine the variables related to the coordination of technical-economical, process-technical, and physicochemical properties of adsorbents, which both researchers and engineers should consider when developing new adsorbents and recovery processes, with emphasis on material processing, capture capacity, selectivity, regeneration cyclicity, and cost. The review also aims to provide help for the seasoned MOF researchers to become conversant with the fundamental relationship between MOF chemical design, functional groups, and gas uptake capacity.
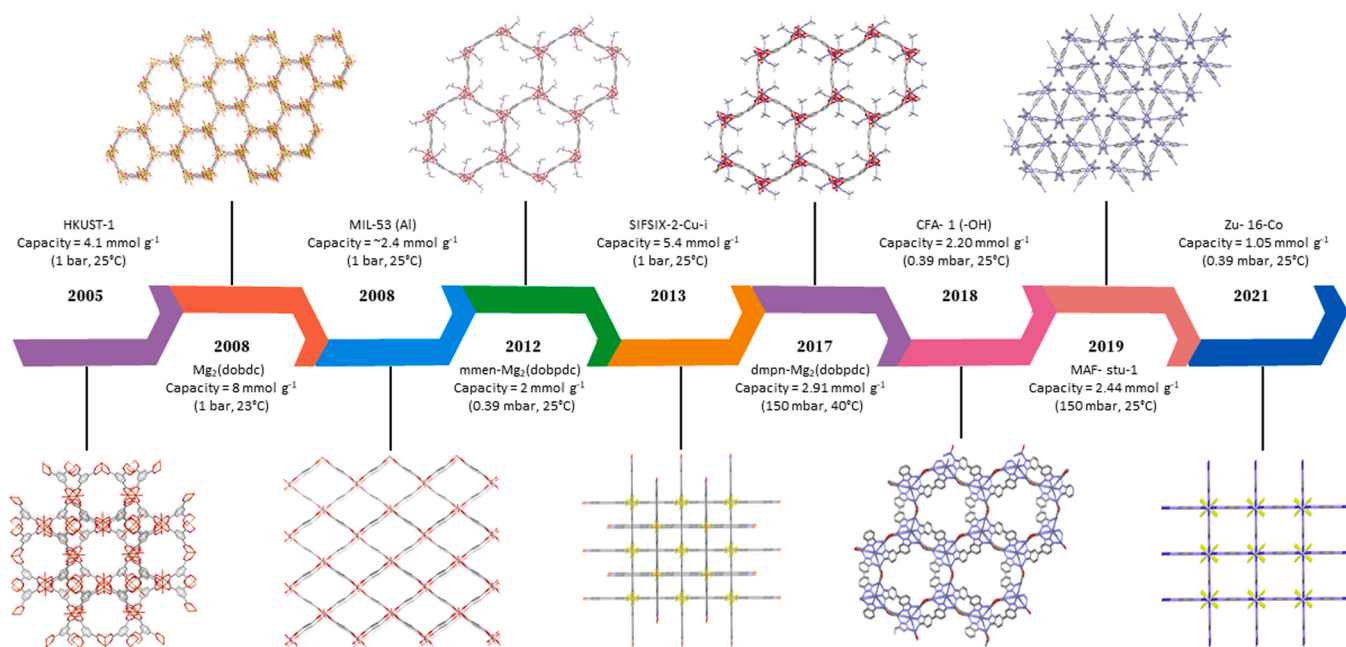


**Fig. 1.** Illustration of CO$_2$ capture capacities for some well-known MOFs (a) HKUST-1 [87] (b) Mg$_2$(dobdc) [99] (c) MIL-53 (Al) [100](d) mmen-Mg$_2$(dobpdc) [101] (e) SIFSIX-2-Cu-i [102] (f) dmpn-Mg$_2$(dobpdc) [103] (g) CFA-1(-OH) [104] (h) MAF-stu-1 [105] (i) Zu-16-Co [106]. CSD entries FIQCEN, VOGTIV, SABVUN, XUXPUD, YEMTIV, ACEWIR, LAWYIV, POVGEP and SUHQUK have been used to create images with Mercury program. [101–111].

## 2. Approaches to improve $CO_2$ capture capacity of a MOF

In the field of $CO_2$ adsorption, with qualifications as mentioned in the Introduction (e.g., high capacity, kinetics, selectivity), the applicable adsorbent needs to bear sufficient resistance against water. Many metals used in the MOF adsorbents are vulnerable to water, which due relatively high affinity of water to the metal ions can cause their hydrolysis, and thereby the chemical deterioration of the network structure. Water has also clearly higher abundance (10–100 times) in the atmosphere compared to $CO_2$ which in turn has a significant effect on the $CO_2/H_2O$ selectivity. In terms of thermodynamics, the $CO_2$ binding enthalpy should be considerably exothermic (at least $-50$ kJ mol$^{-1}$) for an efficient capture process. An adsorbent material should also be chemically and thermally robust to withstand thousands of sorption cycles without loss of activity and chemical integrity [115].

Considering the above criteria, the affinity of a MOF adsorbent for $CO_2$ can further be altered by tailoring the chemical and physical properties of the targeted MOF structure. One of the modification strategies includes the creation of so-called active open metal sites (OMSs) in the network structure. OMSs that are part of the metal-organic framework, can provide potentially higher $CO_2$ intake for the MOF adsorbent, as the inherent rigidity of the framework enables the OMSs to be more accessible throughout the adsorption-desorption events. Also, the pore size of the framework can be controlled via different organic linker unit designs. MOFs sorption properties can also be promoted by functionalizing the organic linkers with nitrogen (N) containing group (s), or via amines that have been appended to the OMSs. By incorporating amine functionalities (e.g., anchored to OMS or as a substitution in the bridging ligand) amidst the pore structure, polar sites (basic property) are generated that in turn interact strongly with $CO_2$. As a result, capturing properties of the MOF may further be improved due the more selective chemisorption occurring between an amino group and $CO_2$. Studies have also shown that MOFs with pore interiors decorated by abundant nitrogen atoms endow stronger quadrupolar interactions between carbon and the nitrogen atoms, thereby affording higher $CO_2$ binding affinities and selectivity. The above design strategies will be reviewed in this paper under four subsections, namely 2.1. targeted modification of metal centers to form active OMS along with ligand extension approach (reticular chemistry concept) to alter density and accessibility of OMS, 2.3. hybrid ultra-microporous materials, 2.4. amine substituted and N-heterocyclic organic linker ligands, and 2.5. post-synthetic amination and adsorption mechanisms on aminated open metal sites. On subsections 2.2. and 2.6., the impact of water as a constant competitor to $CO_2$ in the sorption event is also reviewed. Finally, chapter 2.7. represents coating techniques as further measures to increase the tolerance of MOF adsorbents against water. The literature reviewed is generally limited to publications from 2015 to date, and older studies have been included only when they have represented significant advances in carbon capture research in general. For the sake of simplicity, all the metrics in this review are standardized to the following units: adsorption capacity (mmol g$^{-1}$), temperature (°C) and pressure (mbar or bar).

### 2.1. Modifications of the metal sites and ligand extension approach

The physisorption on a solid surface is viewed as the interaction of $CO_2$ preponderantly through intermolecular weak forces like van der Waals or somewhat stronger hydrogen bonding. Fundamentally, in this process, there is no chemical bond formation owing to the absence of chemical interaction. Simple condensation principles are favored which are inclined towards layer-by-layer deposition. The adsorption heat (-$Q_{st}$) of $CO_2$ is the underlying physical attribute, which prompts the physisorption of $CO_2$ to a MOFs pore structure. Generally, in a weakly binding physisorbent, the binding energies are considerably less than that of a rational chemical bond, and sometimes intermittently lower than a hydrogen bond. Widely acknowledged boundary value for $Q_{st}$

chemisorption–physisorption varies between $-40$ and $-50$ kJ mol$^{-1}$ [55].

As MOFs are generally highly ordered porous materials, the solvent content in the voids, as well as the ones coordinated to metal centers, can be removed either via a solvent exchange, heat, vacuum, or both to form OMSs without changing the original network structure. MOFs with open metal sites utilize Lewis's acidity, imparted by partial positive charges on metal sites, to interact with $CO_2$ molecules (O=C=O⋯M$^{n+}$). Thereby, the aforesaid prerequisite to increase -$Q_{st}$ of $CO_2$ can be fulfilled by forming strong and selective interactions between the host structure and the $CO_2$, via open metal sites. Among the vast family of frameworks, MOF-74 is an extensively studied MOF archetype due to its high density of available open metal sites, and because it can be varied chemically with ease by using a number of different bivalent metals, such as Mg(II), Mn(II), Fe(II), Co(II), Ni(II), Cu(II), and Zn(II) [116]. Structurally MOF-74 also known as $M_2$(dobdc) is consisted of desired metal ion (M) and 2,5-dihydroxy-1,4-benzenedicarboxylic acid ($H_4$dobdc) which forms a three-dimensional framework having one-dimensional (1D) hexagonal channels parallel to the crystallographic *c*-axis. In the network structure, solvent molecules are coordinated at every sixth position of the octahedral metal centers, the removal of which generates an open metal site that serves as a Lewis acidic site and eventually can interact with an incoming $CO_2$ molecule [114,116]. Among the series of M-MOF-74 analogues, the Mg-MOF-74 has so far illustrated the highest so far reported $CO_2$ adsorption capacity of ~9.9 mmol g$^{-1}$ under pure $CO_2$ (25 °C and 1 bar) [117] and adsorption heat of $-47$ kJ mol$^{-1}$ [118] Yazaydin et al. [119] and Caskey et al. [99] made a similar comprehensive screening for $CO_2$ capture performance using different coordination metals in isoreticular series of MOF-74. The study unfolded that with a decrease in the M−O bond length, the $CO_2$ uptake of M-MOF-74 uplifted. It was therefore concluded that the bond lengths seem to define the oxygen affinities of metals in the coordination state (Mg−O (1.969 Å) < Ni−O (2.003 Å) < Co−O (2.031 Å) < Zn−O (2.083 Å)). The obtained adsorption heats for the series were obtained through isotherms that ranged from $-22.1$ to $-43.5$ kJ mol$^{-1}$, of which the highest being on Mg-MOF-74 [116]. Based on the experiments carried out, it could be assumed that the highest affinity for $CO_2$ in the case of Mg-MOF-74 was attributable to the enhanced ionic character of the Mg–O bond, which bestows stronger charge-quadrupole interactions between the OMSs and $CO_2$ [99].

Furthermore, to improve the accessibility and density of OMSs in MOF-74 family, various isoreticular frameworks have been designed by employing the ligand extension approach, wherein a longitudinal dimension of a bridging ligand is elongated but keeping the other properties like the number, type or relative geometrical orientation of functional groups unchanged [101,120,121]. This method utilizes facile incorporation of functionalities by the modulation of the pore size to compensate the moderately small pore size of the native MOF-74 framework that is a limiting factor for the accessibility of OMSs. For instance, McDonald et al. examined pore-expanded MOF-74 variants that were based on the extended analogies of terephthalic acid linkers, such as $H_4$dotpdc (4,4″-dihydroxy-[1,1′:4′,1″-terphenyl]−3,3″-dicarboxylic acid), and $H_4$dobpdc (4,4′-dihydroxy-[1,1′-biphenyl]−3, 3′-dicarboxylic acid) [101]. Also Yoo et al. [121] examined similar pore-expanded structures but using different metal centers such as Ni (II), Mn(II), Zn(II), and Co(II) cations. The adsorption heats calculated from the well-known Clausius-Clapeyron relationship were obtained as $-25.0$, $-33.9$, $-34.5$, and $-25.6$ kJ mol$^{-1}$ for Ni$_2$-, Co$_2$-, Mn$_2$-, and Zn$_2$(dobpdc) MOFs, respectively. The observed trend in adsorption heats implies that there exists a direct relationship between the Lewis acidity of a metal cation and the binding ability of $CO_2$ molecule. Furthermore, Lim and coworkers [122] illustrated a series of Co-based MOF-74 variants [Co$_2$(L)(DMF)$_x$(H$_2$O)$_y$]·zH$_2$O that were made using $H_4$dobdc, -dobpdc and -dotpdc ligands (L), and microwave-assisted solvothermal synthesis (Fig. 2a).

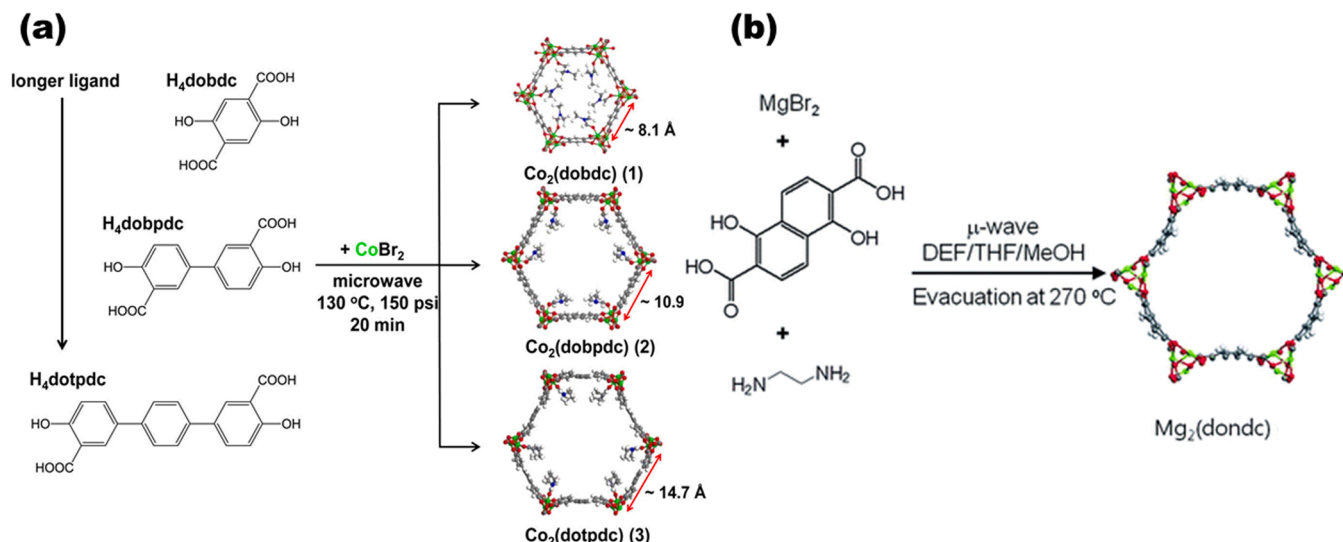Three of the frameworks displayed isoreticular structures as

**Fig. 2.** Synthesis schemes of some (a) Co-, and (b) Mg-based extended MOF-74 structures. Adapted from Ref. [122,123].

validated by powder X-ray diffraction (PXRD) analyses. For the reported systems, Co–Co distances at the edge of pore channels ranged from 8.1 via 10.9–14.7 Å for Co$_2$(dobdc), -(dobpdc) and -(dotpdc), respectively. These studies emphasized the importance of ligand length and how the interchain interaction is systematically governable by the length of the ligand.

Another well-known strategy for a ligand extension is to utilize fused benzene ring bedded ligands, such as naphthalene and anthracene. Yeon *et al.* reported isostructural member of MOF-74 family, that is Mg$_2$(dondc) consisted of 1,5-dihydroxy-2,6-naphthalendicarboxylic acid (H$_4$dondc) [123]. The framework features one-dimensional channels which are nearly 15 Å in size (Fig. 2b), hence settling between Mg$_2$(dobdc) and Mg$_2$(dobpdc) with their channel sizes being approximately on the order of 11 and 18.4 Å, respectively. The study concluded that the availability of OMSs in Mg$_2$(dondc) were the primary binding sites of CO$_2$. The adsorption capacity of Mg$_2$(dondc) was somewhat like on Mg$_2$(dobpdc), thus 4.80 vs. 4.84 mmol g$^{-1}$, respectively but still smaller than on Mg$_2$(dobdc) showing 6.1 mmol g$^{-1}$ capacity at 150 mbar (25 °C). Similarly, Wang and coworkers [124] examined the

effects of the high density of OMSs for carbon capture by designing a porous MOF, Co$_2$(tzpa)(OH)(H$_2$O)$_2$·DMF using 5-(4-(tetrazol-5-yl) phenyl)isophthalic acid (H$_3$tzpa) consisting of tetrazole and two carboxylic acid groups. For the prepared adsorbent, the experimental gas sorption data illustrated good CO$_2$/CH$_4$ selectivity of 31.8 for the gas mixture (1:1 ratio), which was concluded to be the result of high density of open metal sites.

To further investigate properties of the open metal sites, mixed-metal MOFs consisting of two or more different metals have also been prepared. In the case of MOF-74 archetype, the synergistic effect of the bimetallic system demonstrated better gas adsorption and catalytic performances [125–127]. For instance, M/Zn(dobdc) series having evenly distributed metal cations (about 1:1 ratio) in Mg/Zn-, and Ni/Zn-MOF-74 s exhibited adsorption capacities of 6.7 and 6.3 mmol g$^{-1}$ with adsorption heats of − 43 and − 41 kJ mol$^{-1}$, respectively (0 °C and 1 bar) [128]. In Particular, the Ni/Zn-MOF-74 demonstrated a higher heat of adsorption than that of the monometallic Ni-MOF-74 indicating a synergistic effect of mixed metal ions. Similarly, Kim et al. [129] examined bimetallic (M = Mg, Ni, Co, and Mn) MOFs with extended



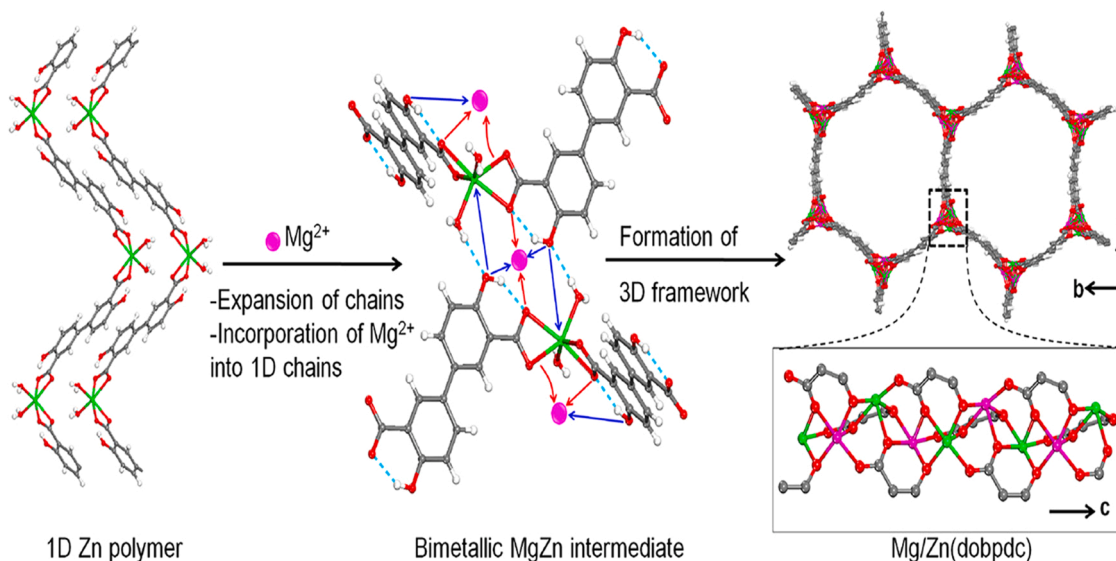**Fig. 3.** Suggested mechanism of dimensional transformation from 1D-chain template to a 3D bimetallic Mg/Zn(dobpdc) framework. Adapted from Ref. [129].

ligand (Fig. 3), namely M/Zn(dobpdc). It was found that based on the energy dispersive microscopy (TEM- and SEM-EDS) only the Mg/Zn (dobpdc) showed a 1:1 ratio between the incorporated metals, and higher adsorption capacity than that reported for the monometallic $Zn_2$(dobpdc), albeit still with a capacity lower than $Mg_2$(dobpdc). On the other hand, adsorption heat for Mg/Zn(dobpdc) was observed to be in the range of $-32.5$–$44.2$ kJ mol$^{-1}$ (Table 1), hence settling in between $Mg_2$(dobpdc) and $Zn_2$(dobpdc) adsorbents.

**Table 1**
Summary of $CO_2$ adsorption for MOFs with targeted modifications of the metal sites.

| MOF | Capacity (mmol g$^{-1}$) | | | -$Q_{st}$ (kJ mol$^{-1}$) | Temp. (°C) | Ref. |
|---|---|---|---|---|---|---|
| | 0.39 (mbar) | 150 (mbar) | 1 (bar) | | | |
| $Mg_2$(dobdc) | 0.088 \0.14$^H$ | 6.1 | ~8–9 | 47 | 25 | [99, 116, 144, 150, 153, 154] |
| $Mg_2$(dobpdc) | 0.13 | 4.85 | 6.42 | 44 | 25 | [101] |
| $Ni_2$(dobdc) | | ~4.06 * * | ~7.0 | 39 | 25 | [116, 119] |
| $Fe_2$(dobdc) | | | ~7.1 | 33 | 25 | [116, 151] |
| $Co_2$(dobdc) | | ~2.81 * * | ~6.90 | 34 | 25 | [99, 116, 119] |
| $Zn_2$(dobdc) | | ~1.30 * * | ~5.61 | 27 | 25 | [99, 116, 119] |
| $Mn_2$(dobdc) | | | ~5.9 | 32 | 25 | [116] |
| $Cu_2$(dobdc) | | | ~2.90 | 22 | 25 | [116] |
| $Mg_2$(dondc) | | 4.80 | 6.42 | 34–44 | 25 | [123] |
| $Mg_2$(dotpdc) | | | ~5.30 | ~40 | 25 | [120] |
| $Mg_2$(pc-dobpdc) | | | ~6.50 | ~38 | 25 | [120] |
| $Mn_2$(dobpdc) | | ~1.95 | | 34 | 25 | [121] |
| $Co_2$(dobpdc) | | ~1.88 | | 35 | 25 | [121] |
| $Ni_2$(dobpdc) | | ~2.70 | | 25 | 25 | [121] |
| $Zn_2$(dobpdc) | | ~1.40 | | 26 | 25 | [121] |
| Mg/Zn (dobdc) | | | 5.10 | 43 | 25 | [128] |
| Ni/Zn (dobdc) | | | 4.80 | 41 | 25 | [128] |
| Mg/Zn (dobpdc) | | | ~5.90 | 33–44 | 25 | [129] |
| SIFSIX-3-Cu | 0.32$^H$ \1.24 | 2.51 | 2.58 | 54 | 25 | [144, 155] |
| SIFSIX-3-Zn | 0.13 | 2.43 | 2.51 | 45 | 25 | [102, 144] |
| SIFSIX-3-Ni | 0.18$^H$ | 2.47 | 2.5 | 47 | 25 | [150] |
| SIFSIX-18-Ni-β | 0.8 * | | | 52 | 25 | [148] |
| SIFSIX-2-Cu-i | 0.03$^H$ \0.068 | 1.25 * * | 5.41 | 32 | 25 | [102, 144, 155] |
| HKUST-1 | 0.05$^H$ | 1.59 | 2.5 \4.1 | 34 | 25 | [87, 150] |
| UTSA-16 | | 2.37 | 4.3 | 34.6 | 25 | [138] |
| MIL-101(Cr) | | | 1.22 | 21 | 25 | [152] |
| ZU-16-Co | 1.05 | | 2.87 | | 25 | [106] |
| TIFSIX-3-Ni | 0.67 \1.7 * | 2.36 | 2.32 | 50 | 25 | [106, 146, 148] |
| NbOFFIVE-1-Ni | 1.8 * \1.3 | 2.15 | 2.2 | 55.4 | 25 | [145, 148] |
| SIFSIX-14-Cu-i | | | 4.70 | 37.7 | 25 | [147] |
| dptz-CuTiF6 | | ~2.86$^H$** | ~4.51 | 38.2 | 25 | [149] |
| MIL-53(Al) | | | ~2.4 | 30 | 25 | [100] |

* Measured at 1 mbar, ** at 100 mbar, and $^H$ humid condition.

### 2.2. Consideration of water effects

Water is a ubiquitous component of the atmosphere, and its competitive adsorption with $CO_2$, and its influence on the chemical stability of MOFs in carbon capture applications is a serious challenge to be considered. The MOF-74 family and many other MOF designs display lower $CO_2$ capture capacities under humid conditions due to the competition between water and $CO_2$ at the active binding sites. In addition, water has significant adverse effects on the chemical stability of many MOF materials, which begin to increase especially when attempting to increase the number of adsorbent regeneration cycles from a few to a practical extent of thousands of cycles, i.e., to extend the life and efficiency of the adsorbent. Inevitably, competition between the guest molecules results in the reduction of reactive sites (e.g., OMSs), as water may permanently terminate the sites and eventually can even break the network structure via hydrolysis [130]. Along with MOFs, also conventional inorganic adsorbents are prone to water, as physisorbents such as zeolite 13X and activated carbon have encountered similar adverse effects [9,131]. To improve the water resistance of MOFs, significantly more research is needed in this area, especially for DAC adsorbents, which struggle with the low concentration of $CO_2$ compared to the concentration of water that is several orders of magnitude higher. For the utilization of OMSs in DAC adsorbents, a better understanding of the adsorption mechanisms is needed for revealing the key factors which may result in better stability and higher selectivity towards $CO_2$ in the presence of competing water [132–134]. In this context, recent studies have demonstrated some progress, e.g., in $CO_2$ selectivity and dynamics in the presence of water, or other molecules competing for absorption. This positive progress gradually will pave the way towards more water-resistant MOFs, which eventually will supersede the moisture-sensitive MOF materials of the previous generations [135–137].

Xiang *et al.* have reported UTSA-16 adsorbent ($K(H_2O)_2Co_3$(cit) (Hcit)) that was prepared using citric acid ($H_4$cit) which showed reduced affinity for water but still having high density of open metal sites [138]. The experimental data on the $CO_2$ working capacity of the adsorbent showed only minor differences between humid and dry conditions (0.94 and 1.30 mmol g$^{-1}$, respectively) indicating improved $CO_2$ separation properties. The observations raised the hope that UTSA-16 could be, at that time, a new efficient adsorbent from both academic and industrial perspectives [139,140]. In addition to the density of OMSs, the pore structure of the adsorbent is also of great importance for the accessibility of the active reaction sites and thus for the total adsorption capacity of the MOF. With a different approach to diminish effects of water, the partial or full substitution of the existing metal centers with metals having a smaller ion radius have been shown to shrink the pore size of MOFs, and causing an increase in -$Q_{st}$ value, which partly defines the adsorption efficiency of the adsorbent [141]. This post-synthetic exchange method offers a promising platform to enhance chemical stability of a MOF and allows to fine-tune its water-resistance while still maintaining the original network structure [142]. For instance, Hu et al. [143] demonstrated a persuasive strategy to functionalize somewhat more water-resistant UiO-66(Zr) MOF by the metalated-ligand exchange (MLE), in which the terephthalic acid (bdc) was exchanged to 1,2,4, 5-benzenetetracarboxylate and its auxiliary sites were occupied by alkali metals (Li$^+$, Na$^+$ and K$^+$). With the described method, the pore size of post-functionalized UiO-66 was able to be altered (for van der Waals interactions) with simultaneous insertion of more polar metal sites (for electrostatic interactions), resulting in to improved $CO_2\backslash N_2$ selectivity and $CO_2$ working capacity. The presented method opens new alternative ways to design water-stable MOFs with potentially higher crystallinity and $CO_2$ separation efficiencies.

### 2.3. Hybrid ultramicroporous materials (HUMs)

One way to avoid adverse effects of water, are the recently developed

anion-functionalized MOFs consisting of metal ions, organic linkers, and inorganic bridging anions. Even though the potential open metal sites are now being used as coordination sites for anionic species, some of these frameworks have shown exceptional $CO_2$ uptakes due to the strong interactions between $CO_2$ and the secondary anionic building units of the framework. Shekhah et al. [144] introduced a new strategy producing novel SIFSIX-3-M ($MSiF_6(pyrazine)_2.2H_2O$) MOFs that contain ultramicropores and have high $CO_2$ capture capacity and selectivity via physisorption in DAC conditions. The reported MOFs were constructed from $MSiF_6$ inorganic units (M = Cu, Ni, and Zn) and a pyrazine ligand (Fig. 4). Resulting adsorbents exhibited excellent $CO_2$ sorption energetics and fully reversible physisorption driven adsorption-desorption process under moderate conditions (at 50 °C under vacuum). This was concluded to have occurred, because of the highly electrostatic inorganic anion ($SiF_6^{2-}$) and the small pore size. Also, in terms of adsorption heat, SIFSIX-3-Cu demonstrated $-54$ kJ mol$^{-1}$ enthalpy in DAC conditions with a steep adsorption isotherm, and 1.24 mmol g$^{-1}$ capturing capacity (Fig. 4d), thus being significantly better than that of previously reported for Mg-MOF-74. Unfortunately, long-term exposure of SIFSIX-3-M MOFs to water vapor ended up to lower $CO_2$ uptake capacities, limiting the applicability of the adsorbents only to dry adsorption conditions. To address this challenge, Bhatt et al. attempted to develop more water-resistant SIFSIX-typed MOFs for carbon capture by selecting octahedrally coordinating Ni(II) as center metal, which has a shorter M−F bond distance ($d_{M-F} = 1.99$ Å) than for example in Cu (II)−F. [145] Secondly, the $(SiF_6)^{2-}$ pillaring anion was changed to a more strongly binding $(NbOF_5)^{2-}$ anion, as it practically supersedes the $SiF_6^{2-}$ anion by having bigger ionic radii of the Nb(V) center, resulting in a longer Nb−F bond length compared to Si−F bond (1.899 Å and 1.681 Å, respectively). Secondly, the better nucleophilic characteristics of the $(NbOF_5)^{2-}$ may potentially contribute to better water resistance of the MOF in humid conditions. The prepared NbOFFIVE-1-Ni MOF indeed exhibited similar 1.3 mmol g$^{-1}$ $CO_2$ capture capacities both in dry and humid conditions indicating clearly improved tolerance against water vapor. The observed capacity is about 15% higher than that obtained for the analogous SiFSIX-3-Cu. In comparison to the reported physisorption adsorbents at the time, NbOFFIVE-1-Ni MOF turned out to be the top adsorbent for $CO_2$ capture both directly from the air and flue gases. Moreover, its straightforward synthesis method has gradually paved the way for economically feasible production of the material in bulk scales (g to kg).

Kumar et al. [146] further investigated SIFSIX analogues using $TiF_6^{2-}$ pillars with an aim to enhance $CO_2$ affinity at lower pressures without worsening their thermal stability and water resistance properties. They synthesized hybrid ultramicroporous material (HUM) TIFSIX-3-Ni which contains $TiF_6^{2-}$ (TIFSIX) and pyrazine (3) connected to Ni nodes. The 14-days accelerated stability tests for the adsorbent showed only a minimal decrease in its $CO_2$ uptake at the end of the runs. The improved thermal stability resulting from the change of an anion type from $SiF_6^{2-}$ to $TiF_6^{2-}$ further underlined how the fine-tuning of the pillaring groups remarkably impacted both the physical and sorption characteristics of otherwise isostructural MFSIX-3-M adsorbents. In a similar study, Jiang et al. [147] presented a twofold interpenetrated copper coordinated network with a sequential pocket-like pore structure known as SIFSIX-14-Cu-i containing $SiF_6^{2-}$ (SIFSIX) anions and 4,4′-azopyridine (14) ligands (Fig. 5a). Mukherjee et al. [148] represented a new member of HUM, namely SIFSIX-18-Ni-β ($[Ni(L)_2(SiF_6)]_n$. It was prepared using 3,3′,5,5′-tetramethyl-1 H,1′H-4,4′-bipyrazole (L) ligands and containing both high-affinity $CO_2$ binding sites and enhanced hydrophobicity resulting from pores coated by methyl groups. It exhibited high $CO_2$ uptakes at low pressures (0.5, 1 and 10 mbar) with 0.4, 0.8 and 2.2 mmol g$^{-1}$ capacities, respectively. It was suggested that the formed hydrophobic pockets in this material resulted in relatively high adsorption heat ($-52$ kJ mol$^{-1}$) and low affinity for $H_2O$. Water adsorption tests for the material (95% relative humidity) revealed somewhat low uptake of 1.66 mmol g$^{-1}$ in comparison to the other three HUMs with 7.5, 8.8 and 10.1 mmol g$^{-1}$ for TIFSIX-3-Ni, SIFSIX-3-Ni and NbOFFIVE-1-Ni respectively. More recently, Liang et al. [149] presented a synthesis method for dptz-CuTiF$_6$ using 3,6-di(4-pyridyl)− 1,2,4, 5-tetrazine (dptz) as the ligand (Fig. 5b). The prepared dptz-CuTiF6 MOF exhibited similar ~2.86 mmol g$^{-1}$ $CO_2$ capture capacities (100 mbar, 25 °C) both in dry and humid conditions indicating the $CO_2$-capture ability of this material is not affected by moisture.

In the year 2021 Zhang and coworkers [106] demonstrated a simple
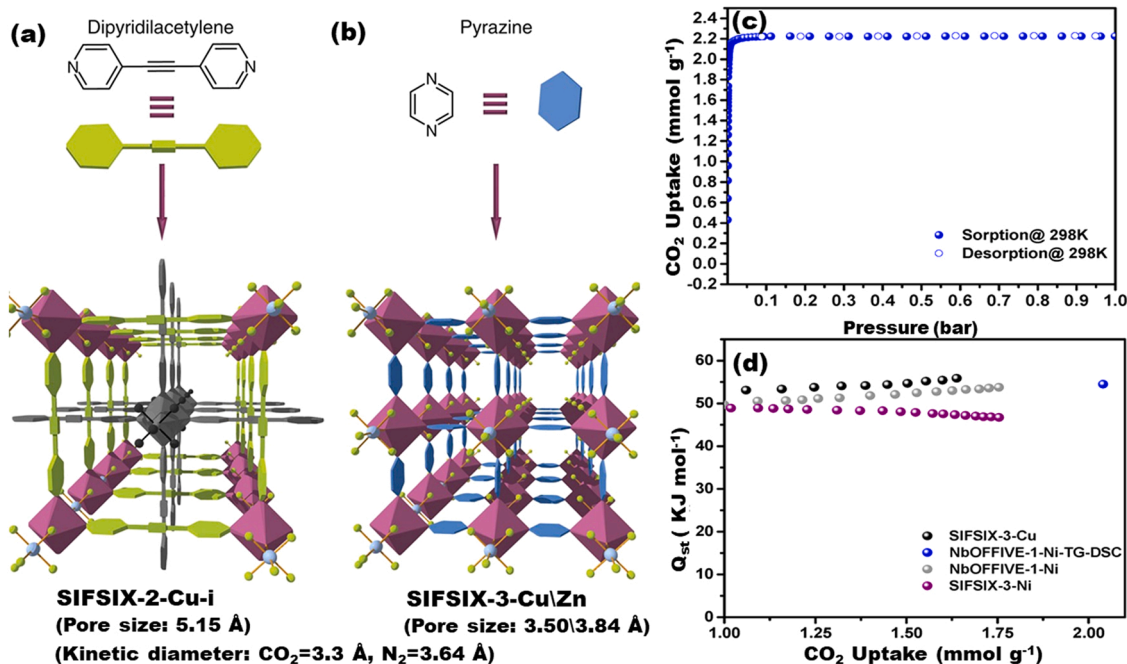


**Fig. 4.** Crystal structures of (a) SIFSIX-2-Cu-i (b) SIFSIX-3-Cu/Zn, (c) $CO_2$ sorption isotherm for NbOFFIVE-1-Ni at 25 °C and (d) comparison of $CO_2$ heat of adsorption for selected HUMs.
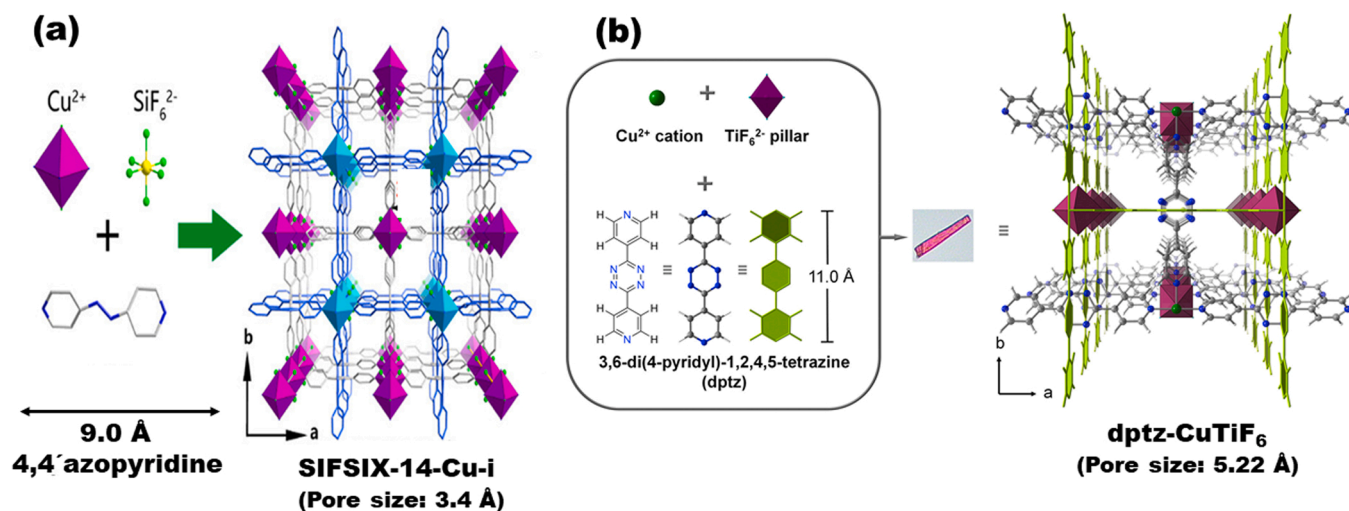Adapted from Ref. [144,145].

**Fig. 5.** Crystal structures of (a) SIFSIX-14-Cu-i, and (b) dptz-CuTiF$_6$ MOFs. Adapted from Ref. [147,149].

synthesis for novel anion-functionalized ZU-16-Co (TIFSIX-3-Co) containing TiF$_6^{2-}$ anions and pyrazine ligands (3). ZU-16-Co demonstrated structural similarities with the NbOFFIVE-1-Ni, thus having one-dimensional (1D) pore channels decorated by fluorine atoms. Among the isostructural MFSIX-3 (M = Si, Ti, Ge) family, the reported ZU-16-Co showed high CO$_2$ uptakes both at low and atmospheric pressures (10 and 1000 mbar) with 2.63 and 2.87 mmol g$^{-1}$ capacities, respectively. Also, a relatively good 1.05 mmol g$^{-1}$ CO$_2$ capacity was observed in DAC conditions. The improved CO$_2$ capture properties were assumed to result from the fine-tuned optimal pore size (~ 3.62 Å) which could arise because of a stronger F···C═O host-guest interaction. Overall, amongst all the HUMs, so far the NbOFFIVE-1-Ni MOF has been found to have the highest CO$_2$ uptake under DAC conditions, along with reasonably low regeneration energy. It is clear, that more research is needed to understand how changing the pore size and shape affects the water tolerance of pillared MOFs and their selectivity towards CO$_2$ in humid conditions. Selected CO$_2$ capture capacities for the adsorbents presented above, as well as for a few well-known physisorbent MOFs, such as HKUST-1, Fe$_2$(dobdc), MIL-53(Al) and MIL-101(Cr) found in the references [100,150–152] are shown in Table 1.

### 2.4. Amine substituted and N-heterocyclic organic linker ligands

Besides the OMSs and HUMs, of which high affinity towards CO$_2$ originates from their Lewis acidic sites, micro-channeled structure, and the electrons of the charged functionalities (e.g., F$^-$), the uncoordinated amino groups substituted on the organic linkers can also act as an active polar binding site for CO$_2$. Amine functionalization can typically be carried out with the help of aromatic or heterocyclic (e.g., N or S containing) organic linker ligands, which are substituted with one or more amino groups. Aliphatic or aromatic free amines can also be added to the framework using post-synthetic methods (PSM), by which the amines can be attached to OMSs, or can be located as free molecules filling the pores of the adsorbent. Along with the amino group, other polar functional groups, such as perfluorinated aliphatic groups (e.g., CF$_3$), halogens (e.g., Cl, Br) and hydroxyl groups can be used as substituents in the bridging ligands. Typically, the backbone structures of aminated bridging ligands are, for example, aminophenyl, aminobiphenyl, aminonaphthyl, aminotriphenyl and aminoazole groups, of which needs to also contain some bonding groups, such as carboxylic acids or tertiary amines contributing to the formation of the actual framework. By incorporating an amine functionality directly to a linker ligand, has some advantages over the amination of OMS or impregnation of amines. In case of the amine-substituted linker ligand the accessible pore volume

for the quest molecules is greater than, if free (poly)amine molecules fill the pores, or are bound to open metal sites of the MOF adsorbent. Also, with aminated linker ligands, an adsorbent can typically be prepared in one or two synthesis steps, whereas with PSM additional preparation steps are needed. For example, aminating OMSs of a pristine MOF includes typically solvent exchange and or further activation steps to remove both the metal coordinated terminal solvents along with solvents in the pores. This is then followed by the actual post-synthetic amination of the freshly created OMSs. Despite of more multi-step synthesis path, PSM is also useful especially when a certain kind of chemical functionality is desired for the adsorbent, but it cannot be a substituent in the bridging ligand in the actual synthesis step of the MOF, for example, due to the chemical reactivity of the group, thermal instability, or unwanted coordination seeking towards the node metal. In the following paragraphs, MOF adsorbents based on various aminated linker ligands and their metrics for CO$_2$ recovery will be reviewed, considering different adsorption conditions, including DAC, flue gases and pure CO$_2$ that is also used to a significant extent for determining the recovery capacities of adsorbents.

Among countless number of aminated linker ligands, 2-amino-terephthalic acid (NH$_2$-H$_2$bdc) can be highlighted as one of the most widely utilized functionalized organic ligand for preparing aminated MOFs since 2001, when Braun *et al.* first published MOF-46 made from NH$_2$-H$_2$bdc [156]. In their study MOF-2 made of terephthalic acid (bdc) was compared to MOF-46 and it was found that the original framework topology of MOF-2 persisted in the aminated MOF-46. Indeed, since the aminated and the original ligand are often structural analogues, the same synthesis methods can be used for the aminated ligand as for the original ligand. Predominantly, the similarity of the ligand structure allows the topology of the network structure to remain unchanged. In 2002 Eddaoudi et al. [157] reported aminated IRMOF-3(Zn) that belongs to isoreticular series of MOF-5 (bdc with Zn) and, which was tested at the time for methane capture but has later utilized also for carbon capture (~1.4 mmol g$^{-1}$ at 25 °C and 1 bar CO$_2$) [158]. Also, some more recent studies for PSM modified IRMOF-3 can be found. For example, Ding *et al.* reported preparation methods for N-doped porous carbon monoliths (NCMs) via direct carbonization of IRMOF-3.[159] In this process, the partial carbonization modifies the originally microporous structure to contain more meso- and macropores which in turn reveal more amino groups to which CO$_2$ can readily chemisorb (Fig. 6). Based on the research, it could be concluded that the modified NCM (IRMOF-3/800 in the sorption plot) demonstrated better CO$_2$ recovery capacity than the pristine IRMOF-3 with 1.64 vs. 0.70 mmol g$^{-1}$ capacities for NCM and IRMOF-3, respectively at 150 mbar of CO$_2$ (0 °C).
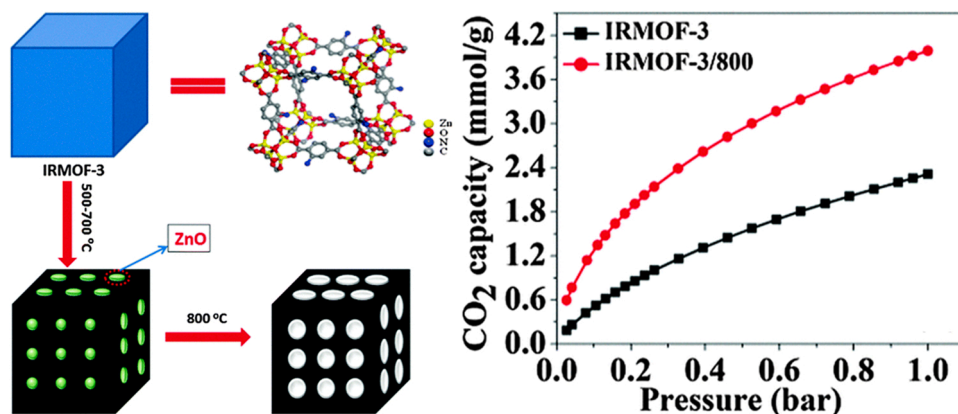
**Fig. 6.** (Left) Illustration for the transformation of IRMOF-3 to NCMs, and (right) $CO_2$ sorption isotherms of IRMOF-3 and modified NCMs at 0 °C. Adapted from Ref. [159].

Nearly doubled capacity (~3.99 vs 2.32 mmol g$^{-1}$) in contrast to IRMOF-3 was observed for NCM at 1 bar $CO_2$ at 0 °C, as can be seen in Fig. 6.

In 2005 Féréy et al. were the first ones to report the nowadays well-known and extensively studied MIL-101(Cr) MOF ([Cr$_3$F(H$_2$O)$_2$O (bdc)$_3$.$n$H$_2$O], ($n$≈25) which has mesoporous structure, remarkable chemical and thermal stability and, when activated contain OMSs [160]. A number of different aminated MOF analogues have also been prepared from the MIL-101 archetype over the years [161–164], as well as plethora of other MOF topologies which are based on NH$_2$-bdc ligand, such as NH$_2$–MIL-101(Al) [165], NH$_2$–MIL-125(Ti) [Ti$_8$O$_8$(OH)$_4$ (NH$_2$–bdc)$_6$] [166], NH$_2$–MIL-68 (USO-3-In-A) [In(OH)(NH$_2$–bdc)] [100], NH$_2$–MIL-53 [Al(OH)(NH$_2$-BDC)][167,168], CAU-1 [Al$_4$(OH)$_2$(OCH$_3$)$_4$(NH$_2$–bdc)$_3$] [169], and NH$_2$–UiO-66 [Zr$_6$O$_4$(OH)$_4$(NH$_2$–bdc)$_6$] [170], to mention a few (Fig. 7). Aminated HKUST-1 framework [Cu$_3$(NH$_2$–btc)$_2$] have also been made from 2-amino-1,3,5-benzenetricarboxylic acid (NH$_2$-btc), as reported by Peikert et al. [171].

Of the above, the NH$_2$-MIL-53(Al) is another interesting example of NH$_2$-bdc containing MOF, as it is known for its specific reversible structural elasticity (breathing network) that can be induced by an external stimulus like heat, or the arrival of a guest molecule in adsorption event. Relatively good $CO_2$ adsorption capacities (e.g., 2.3 mmol g$^{-1}$ at 1 bar $CO_2$) with moderate enthalpy of adsorption (−38.4 kJ mol$^{-1}$) has been reported for it. These are comparable with the other MOFs shown in Table 2. Furthermore, Dhankhar et al. [174] reported mixed ligand MOF1 ([Zn$_2$(NH$_2$BDC)$_2$(dpNDI)]$_n$, having N,N′-di (4-pyridyl)− 1,4,5,8-naphthalenediimide (dpNDI) and NH$_2$bdc ligands. The framework is formed as a 2-fold interpenetrated 3D pillar-layered system with 1D channels decorated by amino groups. The microporous MOF1 demonstrated 1.51 mmol g$^{-1}$ adsorption capacity and enthalpy of − 46.5 kJ mol$^{-1}$ that were clearly better than that observed

for MOF analogue made with bdc (−36.0 kJ mol$^{-1}$). Das et al. [175] designed different mixed ligand MOFs by varying amino, azole and thiophene groups, namely Zn-DAT {[Zn$_2$(TDC)$_2$(DATRZ)]·(3 H$_2$O)· (DMF)}$_n$, including 2,5-thiophenedicarboxylic acid (H$_2$TDC) and 3, 5-diamino-1,2,4-triazole (DATRZ) ligands. Whereas Zn-TAZ {[Zn$_2$(TDC)(TRZ)$_2$]·(DMA)·(MeOH)}$_n$ was made with TDC and 1,2,4-triazole (TRZ) ligands. Interestingly, the amino group containing Zn-DAT showed higher $CO_2$\$N_2$ adsorption selectivity and adsorption heat than the simpler triazole containing Zn-TAZ (−39.5 vs. −31.7 kJ mol$^{-1}$, respectively). In the following study Das et al. [176] reported interesting hydrogen bonded 3D framework, HbMOF1 {[Zn(hfipbba)(MA)]· 3DMF}$_n$ made by using 4,4'-(hexafluoroisopropylene)bis-benzoic acid (hfipbba), and amino-rich melamine (MA) ligands. In this case addition of polar (-CF$_3$) and basic (-NH$_2$) substitution groups adsorbent proved to be even better than the adsorbents reported earlier by Das *et al.*, as its adsorption heat (−36.7 kJ mol$^{-1}$) and particularly adsorption capacity (2.21 mmol g$^{-1}$ at 0 °C) increased significantly.

In addition to the amino group, other N-comprising ligands have been reported to increase the affinity of $CO_2$ into the pores of the framework [177–180]. For instance, Li et al. [181] prepared Cu$_4$[(C$_{57}$H$_{32}$N$_{12}$)(COO)$_8$] consisting of nitrogen-rich triazole-cored octacarboxylic acid ligand (5,5′,5′,5′-((methanetetrayltetrakis(benzene-4,1-diyl))-tetrakis(1 H-1,2,3-triazole-4,1-diyl))-tetraisophthalic acid). The sorption tests revealed remarkable $CO_2$ uptake of 7.18 mmol g$^{-1}$ at 1 bar (0 °C), and it was concluded that the high capacity of the adsorbent resulted from the synergy between the N atoms and open Cu sites while interacting with approaching $CO_2$ molecules. Similarly, bio-MOF-11 [Co$_2$(ad)$_2$(O$_2$CCH$_3$)$_2$] having adenine (ad) ligands and acetate anions, showed high 6.0 mmol g$^{-1}$ capacity along with excellent $CO_2$/$N_2$ selectivity up to 81 at 1 bar (0 °C). The reported MOF consists of mixed acetate/adeninate cobalt paddlewheel units, where
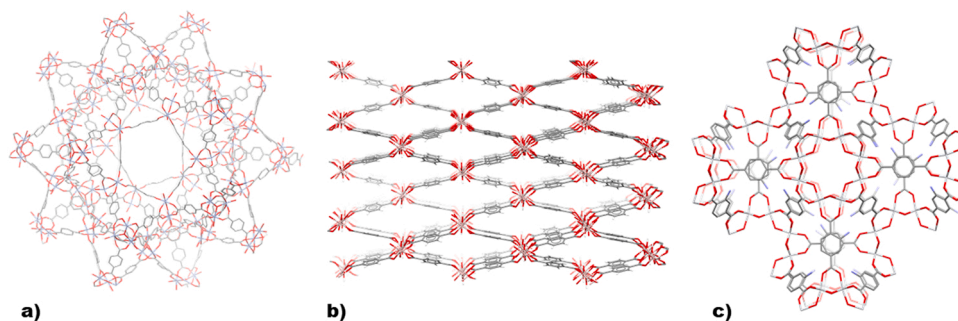


**Fig. 7.** (a) Partial structure views of MIL-101(Cr), (b) MIL-53(Al) having analogous structure to NH$_2$-MIL-53(Al), and (c) NH$_2$-MIL-125. CSD entries OCUNAC, SABWAU01 and MAWBUK have been used to create images with Mercury program
Adapted from Ref. [110,111,160,172,173].

**Table 2**
Summary of $CO_2$ adsorption for MOFs with targeted modifications to linker unit.

| MOF | Capacity (mmol g$^{-1}$) | | -Q$_{st}$ (kJ mol$^{-1}$) | Temp. (°C) | Ref. |
|---|---|---|---|---|---|
| | 150 (mbar) | 1 (bar) | | | |
| IRMOF-3 | | ~1.4 | | 25 | [158] |
| IRMOF-3\800 | 1.64 | 3.99 | 29.6 | 0 | [159] |
| NH$_2$-MIL-101(Cr) | | 1.9 | ~50 | 25 | [161, 164] |
| NH$_2$-MIL-53(Al) | | ~2.3 | 38.4 | 30 | [167, 168] |
| NH$_2$–MIL-125 | | 2.2 | | 25 | [11, 166] |
| CAU-1 | | 3.9 | 48 | 25 | [169] |
| UiO-66 −NH$_2$ | ~1.34 \1.16$^H$~0.25 *$^H$ | ~2.65 | 28 | 25 | [155, 170] |
| Cu$_3$(NH$_2$btc)$_2$ | | 5.26 | | 25 | [171] |
| MOF**1** | | 1.26 | 46.5 | 25 | [174] |
| HbMOF**1** | | 1.39 | 36.7 | 25 | [176] |
| IFMC-1 | | 2.7 | 30.7 | 25 | [211] |
| [Zn(btz)] | | 4.9 | 31.2 | 25 | [212] |
| bio-MOF-11 | | 4.1 | ~45 | 25 | [182] |
| NJU-Bai50 | 0.0018 * \ 0.49 | | 26.6 | 25 | [195] |
| NJU-Bai51 | 0.13 * \ 0.90 | | 33.3 | 25 | [195] |
| IR-MOF-74-III-CH$_3$ | | 2.96 | | 25 | [218] |
| IR-MOF-74-III-NH$_2$ | | 3.18 | | 25 | [218] |
| IR-MOF-74-III-CH$_2$NHBoc | | 2.09 | | 25 | [218] |
| IR-MOF-74-III-CH$_2$NMeBoc | | 1.91 | | 25 | [218] |
| IR-MOF-74-II-CH$_2$NH$_2$ | | 3.35 | | 25 | [218] |
| IR-MOF-74-III-CH$_2$NHMe | | 2.87 | | 25 | [218] |
| IR-MOF-74-III-(CHNH$_2$)$_2$ | | 3.00 | | 25 | [219] |
| MUF-17 | 1.41 | 2.55 | 28.3 | 25 | [193] |
| Cu-TDPAT | | 5.9 | 42.2 | 25 | [197] |
| Cu$_3$(TDPAH) | | 5.2 | 33.8 | 25 | [213] |
| MAF-23 | | 2.5 | 47.4 | 25 | [198] |
| Zn$_2$Atz$_2$Ox | 2.05 | 3.67 | 40 | 20 | [196, 214] |
| MAF-66 | | 4.4 | 26.0 | 25 | [216] |
| ZJNU-43 | | 4.6 | | 25 | [190] |
| ZJNU-44 | | 5.2 | | 25 | [190] |
| ZJNU-45 | | 4.8 | | 25 | [190] |
| HP-e | ~2.33 | ~7 | 35.2 | 25 | [180] |
| ZnF(daTZ) | ~0.96\0.94$^H$ | 3.3 | 33 | 25 | [217] |
| ZnF(aTZ) | ~0.56\0.50$^H$ | 3.1 | 32.3 | 25 | [217] |
| ZnF(TZ) | ~0.27\0.35$^H$ | 2.7 | 23.6 | 25 | [217] |
| FJI-H14 | | 6.5 | 26.6 | 25 | [177] |
| CALF-20 | | 4.0 * * | 39 | 20 | [221] |
| IISERP-MOF4 | | 3.02 | 29 | 25 | [223] |
| HHU-5 | | ~4.78 | 25.6 | 25 | [178] |
| HHU-2 | ~1.35 | ~4.0 | 30 | 25 | [179] |
| MAF-stu-1 | 2.44 | 3.54 | 35 | 25 | [105] |

* Measured at 0.39 mbar, * * Measured at 1.2 bar, and $^H$ for humid condition.

nucleobase adenine comprises an aromatic amine, a pyrimidine and diazole moieties, of which the Lewis basic amino and pyrimidine groups can be assumed to be favorable sites for adsorption. Also, the nano-sized channel structure played a significant role in terms of high $CO_2/N_2$ selectivity (30–77) [182,183]. More recently, Chen et al. [184] prepared a moisture stable N-rich cobalt-based MOF, i.e., Co-PL-1 (Co (Imda)(4,4'-bpy) consisting of imidazole-4,5-dicarboxylic acid (Imda), and 4,4'-bipyridyl (4,4'-bpy) ligands. The reported MOF exhibited $CO_2$ uptakes of 1.20 and 2.02 mmolg$^{-1}$ with high $CO_2/N_2$ adsorption selectivity and good stability under humid conditions both at 150 mbar and 1 bar pressures (25 °C).

In addition to imidazole and triazole groups, an azo group (−N═N–) can have an effect to the selectivity of $CO_2$ adsorption by increasing the polarity of the pore structure [185–187]. For example, with a mixed-ligand approach, Nagaraja et al. [188] made homochiral

3D-MOFs $\{[M(L\text{-mal})(azpy)_{0.5}]\cdot 2\, H_2O\}_n$ and $\{[M(L\text{-mal})(bpee)_{0.5}]\cdot 2\, H_2O\}_n$, with Co or Ni metal ion nodes (M) and L-malate (L-mal) ligand using two different azo and ethylenic group (−CH═CH–) containing secondary linkers, namely 4,4′-bisazobipyridine (azpy) and 1,2-bis (4-pyridyl)ethylene (bpee). For azpy-MOF the $CO_2$ capacity and the adsorption heat were slightly higher than that of the ethylenic analogue being ~4.9 vs. 1.5 mmol g$^{-1}$ and − 37 vs − 31 kJ mol$^{-1}$, respectively. It was suggested that the better sorption properties of azby-MOF originated from more polar azo groups inducing considerably stronger adsorbate−adsorbent interactions in comparison to the ethylenic group. Along with the azo group, the basic non-metalated porphyrin cavity can also enhance the selectivity of $CO_2$ and heat of adsorption. For this, an interesting example is the Mn$^{II}$-porphyrin MOF ([{Mn$_2$(TCPP)·2 H$_2$O· DMF]$_n$), where 5,10,15,20-tetrakis(4-benzoate)porphyrin (TCPP) ligand was used. The relatively high $CO_2$ capacity 2.63 mmol g$^{-1}$ (0 °C, 1 bar) and heat of adsorption of − 32.1 kJ mol$^{-1}$ values observed for the adsorbent were assumed to occur due to the basic -NH groups of the pyrrole macrocyclic cavity [189].

It is also good to point out that in the formulation and construction of MOFs for $CO_2$ adsorption, one should not only emphasize the abundance of NH$_2$ or other N-containing groups but also more critically focus on the impact of the accessibility of active binding sites by approaching $CO_2$. Song et al. [190] studied array of isoreticular copper-based MOFs, namely ZJNU-43, ZJNU-44, and ZJNU-45 by utilizing three rigid organic ligands, 5,50-(quinoline-5,8-diyl)-diisophthalic, 5,50-(isoquinoline-5, 8-diyl)-diisophthalic, and 5,50-(quinoxaline-5,8-diyl)-diisophthalic acids (Fig. 8). Although all three network structures have almost the same active surface area, they showed pronounced differences in their $CO_2$ uptakes due to the different number, and dissimilar orientation of N-containing groups inside the framework, which consequently defined accessibility of $CO_2$ toward the available binding sites. In ZJNU-43 the nitrogen atom of the heterocyclic aromatic ring is in the α-position, demonstrating 4.6 mmol g$^{-1}$ $CO_2$ uptake. Whereas when located in $\beta$-position in ZJNU-44 the $CO_2$ capture capacity increased significantly to 5.2 mmol g$^{-1}$ (1 bar, 25 °C). On the ZJNU-45 the number of nitrogen atoms were doubled resulting somewhat lower 4.8 mmol g$^{-1}$ capacity under the same adsorption conditions. The difference in the determined capacities were also examined by quantum chemical calculations that suggested $CO_2$ trapping to occur in the narrow windows in case of the structures ZJNU-43 and ZJNU-45. Whereas in ZJNU-44 framework, N-containing sites pointed into the pore centers and by this allowed $CO_2$ bridging with the organic linkers. The binding energy was found to be highest for ZJNU-44 (−27.6 kJ mol$^{-1}$), whereas − 18.1 and − 18.7 kJ mol$^{-1}$ were calculated for ZJNU-43 and ZJNU-45, respectively. Based on the results, the orientation of the nitrogen-containing sites in the pore structure seem to play an important role in the efficiency of $CO_2$ adsorption. Similar conclusions have been drawn recently by studies in which the subtle changes in the chemical construction and orientations of N-containing sites in MOFs have significantly impacted to the adsorption capacity [191,192].

Recently Qazvini et al. [193] investigated $CO_2$ capturing properties of MUF-17 ([Co$_5$(μ$_3$- OH)$_2$(aip)$_4$(H$_2$O)$_2$], prepared using 5-amino-isophthalic acid (aip) and cobalt ion nodes. In this framework, the primary $CO_2$ binding sites were positioned at the median of the narrowest channel neck. As can be seen in Fig. 9b, the electrostatic and hydrogen-bonding interactions with short contact distances prevailed between the framework and the $CO_2$ molecule. It was found that up to 85 % relative humidity, the adsorption efficiency of the MUF-17 remained unchanged. The compatibility of MUF-17 with a polymeric binder, poly-vinylidene fluoride, (PVDF) was also examined. The resulted MUF-17/PVDF composite in form of pellets exhibited similar behavior in gas adsorption experiments as the pristine MOF (Fig. 9c).

With a somewhat different approach, the chelate effect of bridging ligands was investigated by Wang et al. [105]. They reported Zn (imPim), also known as MAF-stu-1 which belongs to the group of metal azolate frameworks (MAF). It consisted of imidazole derivative ligand,
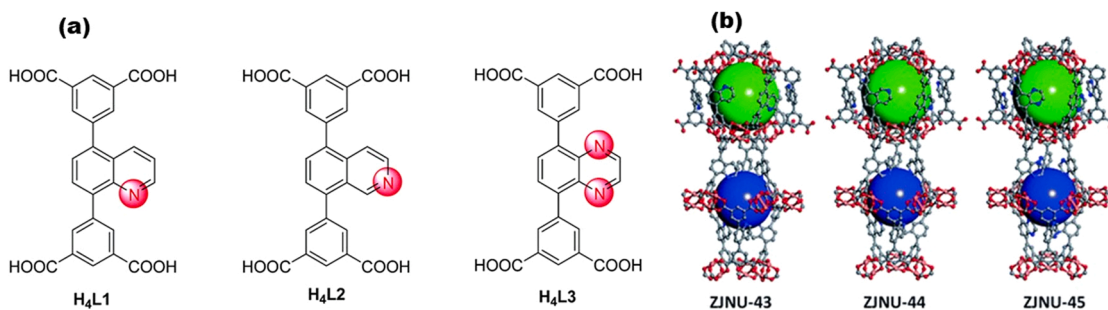
**Fig. 8.** (a) The organic linker ligands with heterocyclic N-containing core units, and (b) polyhedral nanocages of ZJNU-43, ZJNU-44, and ZJNU-45 MOFs. Adapted from Ref. [190].
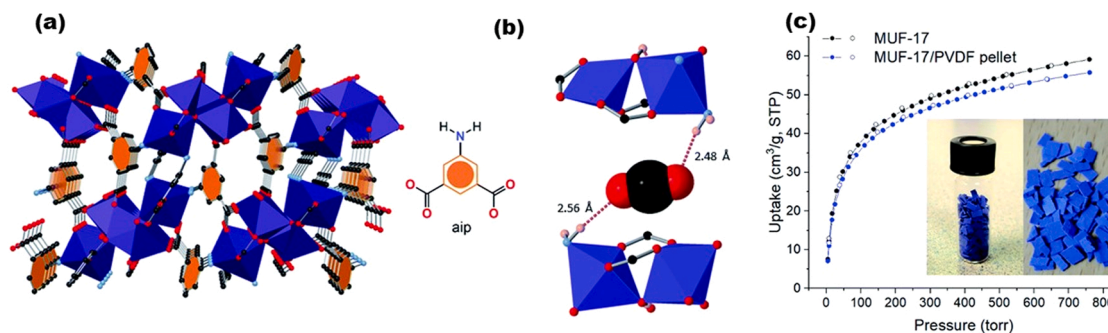


**Fig. 9.** The structure of (a) MUF-17, (b) Hydrogen bonding interactions with adsorbed $CO_2$ molecules, and (c) $CO_2$ adsorption and desorption isotherm of MUF-17/ PVDF pellets at 20 °C.
Adapted from Ref. [193].

2-(1 H-imidzol-2-yl)– 3 H-imidazo[4,5-*c*] pyridine (H₂imPim), which offers binding pockets for $CO_2$ molecules in a "fit like a glove" manner (Fig. 10). The reported MOF exceeded the earlier benchmarks with a record-breaking thermal (up to 680 °C) and chemical stabilities coupled with a simple synthesis procedure in bulk quantities. Owing to its shape-complemented binding pockets, MAF-stu-1 also demonstrated an excellent capacity (3.54 mmol g$^{-1}$), high $CO_2/N_2$ (15:85, v/v) selectivity (106), and a low level of energy cost on regeneration (35 kJ mol$^{-1}$). Although MAF-stu-1 is a physisorbent, the obtained metrics are promoting its potential use in $CO_2$ recovery also in DAC conditions.

One of the available strategies for trapping $CO_2$ molecules is based on its physical (size and shape) and chemical (polarity) properties. As suggested by Li et al. for instance, by tuning the bridging ligands, molecular

cavities with accurate size and desirable properties can be designed, like a single-molecule-trap (SMT). In their study, the distance of 6.4–8.0 Å was suggested to be optimal for holding $CO_2$ molecules between two OMSs through electrostatic interaction [194]. This idea was further utilized by Song et al.[195] as they made NJU-Bai50 [Sc₃O(L1)₂(H₂O)₃(NO₃)]$_\infty$ and NJU-Bai51[Sc₃O(L2)₂(H₂O)₃(NO₃)]$_\infty$ MOFs using 1,10-(4-carboxypyridine-2,6-diyl)bis(1 H-pyrazole-4-carboxylic acid (H₃L1) and 1,10-(4-carboxypyridine-2,6-diyl)bis(3-bromo-1 H-pyrazole-4-carboxylic acid (H₃L2) ligands. To fit $CO_2$ adequately to pores, the contact distance between two opposite OMSs were tuned from 6.45 Å (NJU-Bai50) to 6.75 Å (NJU-Bai51) by regulating the torsion degree of the ligand. The $CO_2$ trap of NJU-Bai51 resulted in enhanced host–guest interactions, locking on to a single $CO_2$ molecule through its two O atoms without chemical bond formation. The increase in $CO_2$ uptake capacity was observed to be
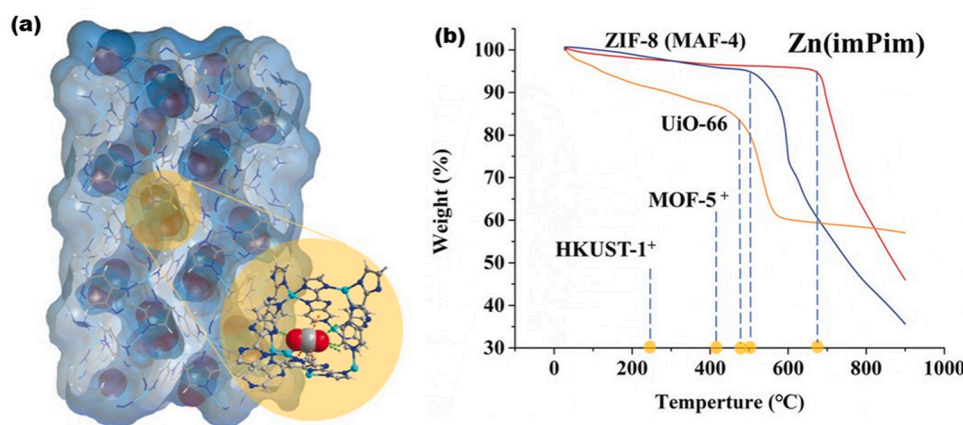


**Fig. 10.** (a) Partial view of periodic $CO_2$ binding pockets on Zn(imPim), and (b) Thermogravimetric curves of few selected MOFs compared with Zn(imPim)
Adapted from Ref. [105].

0.13 mmol g$^{-1}$ (72 times higher) and 0.90 mmol g$^{-1}$ (nearly double) in comparison to NJU-Bai50 (0.0018 and 0.49 mmolg$^{-1}$) both at 0.4 and 150 mbar (25 °C), respectively. In terms of $CO_2/N_2$ selectivity (15/85 ratio at 1 bar, 25 °C) NJU-Bai51 showed a significantly better selectivity compared to NJU-Bai50 (545.7 vs. 30.5), most likely due to its custom designed size-matching cavities for $CO_2$. In addition to the examples discussed above, other N-containing linkers such as pyrimidines, triazines, and azole derivatives have been utilized in functionalized MOFs, and have also demonstrated intriguing new results [191,196–217].

### 2.4.1. Consideration of water effects

The affinity, selectivity, and overall $CO_2$ uptake properties of N-containing ligands in the frameworks are just as prone to the effects of water as the OMSs are. Fracaroli et al. [218] examined a series of IR-MOF-74-III by incorporating differently functionalized ligands containing –CH$_3$, –NH$_2$, –CH$_2$NMeBoc, and –CH$_2$NHBoc (Boc = tertbutyloxycarbonyl) functional groups (Fig. 11). On IRMOF-74-III-CH$_2$NHBoc and –CH$_2$NMeBoc the protective Boc groups were removed by protonation to embody –CH$_2$NH$_2$, and –CH$_2$NHMe in the framework. The conversion was confirmed by $^1$H and $^{13}$C NMR, ESI-MS, and SC-XRD data. Of the tested adsorbents IRMOF-74-III-CH$_2$NH$_2$ revealed the highest $CO_2$ uptake being 3.2 mmol g$^{-1}$ (1 bar $CO_2$), and a combination of carbamic acid (RNHCOOH) and ammonium carbamate (RNHCOO$^{-+}$H$_3$NR) species were ascertained by solid-state cross-polarization magic angle spinning (CP-MAS) $^{13}$C NMR spectra to be the main chemisorption products. In addition, the water did not seem to have any effect on the adsorption properties of the adsorbent, because similar retention times were observed with NMR for samples representing both dry and humid conditions. The adsorbent's high selectivity and capacity sustained even at 65 % relative humidity. Thereby it could be assumed that $CO_2$ is likely to bound to the ligand-substituted alkylamine groups rather than to OMSs, as in case of humid condition OMSs should virtually be inaccessible due the water molecules have bound to them.

Furthermore, Flaig and coworkers [219] presented a doubling of the linker-substituted alkylamines in the framework to yield IRMOF-74-III-(CH$_2$NH$_2$)$_2$. At lower $CO_2$ pressures, the adsorbent demonstrated about 2.3 times higher $CO_2$ adsorption capacity than IR-MOF-74-III-CH$_2$NH$_2$ indicating that two alkyl-amines per organic linker further promoted chemisorption. Notably, based on the solid-state NMR ($^{13}$C and $^{15}$N) data, carbamic acid was observed under dry conditions, whereas under water vapor ammonium carbamate was observed (Fig. 12). The reported study was one of the first ones to demonstrate the actual chemical composition of the adsorption products. It also highlighted the significance of the participation of water in dictating the

adsorption mechanism within the pores of the framework. The different sorption mechanisms of chemisorption are described in more detail in Section 2.5.2.

Along with the MOF-74 family, zeolitic imidazolate frameworks (ZIFs) have also proven to be promising adsorbent candidates for carbon capture due to their intrinsic hydrophobic behavior. Nguyen et al. [220] reported ZIF adsorbents resembling the structural topology of chabazite (CHA), namely ZIF-300 (Zn(2-mIm)$_{0.86}$-(bbIm)$_{1.14}$), ZIF-301 (Zn (2-mIm)$_{0.94}$(cbIm)$_{1.06}$), and ZIF-302 (Zn(2-mIm)$_{0.67}$(mbIm)$_{1.33}$) which were made using 2-methyl-imidazo (2-mIm), 5(6)-bromobenzimidazole (bbIm), 5(6)-chlorobenzimidazole (cbIm), and 5(6)-methylbenzimidazole (mbIm), respectively. For all three adsorbents, remarkably low affinity for water was observed in water adsorption tests with uptake capacities varying from 0.33, 0.32–0.25 mmol g$^{-1}$, respectively at P/P$_0$ ≈ 0.8 (25 °C). The ZIF-300 proved to be the most effective adsorbent for the dynamic separation of $CO_2$ from $N_2$ as the $CO_2$ adsorption isotherms showed uptakes of 1.3, 1.2, and 0.1 mmol g$^{-1}$ for ZIF-300, ZIF-301, and ZIF-302, respectively (at 1 bar, 25 °C). The experiments were made under dry and humid conditions, and no loss of activity was observed within three subsequent cycles. Furthermore, Lin *et al.* reported CALF-20 [Zn$_2$(1,2,4-triazolate)$_2$(oxalate)] MOF which demonstrate low water affinity and high uptake of 4.07 mmol g$^{-1}$ (1.2 bar, 20 °C) but with modest heat of adsorption of − 39 kJ mol$^{-1}$ indicating physisorption of $CO_2$. [221] With atomistic grand canonical Monte Carlo (GCMC) simulations, the $CO_2$ binding sites were found to be in the centers of pores that impede forming of a hydrogen-bonding network between water molecules. The calculated $CO_2$ binding energy of − 34.5 kJ mol$^{-1}$ indicated electrostatics and attractive dispersion interactions (85 %) being predominant in interactions between the framework and $CO_2$. For water adsorption studies, simulations demonstrated that in the absence of $CO_2$, water uptake (20% RH) was 6 mmol g$^{-1}$, but with presence of $CO_2$ it was negligible. However, at 40 % RH, water uptake was observed to be 6 mmol g$^{-1}$ in the presence of $CO_2$. Thus, below 40 % RH, CALF-20 demonstrates not just preferential $CO_2$ physisorption but also shows suppression of water adsorption by $CO_2$. In addition, adsorbent showed low enthalpic regeneration penalty in flue gas conditions and displayed durability towards steam > 450,000 cycles. [221].

Although with moderately water-resistant MOFs exemplified above and few others found in the literature [222,223], most MOFs will go through structural degradation under humid conditions. The metal centers of the framework, in the long run, end up gradually interacting with a water molecule instead of $CO_2$ owing to its quadrupole moment [131,224,225]. The long-term chemical stability of the adsorbents against water is an important property, particularly for those designed to function in DAC conditions, wherein water will always be present in
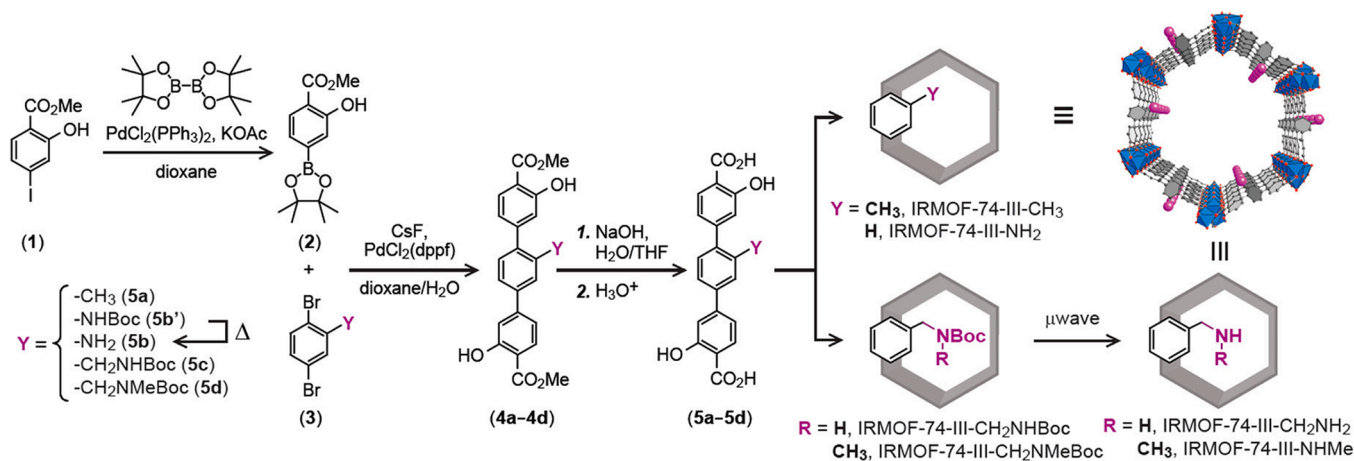


**Fig. 11.** Synthetic route for the functionalized organic linkers incorporated in IRMOF-74-III Adapted from Ref. [218].
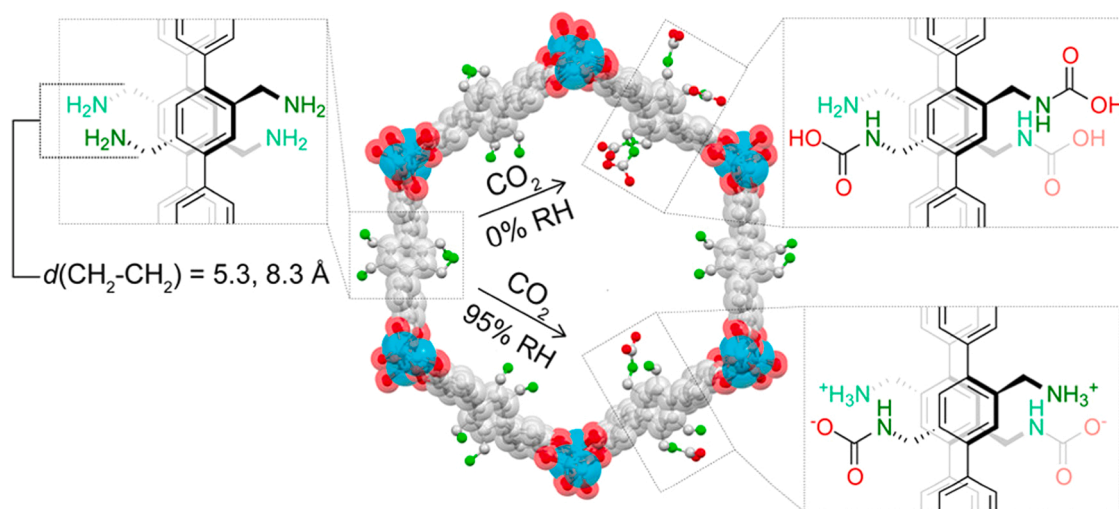
**Fig. 12.** Modelling of the IR-MOF-74-III-$(CH_2NH_2)_2$ structure and schematic of the chemisorption species upon reaction between linker-based alkylamine and $CO_2$ under dry and humid conditions.
Adapted from Ref. [219].

magnitudes several times higher than $CO_2$. Selected $CO_2$ capture capacities for all the adsorbents presented above are shown in Table 2.

### 2.5. Post-synthetic amination and adsorption mechanisms on aminated open metal sites

Water molecules are in constant competition with $CO_2$, and the unsaturated open metal sites are particularly attractive to water. To overcome the adverse effects of water, particularly on physisorbent MOFs that are typically based on the adsorption of $CO_2$ to OMSs, amine-containing species can be anchored post-synthetically in OMSs. Methods commonly found in the literature are called as amine grafting, tethering, or appending of amines. Two of the well-known MOF-families, namely MOF-74, and MIL-100/101 based MOFs serve again as good examples of recent advances in MOFs that include OMSs (chapters 2.5.1 and 2.5.3). Many of the $CO_2$ adsorbents of both families are among the best performing adsorbents in dry conditions but many of them, like most other MOF adsorbents, face difficulties in humid conditions due to the gradual deterioration of the chemical structures by hydrolysis [226]. Adsorption mechanisms, which inevitably depend on whether adsorption takes place in dry or humid conditions, are also reviewed in Section 2.5.2.

#### 2.5.1. MOF-74 family

According to Choi et al. [227] OMSs in MOF-74 are capable to form stable bonds with diamine by receiving electrons from the N atom of the first amino group of the diamine, and by this, the second amino group is still available for interaction with $CO_2$. Among the first post-synthetic modification studies, ethylenediamine (en) was tethered into $Mg_2(dobdc)$ to produce en-appended MOF-74. The thermogravimetric analysis (TGA), nitrogen sorption, and DFT calculations of the product revealed that approximately one ethylenediamine molecule was associated per one OMS in each unit cell. After functionalization, the surface area of the modified material was clearly lower than that of the pristine MOF, as it decreased from 1094 to 469 $m^2/g$. However, some 12% increase in $CO_2$ uptake (from 1.35 to 1.51 mmol $g^{-1}$) was observed between aminated and pristine MOF-74 under 0.39 mbar $CO_2$. The regeneration tests with four sorption cycles were made for both aminated and pristine MOF-74 and revealed some 21% decrease in the capacity at the end of the cycles for pristine adsorbent, whereas no change in capacity was observed for the aminated one.

Bernini et al. [228] screened several reported and some hypothetical en-$Mg_2(dobdc)$ MOF variants by Monte Carlo simulations to determine the optimized amine loadings for capturing $CO_2$ both from flue gas and

ambient air. Ethylenediamine compositions of 3.14, 5.99 and 6.74 wt.-% were incorporated to $Mg_2(dobdc)$, and as a result diamine content of about 50% of the available OMSs turned out to be the optimal fill rate for affording the best adsorption capacity. Also, the correlation between thermal stability and amine loadings was investigated by TGA. The superior stability was demonstrated by the lowest amine loading (3.14 wt.-%) followed then by 5.99 and 6.74 wt.-% amine loads. This indicated a clear decrease in thermal stability with an increase in amine loads, as temperature ranges for primary thermal degradation step varied from 278 to 430 via 252–440–228–430 °C, correspondingly. Hydrazine (HZ), the smallest and the lowest boiling diamine (114 °C), was appended in various loads to $Mg_2(dobdc)$ by Liao et al. [229] resulting in the highest capture capacity of 3.89 mmol $g^{-1}$ in DAC (25 °C) with HZ-MOF-74 containing 6.01 mmol $g^{-1}$ amine load. Interestingly, the thermal stability of the afforded adsorbent was high even though low boiling diamine was incorporated into the framework. The aminated adsorbent was subjected to 5 sorption cycles with desorption at 130 °C ($N_2$), and virtually no capacity loss was observed at the end of the cycles.

As can already be seen from the above examples, amine basicity also plays an important role both in the adsorption and selectivity of $CO_2$. Yeon et al. [123] investigated the effects of amine basicity using an amine-functionalized isoreticular Mg-MOF-74 analogue, namely $Mg_2(dondc)$ made of 1,5-dihydroxy-2,6-naphthalenedicarboxylic acid. Pristine adsorbent showed pore size of about 15 Å, which was then modified using primary, secondary and tertiary amines: ethylenediamine (en), *N,N'*-di-methylethylenediamine (mmen), and piperazine (ppz), respectively. Due to the relatively small channel sizes of the unmodified adsorbent, the available open metal sites were found to be 75 (en), 55 (ppz), 60 % (mmen) occupied by the amines. Nevertheless, adsorbents exhibited good $CO_2$ capacities ranging from 1.99 (en) via 2.04 (ppz) to 3.20 (mmen) mmol $g^{-1}$ under post-combustion flue gas conditions. Surprisingly, the adsorption mechanism was attributed to be both physi- and chemisorption, as indicated by the IR spectroscopic analyses. The major weakness of the adsorbents proved to be their poor thermal stability, as leakage of the amines out of the pores was thermogravimetrically evidenced during regeneration cycles. After five cycles, the ethyleneamine containing adsorbent already lost 10% of its initial $CO_2$ adsorption capacity at 150 °C, and mmen- and ppz-appended ones lost 15% and 14% already at 130 and 120 °C, respectively. For en- and ppz-appended adsorbents the uptake losses were associated to 17 and 12 wt.-% amine leakage, whereas mmen-$Mg_2(dondc)$ showed only weight loss of 2 %. To examine long term regeneration characteristics,

ppz-Mg$_2$(dondc) was regenerated 50 times resulting in dramatic 43 % decrease in CO$_2$ uptake capacity under tested desorption conditions (with Ar at 130 °C). McDonald et al.[101] made similar amination tests but with Mg$_2$(dobdc) and the OMSs were post-synthetically aminated by mmen. In DAC the aminated mmen-Mg$_2$(dobpdc) showed a significantly higher 2.0 mmol g$^{-1}$ capacity (0.39 mbar, 25 °C) being about 15 times higher than the pristine Mg$_2$-(dobpdc) showing only modest ~0.13 mmol g$^{-1}$ capacity under the same conditions. The high adsorption heat determined for the adsorbent indicates that CO$_2$ is chemisorbed to the diamine sites of the adsorbent. Based on the above examples and the literature, it has been suggested that the mmen-Mg$_2$(dobpdc) adsorbent would be more efficient than, for example, conventional amine-grafted silica-based adsorbents or aqueous amine scrubbers. [230].
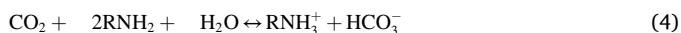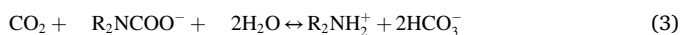
*2.5.2. Adsorption mechanisms*

Regarding the aminated MOF adsorbents already discussed above, the variables related to their adsorption and regeneration process (desorption) can also be considered, of which the actual adsorption mechanism is one of the key factors, and it is dependent on the properties of the available adsorption sites e.g., amines appended on open metal sites, as well as whether sorption conditions are dry or humid and at what temperature. For instance, the mmen-Mg$_2$(dobpdc) has been designated as a ´phase-change´ type of CO$_2$ adsorbent, as it shows step-shaped isotherms with a relatively large working capacity at a small temperature increase. However, classical adsorbents (mostly amine-functionalized inorganic solids) show Langmuir-type isotherms demanding higher desorption temperatures to attain large working capacities. The sudden step-shaped rise in the CO$_2$ isotherm at a precise pressure signifies cooperative insertion of CO$_2$ amongst the metal centers and the amine clusters. Therefore, it is expected that carbamate species will be created that leads to the generation of ion pairs with neighboring ammonium ions [231]. The foundations for the generation of carbamate species lay on the sorption environment favoring chemisorption in the presence of amino group, wherein water acts as a catalyst and protic solvent for the deprotonation via which the carbamate is generated. When chemisorption governs the CO$_2$ adsorption, the kinetics of CO$_2$ uptake is very fast and highly selective above any other gases [55]. For instance, in the case of tetraethylenepentamine (TEPA) aminated Mg$_2$(dobdc), humid condition promotes CO$_2$ adsorption considerably, which can be seen as an increase in capacity from 6.06 to 8.31 mmol g$^{-1}$ on TEPA-Mg$_2$(dobdc), compared to non-aminated one, due to bicarbonate formation favored by the water-assisted stoichiometry.

Based on theoretical and experimental considerations, it is well-known that amino groups of polyamines, both primary and secondary, prefer the formation of carbamate species with CO$_2$, which converts into bicarbonate in the presence of water. In terms of stoichiometry CO$_2$ capture in dry conditions needs two amino groups per CO$_2$ to be adsorbed (reactions 1 and 2), whereas in humid conditions only one amino group is needed for adsorption, as can be seen from the reaction formulas 3–5:

$$CO_2 + \quad 2RNH_2 \leftrightarrow NH_4^+ + R_2NCOO^- \tag{1}$$

$$CO_2 + 2R_2NH \leftrightarrow R_2NH_2^+ + R_2NCOO^- \tag{2}$$
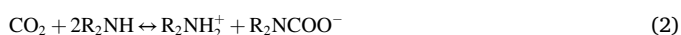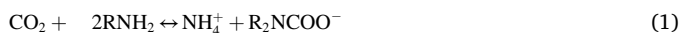
The addition of moisture accelerates the reaction of carbamic acid with water and CO$_2$, eventually bicarbonate; is formed (3). There is also a tendency of the amine group to react directly both with CO$_2$ and H$_2$O to form a bicarbonate unit (4−5). [232].

$$CO_2 + \quad R_2NCOO^- + \quad 2H_2O \leftrightarrow R_2NH_2^+ + 2HCO_3^- \tag{3}$$

$$CO_2 + \quad 2RNH_2 + \quad H_2O \leftrightarrow RNH_3^+ + HCO_3^- \tag{4}$$

$$CO_2 + 2R_2NH + \quad H_2O \leftrightarrow R_2NH_2^+ + HCO_3^- \tag{5}$$

The study made by Planas et al. [233] verified that an increase in CO$_2$ capture capacity is not merely based on the interaction between a positive carbon and a negative nitrogen atom, in CO$_2$ and amine respectively. They examined CO$_2$-amine chemisorption mechanism in mmen-Mg$_2$(dobpdc) using computational chemistry. With density functional theory (DFT) studies, they proposed that N−C bond formation steps are stabilized by cleavage of N−H bonds and the concurrent generation of hydrogen-bonded adducts (Fig. 13). It was also suggested that the hydrogen bonds have a crucial role in preventing unwanted reactions from occurring that may lead to unwanted intermediates and side-product formation.

As can be seen in Fig. 13, the preliminary lowermost-energy state (A$_I$) comprises two amines allied on a neighboring Mg$^{2+}$ cation. The single H atom of an amine can form a hydrogen bond with N atom of an adjacent amine group. The O atom of confronting CO$_2$ interacts with H atom of the amine and forms a weak early-stage hydrogen bond. After the rotation of the amine group and CO$_2$ molecule, the H-N bond cleaves, consequently followed by the formation of N−C bond between an amine and CO$_2$, respectively. In this mode, the amine N atom tethers to the C atom and donates its H to the adjacent amine N atom, thereby forming a carbamic unit. Concurrently, the other amine N atom accepts the H atom and forms RNH$_3^+$ cation. In accordance with Coulombic force, the positive RNH$_3^+$ seeks $N - CO_2^+$ to form new hydrogen bonds (N−H and O−H) with minimal energy states (B$_I$). Interestingly, it was suggested that with the addition of a second CO$_2$ molecule, hydrogen bond will be formed between the carbamic acid−amine adduct (B$_{II}$ to B$_{III}$) and CO$_2$, thus producing a second zwitterionic unit that is stabilized by two-fold hydrogen bonds. Consequent exchange of protons followed by a reorganization of the product leads to the formation of bis(carbamic acid), which is stabilized by dual hydrogen bonds in the ultimate structure. Based on the suggested mechanism, the adsorption energy of − 138.25 kJ per 2 moles of CO$_2$ corresponds to an average adsorption energy of − 69.13 kJ mol$^{-1}$ which is a reasonably good agreement with the experimental value of − 71 kJ mol$^{-1}$ for chemisorption of CO$_2$.[234] The presented mechanism emphasized the importance of the physical length of the amine as the structural constraints of the adsorbent dictate the amine−amine interaction distances.

Encouraged by the presented mechanism Lee et al. further studied CO$_2$ adsorption in DAC using a system wherein primary amine ethylenediamine was appended into a pore size expanded Mg$_2$(dobpdc) [235]. A significantly higher 2.83 mmol g$^{-1}$ CO$_2$ capacity (0.39 mbar, 25 °C) was measured for en-Mg$_2$(dobpdc), and even higher 3.62 and 4.57 mmol g$^{-1}$ were obtained at 150 mbar and 1 bar CO$_2$ pressures in dry conditions, respectively. In regeneration cycles, the capacity remained practically unchanged both in DAC, as well as on CO$_2$ richer conditions corresponding to the flue gas. En-Mg$_2$(dobpdc) was also exposed to humid conditions, wherein the capacity also remained unchanged after several cycles. However, the adsorption mechanism proved to be different than the previously suggested carbamate formation, as based on the FTIR and DFT calculations carbamic acid resulted in the adsorption event. In FTIR spectra, the characteristic O−H peak at 3412 cm$^{-1}$ disappeared with an increase in temperature followed by emerging of N − H stretching at 3337 and 3281 cm$^{-1}$, therefore indicating adsorption of CO$_2$. The calculated adsorption heat was found to be in the range of − 49–51 kJ mol$^{-1}$ being consistent with the enthalpy of carbamic acid formation determined by DFT calculations.

In another study, Lee et al. [236] prepared dmen-Mg$_2$(dobpdc) using *N,N*-dimethyl-ethylenediamine (dmen) as amine loading. Dmen-Mg$_2$(-dobpdc) showed 4.34 mmol g$^{-1}$ CO$_2$ capacity (1 bar, 40 °C) with adsorption heat in the range of − 71–75 kJ mol$^{-1}$ resembling overall features of mmen-Mg$_2$(dobpdc). The modified adsorbent was subjected to 24 sorption cycles (desorption at 75 °C under Ar) where it showed virtually no capacity loss at the end of the cycles, indicating good thermal stability of dmen-Mg$_2$(dobpdc) under the tested conditions. Time-dependent in situ FTIR spectroscopic analyses were also made
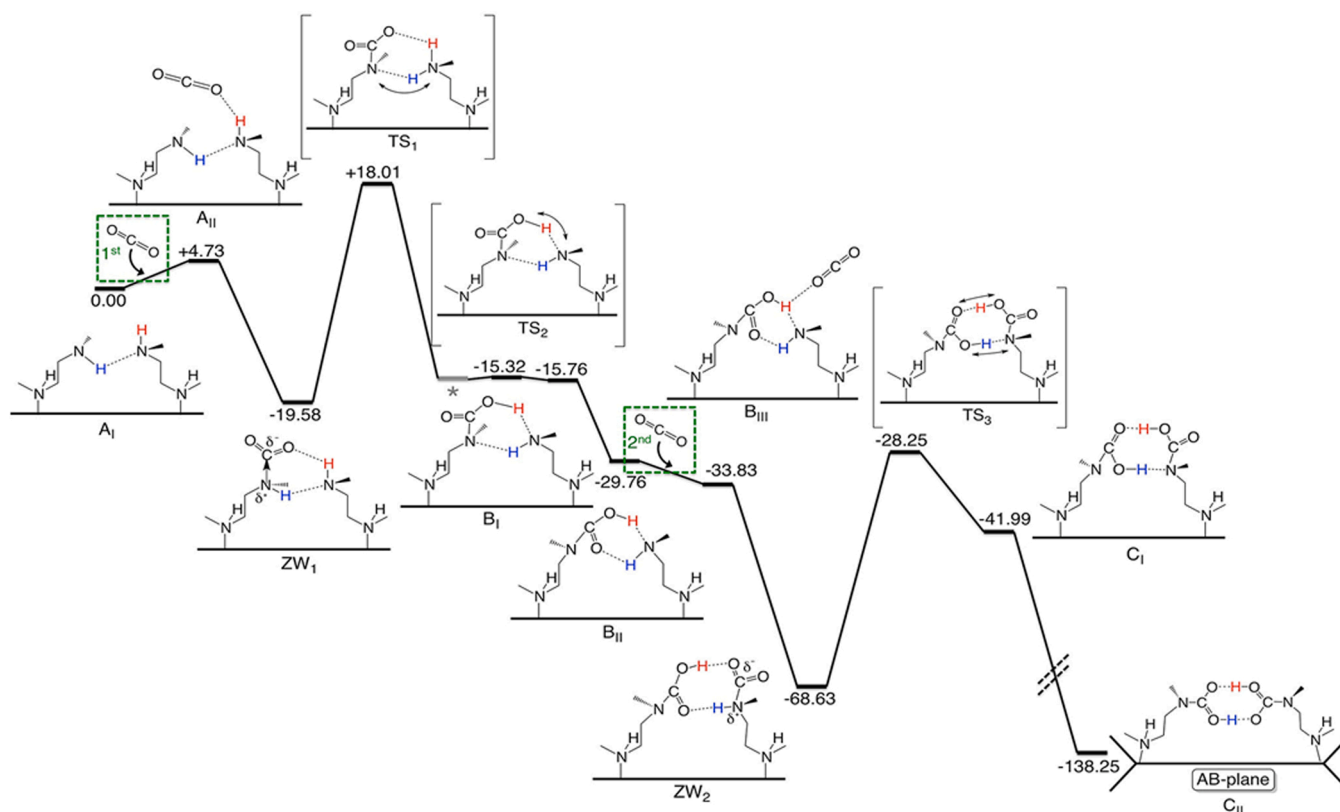
**Fig. 13.** Possible pathway of stepwise $CO_2$ adsorption on mmen-Mg$_2$(dobdc) Adapted from Ref. [233].

under humid conditions using 100 % relative humidity (RH) and 150 mbar $CO_2$ pressure to simulate flue gas conditions. Notably, under humid $CO_2$ conditions, the N − H stretching peak at 3397 cm$^{-1}$ appeared in the FTIR spectrum and it was still visible after purging with $N_2$. However, the characteristic peaks of $CO_2$ disappeared with purging. These observations are well aligned with the dmen-Mg$_2$(dobpdc) examined under similar $CO_2$ adsorption conditions.

In the studies of McDonald et al. [231] and Lee et al. [236] a somewhat modified adsorption mechanism describing cooperative intake of $CO_2$ on mmen- and dmen-loaded Mg$_2$(dobpdc) was suggested. As in earlier models, one end group of a diamine was assumed to be bound with an open metal site, whereas the other terminal amine remained accessible for $CO_2$. With exposure to $CO_2$, the free diamine group adheres to $CO_2$ and the resulting carbamic species are formed with similar fashion as suggested by Planas *et al.*, thus via proton transformation from one amine to the adjacent metal coordinated amine N atom (Fig. 14). Based on the DFT calculations, carbamic acid O atom favors binding with Mg over the N atom of amine, originally bound with Mg center. Thus, as illustrated in Fig. 14, highly ordered chains are

generated upon synchronized breakage of the Mg−N bond followed by the consequent forming of Mg−O bond. To validate the suggested model, thorough structural studies were carried out using isostructural series of mmen-M$_2$(dobpdc) MOFs (M = Co, Ni, Mg, Mn, Fe, and Zn) for which $CO_2$ adsorption isotherms were determined [231]. All the obtained isotherm curves consistently displayed a sharp isothermal step that moved to higher pressure with an increase in temperature, thereby implying a cooperative process wherein $CO_2$ displace M–N bonds upon its chemisorption. The subsequently formed carbamate and adjoining ammonium ion pairs align in the channels, forming ammonium carbamate chains that are periodically bound to the Mg center via oxygen. This arrangement was suggested to cause sudden increases in the adsorption curves. Adsorption mechanisms were further examined by in situ FTIR and solid-state NMR ($^{13}$C and $^{15}$N) to identify the actual chemical species formed during the sorption process. FTIR spectra displayed a broad peak positioned at 2200 cm$^{-1}$ and multiple peaks in the range of 1700 − 1630 cm$^{-1}$ indicating the presence of ammonium cation and C−O stretching of the amide group and asymmetric deformation of the ammonium cation. These peaks, along with the N − H
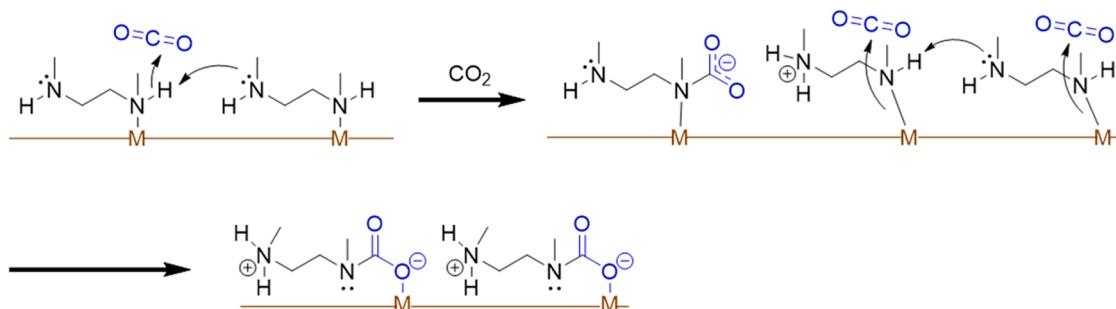


**Fig. 14.** A cooperative insertion mechanism of $CO_2$ on mmen-Mg$_2$(dobpdc).

stretching peak at 3397 cm$^{-1}$ disappeared with the progress of adsorption, implying forming of the carbamate species. NMR experiments suggested interconversion of coordinated and uncoordinated ends of the mmen molecule in mmen-Mg$_2$(dobpdc), which could be detected as $^{15}$N chemical shifts at 31 and 72 ppm along with CO$_2$ adsorption and can be expected to result from ammonium cation and carbamate species, respectively. On the other hand, with a lack of CO$_2$, only a single $^{15}$N resonance peak was found for mmen-Mg$_2$(dobpdc). Next, the X-ray absorption near edge structure (NEXAFS) spectroscopy was used for the elucidation of the CO$_2$ adsorption mechanism. A new peak was found at 402.3 eV corresponding to carbamate nitrogen, thus explaining the insertion of carbamate into the metal−nitrogen bond. The reported work is of profound significance as the combination of spectroscopic and diffractometric measurements, including computational studies, provided deep insight into the chemisorption mechanism, and associated chemisorbed species (carbamate or carbamic acid) formed with CO$_2$ adsorption. Further confirmation of the proposed mechanism was obtained by Drisdell *et al.* as their detailed study, including computational and spectroscopic measurements on the CO$_2$ adsorption on mmen-Mg$_2$(dobpdc) also evidenced the formation of either ammonium carbamate or carbamic acid between CO$_2$, and that the chemisorption with the presence of an amine is clearly favored in contrast to the physisorption adsorption [237].

To investigate adsorption rates and side groups effects on the CO$_2$ desorption mechanism, Jo et al. [238] made a comprehensive study on diamine aminated MOFs compared with number of different types of MOF adsorbents, such as MOF-5, Zn(pyrz)(SiF$_6$), as well as inorganic adsorbents like zeolites and activated carbon. Branched primary diamines of 1-methylethylenediamine (men) and 1,1-dimethylethylenediamine (den) and linear ethylenediamine (en) were loaded to Mg$_2$(dobpdc). The modified materials en-, men- and den-Mg$_2$(dobpdc) exhibited 3.53, 3.6 and 2.15 mmol g$^{-1}$ adsorption capacities under simulated flue gas conditions, respectively. Based on the correlation diagram determined for the working and capture capacities at 30 mbar CO$_2$, both capacities appeared to be dependent on the structural properties of the incorporated diamines. Several samples were tested and categorized into four groups (Fig. 15). Group I included adsorbents with or without OMSs that showed both working and adsorption capacities to be lower as an example for pristine MOF-74 ~1.02 mmol g$^{-1}$ has been presented (4.5 wt.-%, as illustrated in Fig. 15). Group II comprises primary diamines aminated MOFs demonstrating low working capacity but

high adsorption capacity due to the strong chemisorption between the primary amine and CO$_2$. Group III constitutes hetero-diamine-aminated Mg$_2$(dobpdc) showing high working capacity but low adsorption capacity due to the weaker interactions between the CO$_2$ and the mixed amine groups. Group IV includes den-Mg$_2$(dobpdc) exhibiting high ~2, 49 mmol g$^{-1}$ adsorption capacity due to the presence of primary amine groups. The dimethyl groups on the ethylene linker in den-Mg$_2$(dobpdc) were expected to be responsible for the weakening of Mg–carbamate interaction, thus promoting facile desorption and subsequently higher working capacity of ~2.77 mmol g$^{-1}$ was observed. In the reported study, the adsorbent was also subjected to SO$_x$ exposure (500 ppm SO$_2$/N$_2$) for a single sorption cycle with adsorption at 40 °C (150 mbar) and desorption at 130 °C under Ar. As the result of test, CO$_2$ capacity dropped about 6 % under dry, and 13 % in humid conditions. Based on the observed sorption characteristics, den-Mg$_2$(dobpdc) was suggested to be a suitable adsorbent for a fluidized bed system for continuous CO$_2$ capture.

In the study of Lee et al. [239] diamine aminated Mg$_2$(dobpdc) adsorbents were made using ethylenediamine (en), primary-secondary diamines, such as *N*-ethylethylenediamine (een) and *N*-isopropylethylenediamine (ipen), and various combinations of primary-tertiary and secondary-secondary diamines. MOF adsorbents were then subjected to CO$_2$ sorption tests under real flue gas conditions. The study demonstrated how the change in diamine chain length or in the number of alkyl substituents define the desorption properties, such as desorption temperature and the temperature difference between the adsorption and desorption processes ($\Delta T$). The amine bulkiness was shown to play an essential role in elevating robustness of the framework when exposed to realistic flue gas conditions which contain some O$_2$, SO$_2$, and water vapor. Interestingly, DFT calculations revealed two-step adsorption behavior for the ipen-Mg$_2$(dobpdc), which was concluded to be caused by the steric bulkiness of the branched diamines. The presented study clearly emphasized the importance of the proper selection of diamine, as it can have a considerable effect on the durability of the framework and CO$_2$ uptake efficiency. In this context, Kang et al. [240] presented een-Mn$_2$(dobpdc) which exhibited at the time the smallest temperature difference between adsorption and desorption processes ($\Delta T = 30$ °C), low regeneration temperature ($\leq 100$ °C), and high cyclic working capacity of 3.18 mmol g$^{-1}$ over the tested 600 sorption cycles. The overall efficiency of this adsorbent was further improved by coating the MOF particles with polydimethylsiloxane (PDMS) to enhance water
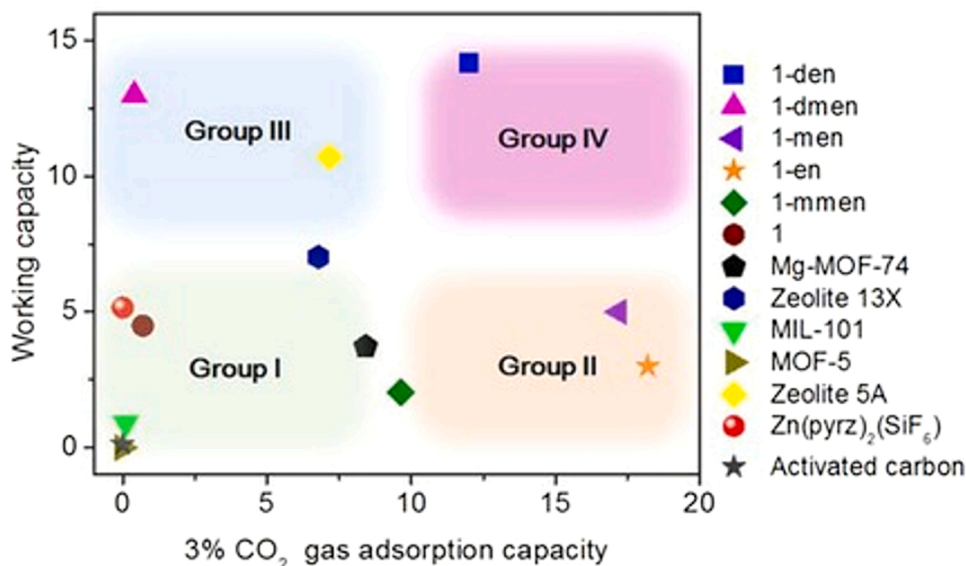


**Fig. 15.** Correlation diagram for working and adsorption capacities (wt.-%) obtained at 30 mbar
Adapted from Ref. [238].

resistance of the adsorbent, and thereby also affecting the adsorption properties of the adsorbent (for coating methods see chapter 2.7).

It has been well-established by now that the cooperative adsorption threshold is governed by two key variables: $CO_2$-inserted sites and the relative stability of an amine bound to the MOF. As a continuation to earlier studies Siegelman et al. [241] investigated the effect of an amine structure on the interaction of the metal−amine bond (M-A), and ammonium carbamate ion-pairing (Fig. 16). Nine diamine aminated $Mg_2$(dobpdc) adsorbents were prepared, including *N*-dimethylethylenediamine (m-2-m), *N,N′*-diethylethylenediamine (e-2-e), *N, N′*-diisopropylethylenediamine (i-2-i), *N*-methylethylenediamine (m-2), *N*-ethylethylenediamine (e-2), *N*-isopropylethylenediamine (i-2), *N, N*-dimethylethylenediamine (mm-2), *N,N*-diethylethylenediamine (ee-2) and *N,N*-diisopropylethylenediamine (ii-2). Products were examined with combination of single crystal X-ray diffraction, spectroscopic and volumetric gas adsorption methods. In the study, it was found that even small changes in the molecular structure of the diamine can affect the threshold pressure of cooperative $CO_2$ adsorption up to four times at a single temperature. For instance, bulky diamine bound to a metal center would cause steric hindrance, which causes instability of the amine-bound adsorption product (e.g., carbamate) and consequently lowers the step pressure. Also, when substituent groups are coupled on the terminal amine side, the step pressure will increase, because of the weakened ion-pairing interactions in ammonium carbamate chains that are formed by $CO_2$ adsorption. It was also observed that hydrogen bonding and ion-pairing interactions would stabilize $CO_2$-inserted phases, and subsequently lower the step pressure for the continuation of cooperative $CO_2$ adsorption. The critical principles outlined by the study can be assisted in forthcoming designs of diamine-appended MOFs to achieve increasingly optimized adsorption properties for $CO_2$ capture.

In the same year, Milner et al. [103] made 3-diaminopropane (pn), 2-methyl-1,3-diaminopropane (mpn) and 2,2-dimethyl-1,3-diaminopropane (dmpn) aminated $Mg_2$(dobpdc) adsorbents and examined their sorption properties including cyclic stability tests. Of the tested adsorbents in flue gas simulated conditions, dmpn-$Mg_2$(dobpdc) showed the best step-shaped adsorption at 40 °C (150 mbar) and almost complete desorption at 100 °C (1 bar) with high 2.42 mmol $g^{-1}$ working capacity. Also, high differential adsorption heat of $-74$ kJ $mol^{-1}$ with narrow $\Delta T = 60$ °C temperature swing window was determined for the dmpn-$Mg_2$(dobpdc). Based on the extensive sorption and regeneration tests made, the dmpn-$Mg_2$(dobpdc) demonstrated substantial long-term stability, as only about 3% decrease in amine load was observed without

significant change in work capacity after 1000 regeneration cycles. Due to the fast kinetics observed for the system, the sorption cycles could be run using 5 min adsorption and 1 min desorption steps. The authors concluded that, particularly the dmpn-$Mg_2$(dobpdc) would be a very promising adsorbent for capturing $CO_2$ from flue gas. In 2019 Choe et al. [242] reported a series of tetraethylenepentamine (TEPA) appended $Mg_2$(dobpdc) adsorbents containing different amine loadings (with 0.2, 2, 20, and 200 equivalents, samples named T02, T2, T20, and T200, respectively). Surprisingly, on higher TEPA loadings (T20 and T200) a significant increase in the $CO_2$ adsorption capacity from 1.47 to 2.36 mmol $g^{-1}$ was observed but with an increase in adsorption temperature accordingly from 40° to 80 °C. At first, the obtained results seemed to be slightly inconsistent with the previously investigated aminated MOF adsorbents. Eventually, it was found that observations related to the temperature-dependent behavior of the long-chained TEPA molecules, which at lower temperatures obstructed diffusion of $CO_2$ into the pores but at higher temperatures with increased flexibility of their alkyl chains this obstacle was overcome. Based on the sorption tests TEPA-$Mg_2$(dobpdc) adsorbs $CO_2$ via similar cooperative insertion mechanisms as have been observed, for instance on mmen-, and dmpn-$Mg_2$(dobpdc), and many other diaminated MOF-74 analogues, because the similar type of sharp increases in $CO_2$ adsorption isotherms were seen.

As a natural continuation of linear and branched diamines are cyclic diamines, which Rebecca et al. [243] used to functionalize $Mg_2$(dobpdc) with 2-(aminomethyl)piperidine (2-ampd) for capturing $CO_2$ in simulated natural gas flue emission stream. The sorption isotherms showed two adsorption steps, and 3.46 mmol $g^{-1}$ $CO_2$ uptake was determined for the adsorbent in 40 mbar $CO_2$ pressure (40 °C). Under humid conditions uptake was further improved, which assumed to be resulted from the hydrogen bonding interactions between water and carbamate chains to form ammonium carbamate species. The sorption tests with 700 cycles under humid conditions at 140 °C for 12 h indicated good stability of the adsorbent as the adsorption capacity remained virtually unchanged. Currently the reported 2-ampd-$Mg_2$(dobpdc) is still one of the best adsorbents among the MOFs developed for the natural gas flue emission technology. Recently, Kim *et al.* [244] demonstrated the $CO_2$ adsorption properties of tetraamine functionalized MOFs utilized in emission conditions corresponding to the combustion of natural gas, wherein the emission of $CO_2$ is only a quarter (~4%, 40 mbar) of the amount released from coal combustion. Again, the ordered, multi-metal coordinated tetramines showed high thermal stability and enabled regeneration of
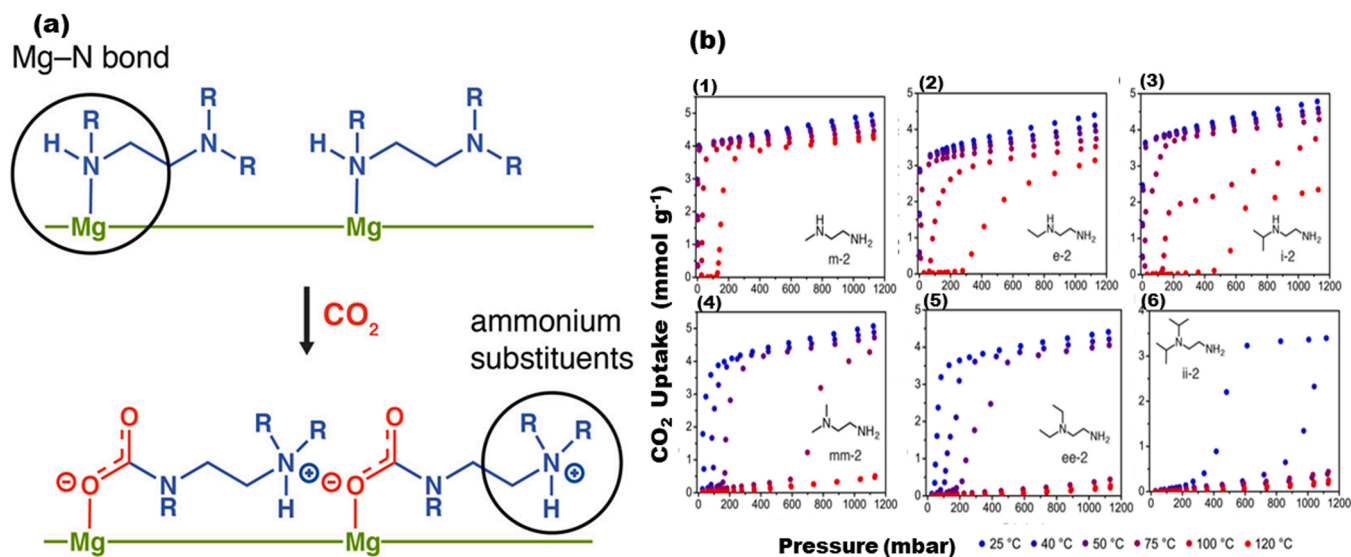


**Fig. 16.** Illustration of cooperative $CO_2$ insertion into Mg(II)-diamine sites to form ammonium carbamate chains. Adapted from Ref. [241].

the adsorbent with inexpensive low-temperature steam. A range of tetraamine appended-$Mg_2$(dobpdc) were synthesized by Kim et al. with varying alkyl chain lengths between the adjacent nitrogen atoms in the chain as follows (Fig. 17): triethylenetetramine (2−2−2), *N,N'*-bis (2aminoethyl)− 1,3-propanediamine (2−3−2), 1,2-bis(3-aminopropylamino)ethane (3−2−3), *N,N'*-bis(3-aminopropyl)− 1,3-diaminopropane (3−3−3), *N,N'*-bis(3-aminopropyl)− 1,4-diaminobutane (3−4−3), diethylenetriamine (3−3), and *N*-(3-aminopropyl)− 1,4-diaminobutane (3−4). So far among the various tetramine modified $M_2$(dobpdc) adsorbents, the 3−4−3-tetraamine appended $Mg_2$(dobpdc) holds the highest $CO_2$ adsorption enthalpy of − 99 kJ $mol^{-1}$ with a two-step shaped adsorption curve, breakthrough capacity of 2 mmol $g^{-1}$ under humid conditions, while also meeting the U.S. Department of Energy (DOE) ambitious target for capturing 90% of $CO_2$ from natural gas flue emissions. Based on spectroscopic analyses, the step-shaped adsorption curve was again caused by the cooperative insertion mechanism originating from the formation of chained ammonium carbamate species. The determined working capacity remains unchanged under humid conditions with over 1000 sorption cycles indicating strong selectivity for $CO_2$ over water vapor. With the above-described characteristics, the reported 3−4−3-tetraamine appended MOF could potentially be a promising candidate for direct air capture of $CO_2$ as well.

In 2020, Mao et al. [245] designed alkanolamine and alkoxyalkylamine functionalized $Mg_2$(dobdpc) variants, for which extensive computational and structural studies were combined to evaluate five different possible mechanisms for cooperative $CO_2$ adsorption. Tested alcoholamines included bulky secondary amine groups, such as ethyl (e-2-OH), n-propyl (nPr-2-OH), isopropyl (iPr-2-OH), n-butyl (nBu-2-OH), cyclohexyl (cy-2-OH), isopentyl (iPent-2-OH), and 3-aminopropanol (3-OH) as shown in Fig. 17d. Altogether, with solid-state NMR ($^{13}$C and $^{15}$N) and gas-adsorption studies, they presented the most likely mechanism, wherein subsequently to $CO_2$ adsorption, the hydrogen bonds of the methoxy groups across the *ab* lattice plane further stabilize the formed ammonium carbamate ion-pairs, and as a result continuous cooperative adsorption propagates along the crystallographic *c*-axis. Park et al. functionalized $Mg_2$(dobpdc) with *N*-methyl-1, 3-diaminopropane (Nmpn), 1,3-diaminopentane (epn), 1,

3-diaminopropane (pn), 2,2-dimethyl-1,3-diaminopropane (dmpn) and *N,N*-dimethyl-1,3-diaminopropane (Ndmpn) and tested their adsorption properties in dilute $CO_2$ concentration (1 mbar) with comparison to many other adsorbent materials (Fig. 18) [246]. The study focused mainly on lowering the regeneration temperature, as for practical real-world applications high desorption temperature is undesirable as it effects adversely to the chemical and structural stability of the adsorbent, and consumes more energy. Interestingly, regeneration of epn-$Mg_2$(dobpdc) at moderate 70 °C still demonstrated notable 2.88 mmolg$^{-1}$ adsorption in 1 mbar $CO_2$ pressure. However, when the similar sorption cycles were made under humid conditions, a significant decrease in the recovery capacity was observed. Authors, attempted to solve the problem by coating the adsorbent particles with a hydrophobic agent polydimethylsiloxane (PDMS) and indeed, with the help of the hydrophobic coating, $CO_2$ uptake decreased only slightly from that of observed in dry conditions, thus being ~2.77 mmol $g^{-1}$ (for coating methods see chapter 2.7).

As discussed above, for designing new cooperative $CO_2$ adsorption MOFs for carbon capture it is essential to unravel the interrelationship between the $CO_2$ insertion mechanism and the chain length of diamine. To this end, Hong et al. [247] made further efforts to clarify $CO_2$ adsorption mechanisms by functionalizing $Mg_2$(dobpdc) with primary diamines with varying chain lengths of ethylene- (1-en), propylene- (1-pn), butylene- (1-bn), pentamethylene- (1-pen), hexamethylene- (1-hn), and octamethylene- (on) diamine (Fig. 19). Intriguingly $CO_2$ isotherms, with the support of FTIR spectroscopy and computational chemistry, evidenced that the $CO_2$ insertion mechanism is dominant up to the alkyl chain length of four carbons, while the mechanism was not found to occur with longer alkyl chains. With the van der Waals corrected density functional theory (DFT) it was further evidenced that the $CO_2$ insertion process was proved to be dependent on the relative location of diamines across the hexagonal pore structure as based on the calculated models the longer chained 1-pen, 1-hn, and 1-on diamines seem to follow non-cooperative adsorption mechanism. This was particularly clear with the 1-hn and 1-on diamines, as they coordinate across the pore to two distinct $Mg^{2+}$ sites, and thus cannot participate in chemisorption. Surprisingly, bn-$Mg_2$(dobpdc) displayed three distinct
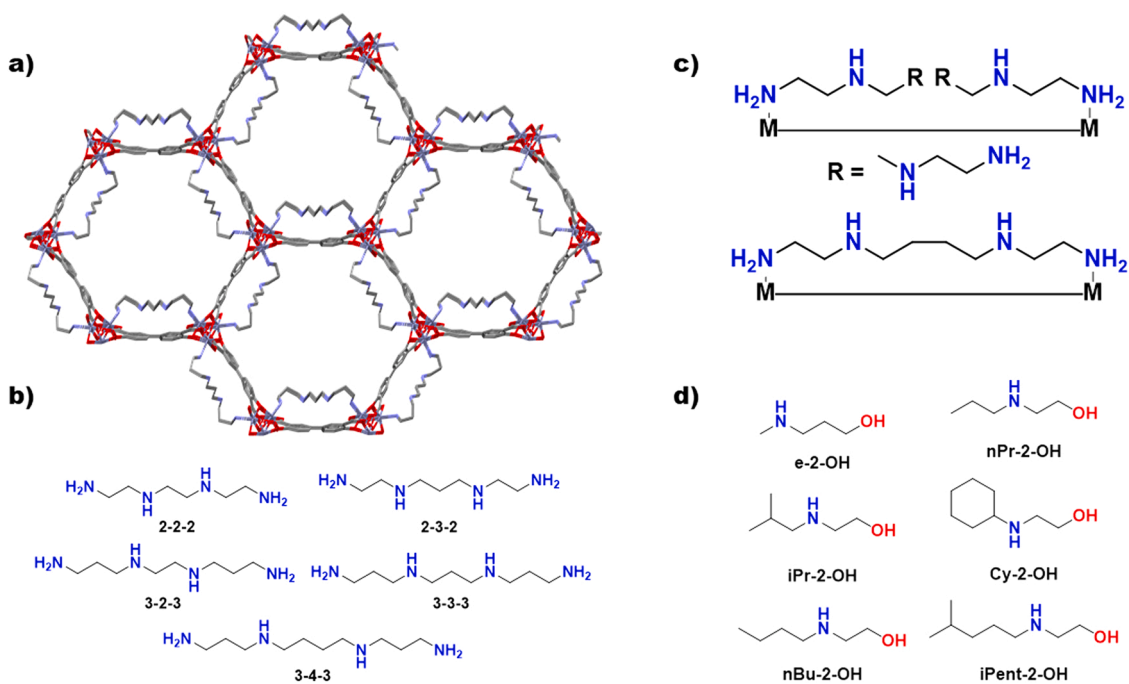


**Fig. 17.** (a) Illustration of pore structure of amine appended $Mg_2$(dobpdc) (CSD entry: FUYGUE), (b) different tetraamines appended to $Mg_2$(dobpdc), (c) structural modeling of 2−3−2 appended and 3−4−3-appended metal sites, and (d) selection of alkanolamines used to functionalize the open metal sites of $Mg_2$(dobpdc) [110, 244,245].
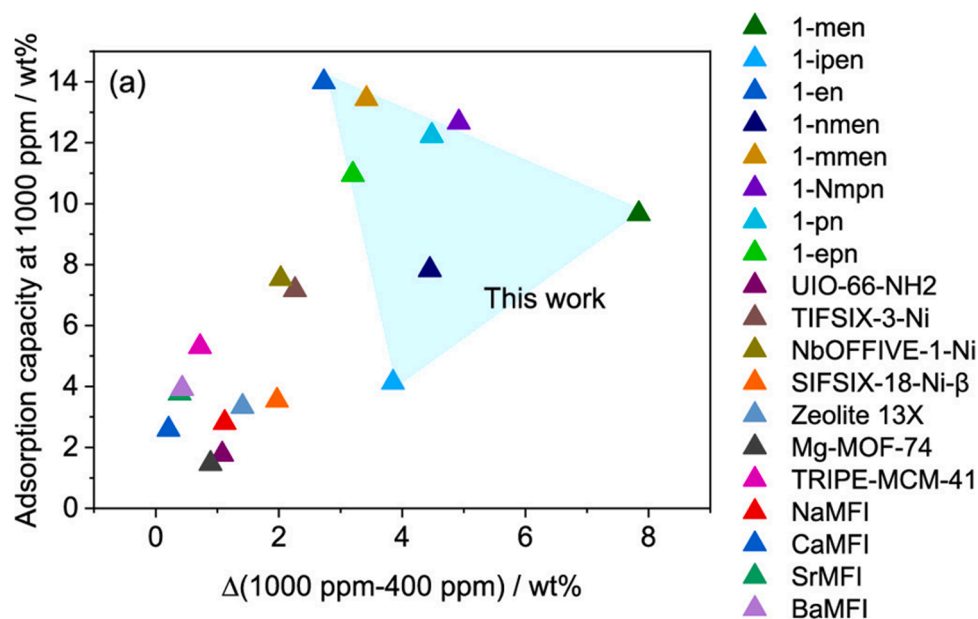
**Fig. 18.** Comparison diagram of the adsorption capacities at 1 mbar (1000 ppm) $CO_2$ for selected MOF adsorbents. Adapted from Ref. [246].
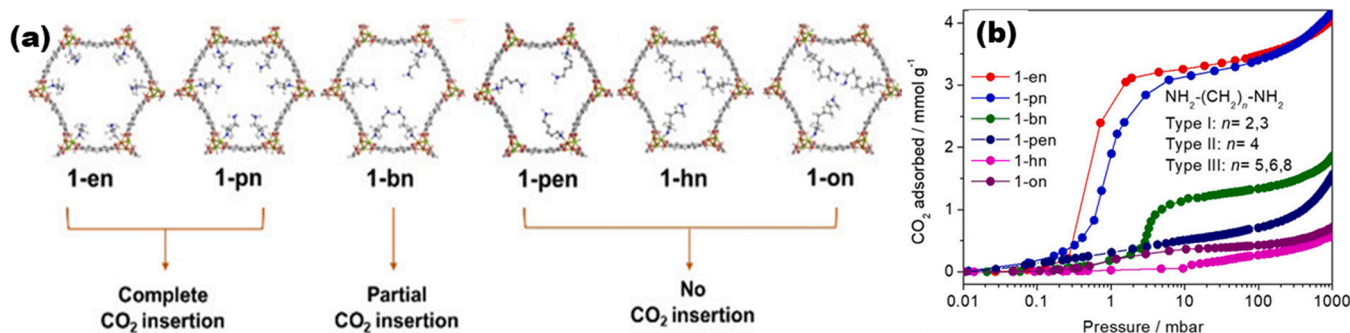


**Fig. 19.** *n*-alkyl diamine functionalized $Mg_2$(dobpdc) series (a) $CO_2$ adsorption mechanism, and (b) $CO_2$ sorption isotherm measured at 40 °C. Adapted from Ref. [247].

chemical environments for the carbamate species, which are attributed to the varied relative conformations of carbon chains upon $CO_2$ addition. With this study, new essential chemical insights were acquired for the interrelationship between the $CO_2$ insertion mechanism and diamine chain length that can further be utilized by the researchers for developing new more efficient amine appended MOF adsorbents for carbon capture.

*2.5.3. Post-synthetically aminated MOFs in MIL-family*

Although aminated $M_2$(dobpdc), as well as other MOF-74 analogs have been the subject of intensive research, many other MOF adsorbents with large pore structures have been reported and can also be post-synthetically modified. For instance, MIL-100(Cr) is known for its high thermal stability, large pore size, and has been incorporated with different amines, such as ethylenediamine (en) and *N,N'*-dimethylethylenediamine (mmen). En-MIL-100(Cr) has demonstrated adsorption capacity of 2.4 mmol $g^{-1}$ (30 °C, 1 bar $CO_2$) and adsorption heat of about − 80 kJ $mol^{-1}$ indicating favoring of a chemisorption mechanism in contrast to the pristine MIL-100(Cr) having 1.6 mmol $g^{-1}$ and − 63 kJ $mol^{-1}$ values for capacity and adsorption heat, suggesting physisorption mechanism even though it shows relatively high adsorption heat, no chemisorption capable functional groups exist in the original framework. In the literature, $CO_2$ capturing efficiency for

ethylenediamine aminated frameworks have been shown to be somewhat higher than on mmen-MIL-100(Cr) having ~1.7 mmol $g^{-1}$ $CO_2$ uptakes reported under the same adsorption conditions [248].

Due to very large pore structure of MIL-101, besides discrete amines used with the MOF-74 family, also polymeric amines can be used. Polyethyleneimines (PEIs; both low and high molecular weight) are the most widely used of them, due to e.g., for their reasonably high thermal stability. Lin et al. [249] showed in their study that porosity and physical size of the MIL-101(Cr) particles as well as molecular weight and the structural properties of the loaded polyamines, all are important variables to be optimized to afford better $CO_2$ capturing properties for such hybrid materials. In terms of particle size, it was observed that small particle-sized samples enhanced the impregnation of PEI into the inner pores of the adsorbent but at the same time brought down the surface area/pore volumes, and consequently the adsorption capacity decreased. Also, the low molecular-weight PEI diffused more easily into the inner pores compared to the high-weight PEI, which was not fully loaded in, as it more preferably settled on the surface of MOF particles. The highest adsorption capacity of 3.6 mmol $g^{-1}$ was obtained for PEI-300-MIL-101(Cr) with ultrahigh $CO_2/N_2$ selectivity at 150 mbar $CO_2$ pressure (25 °C). In terms of thermal properties, similar thermal stabilities were observed regardless of considerably different MWs as MIL-101(Cr) was impregnated both with linear (MW = 300 Da) and

branched PEI (MW = 1800 and 10,000 Da). Of the above, the linear PEI displayed better regenerability, albeit after 50 sorption cycles the $CO_2$ uptakes were already decreased about 20%. Similarly to PEI- impregnated MIL-101(Cr), Jiang et al. [250] investigated incorporation of PEI into the pores of light-responsive azobenzene-decorated MOF (azoMOF). They used a wet-impregnation technique with various PEI loadings (e.g., 0.39, 0.66, 0.98 and 1.28 mmol $g^{-1}$), of which the best adsorption capacity was afforded by 0.98 mmol $g^{-1}$ loading of PEI ($P_3$/azoMOF). The specific surface determined for the modified azoMOF proved to be significantly lower (324 $m^2$ $g^{-1}$) than on pristine azoMOF (1275 $m^2$ $g^{-1}$) but nonetheless, $P_3$/azoMOF demonstrated ~2.9 mmol $g^{-1}$ (25 °C, 1 bar $CO_2$) adsorption capacity. The higher adsorption heat (−64 kJ $mol^{-1}$) of polyaminated adsorbent referred to chemisorption mechanism, whereas the pristine azoMOF with lower adsorption heat and the capturing capacity (~1.5 mmol $g^{-1}$) indicated favoring the physisorption. With UV–vis spectroscopy, the effects of light-response on adsorption properties were examined with $P_3$/azoMOF. In the case of *cis*-isomer the capacity and adsorption heat were about 33% and 26% lower (2.2 mmol $g^{-1}$ and −47.5 kJ $mol^{-1}$, respectively) than that of found for *trans*-configuration. This suggests *cis*-$P_3$/azoMOF structure modification to have considerably lower adsorbate−adsorbent interactions than in *trans*-isomer. For *trans*-isomer, DFT calculations revealed surface potentials around amine to be − 0.048 eV indicating negligible interaction between *trans*-azobenzene and amine. On the contrary, *cis*-isomer showed a significant interaction between *cis*-azobenzene and amine (−0.025 eV) and with higher interaction, the adsorption sites were more shielded resulting in lower $CO_2$ capacity of *cis*-isomer. The strategy outlined by the study can be utilized in forthcoming designs of new light-responsive MOFs to achieve increasingly controllable $CO_2$ adsorption separation.

Besides polymeric PEI, various smaller polyamines, such as tris(2-aminoethyl)amine (TAEA), triethylenediamine (TEDA), *p*-phenylenediamine (PPD), tetraethylenepentamine (TEPA) have been appended to the MIL-101 framework. Although in many studies the above amines have been shown to be inferior in thermal stability to polymeric amines like PEI. Darunte et al. [26] examined adsorption properties of tris-(2-aminoethyl) (tren) and branched low molecular weight polyethyleneimine (PEI- 800) loaded to MIL-101(Cr) under DAC conditions. At first modest 0.35 mmol $g^{-1}$ capacity was observed at a 0.4 mbar $CO_2$ pressure for tren-MIL-101(Cr). With an increase in the amine loading by wet impregnation, the $CO_2$ capacity was increased to 2.8 mmol $g^{-1}$. Unfortunately, due to the high volatility of low boiling tren-amine, adsorbent demonstrated some 13 % uptake loss already after three cycles, whereas only 4 % amine loss occurred on PEI-MIL-101(Cr) in the same conditions. To further examine the optimal amine content on MIL-101, a range of different PEI loadings from 0.18 to 1.8 mmol $g^{-1}$ were tested. The results unfolded that capture efficiency was found to be directly dependent on amine content until the step-like increase was observed with the amine loads higher than 0.8 mmol $g^{-1}$. Kyu et al. [251] incorporated polymethacrylamide (PM) into MIL-101 (PM@MOF) via double solvent method and free $NH_2$ groups were further post-synthetically introduced to the material to obtain R-PM@MIL-101. Based on the higher adsorption heat (−50 kJ $mol^{-1}$) the modified material exhibited chemisorptive $CO_2$ uptake on its amino sites both at low and atmospheric pressures (150 and 1 bar $CO_2$) with 3.6 and 1.4 mmol $g^{-1}$ capacities, respectively. Further studies on polymeric amine loads were carried out by Sokhrab et al. [252] as they examined intra-channel polymerization of aniline on MIL-101(Cr) to obtain PANI@MIL-101(Cr) hybrid material. With XPS, amine (–NH–), protonated amine (–$NH_2^+$–), imine (=N–) and protonated imine (=$NH^+$–) signals at 399.2, 400.2, 397.9 and 400.6 eV, respectively were observed. The calculated amine\imine ratio of 2.35 indicated the presence of partially protonated PANI which originates from the intermediate oxidation states between the proto-emeraldine and emeraldine species. The modified material demonstrated $CO_2$ adsorption capacities of 2.26 and 1.62 mmol $g^{-1}$ at 0 and 20 °C (1.2 bar $CO_2$), respectively. Moreover,

high $CO_2$/$N_2$ selectivity was observed at 0 °C. Shin et al. [253] incorporated polyvinylamine (PVAm) to MIL-101 (PVAm@MIL-101) via the "ship in a bottle" method. Among the various PVAm loadings tested, the PVAm (0.7)@MIL-101 with the 70% volume filled of full volume by the N-vinylformamide, showed high $CO_2$ uptake of 1.5 and 3.3 mmol $g^{-1}$ at 150 mbar and 1 bar $CO_2$ (25 °C), respectively. With N-vinylformamide load, the $CO_2$/$N_2$ selectivity of the adsorbent increased approximately 11-fold compared to the unmodified adsorbent.

Babaei et al. [254] conducted a comparative study with amine-impregnated MIL-100 and MIL-101 using *p*-phenylenediamine (PPD). For the aminated MOFs, the adsorption capacity of MIL-101 was found to be somewhat higher than on MIL-100 with 1.7 vs. 1.3 mmol $g^{-1}$ at 1 bar $CO_2$, respectively, as expected due to the higher surface area and pore volume of MIL-101. Zhong et al. [255] surveyed a double-solvent incorporation technique in which the amines are promptly "squeezed" into the MOF pores without collapsing the framework. With the presented technique, MIL-101(Cr) was functionalized using tris (2-aminoethyl)-amine (TAEA), ethylenediamine (en) and triethylenediamine (TEDA). Interestingly, the $CO_2$ uptake of TAEA-MIL-101(Cr) was observed to be 1.5 times higher than for pristine MIL-101(Cr) with uptakes of 5.05 and 3.26 mmol $g^{-1}$, respectively (at 1 bar $CO_2$, 0 °C). For these aminated adsorbents, the adsorption heats varied from exceptionally high − 118.7 kJ $mol^{-1}$ to − 49.2 kJ $mol^{-1}$ of which the lower values indicate physisorption instead of chemisorption as with unmodified MIL-101(Cr) showing − 22.4 kJ $mol^{-1}$ adsorption heat.

Li et al. took a different approach for amine appending as they aminated MIL-101(Cr) with tris(2-aminoethyl)amine (TAEA) in cyclohexane [256]. The idea behind this concept is that the low polarity solvent will have weaker interaction with the alkylamine than a high polarity solvent. Consequently, the better chemical potential of the dispersed alkylamine molecules will transfer more alkylamine molecules from the solution into the framework (Fig. 20). The prepared TAEA-MIL-101(Cr) exhibited high 4.21 mmol $g^{-1}$ $CO_2$ uptake at 150 mbar and 25 °C. Regeneration tests with five cycles, under 15:85 $CO_2$/He mixture during adsorption (40 °C), and pure He on desorption (90 °C) revealed no appreciable decrease in $CO_2$ capacity indicating good stability of the adsorbent. The yet different approach was introduced by Li et al., wherein MIL-101(Cr)-$SO_3H$ was loaded with tris (2-aminoethyl)amine (TAEA) via Brønsted acid-base reaction between sulphonic acid and amine groups. $CO_2$ uptakes for the prepared adsorbents varied from 1.12 to 2.28 mmol $g^{-1}$ at 0.4 and 150 mbar (25 °C). In the same study, experimental conditions for adding the amines to the frameworks were also optimized from a thermodynamic point of view. It was concluded that the most practical procedures included a reaction time of about 5 min at room temperature. Authors suggested that with given simple synthetic techniques and economical starting materials, this adsorbent may hold great potential for its large-scale production in the future [257].

Recently, Vo et al. reported amine appended $NH_2$-MIL-101(Cr) which was further aminated by the incorporation of ethylenediamine (en) into the pores, because of which the recovery capacity of the adsorbent increased by 62% (3.4 vs. 2.10 mmol $g^{-1}$) compared to that observed for $NH_2$-MIL-101(Cr)-$NH_2$ having only amino groups substituted on its linker ligands [258]. Furthermore, Li et al. [259] fine-tuned the hydrophobicity of MIL-101(Cr) by varying the alkyl chain lengths of the primary amines (*n*-propylamine, *n*-hexylamine, and 1-dodecylamine), as shown in Fig. 21. With the longer alkyl chained amines, the initially hydrophilic MIL-101(Cr) was converted into a more hydrophobic one. Of the ones tested, dodecylamine-MIL-101 exhibited the highest hydrophobicity by showing an exponential increase in the contact angle measurements.

Likewise, other MOFs and their aminated variants, such as CuBTTri, HKUST-1, MIL-101(e.g., Fe, Mg), UiO-66, UiO-66-$NH_2$, and MOF-177 [260–267] have been examined for carbon capture but are not reviewed in detail in this review. Selected $CO_2$ capture capacities for all the adsorbents presented above, are shown in Table 3.
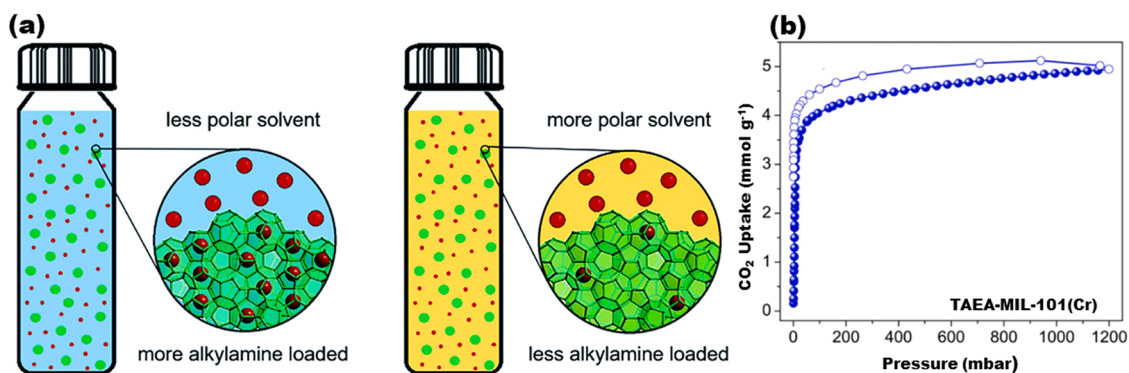
**Fig. 20.** (a) Illustration of the different alkylamine loading amounts in MOF, and (b) $CO_2$ sorption isotherm for TAEA-MIL-101(Cr) measured at 25 °C. Adapted from Ref. [256].
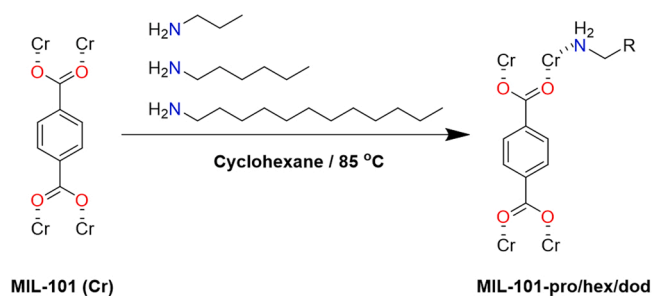


**Fig. 21.** Illustration of the different alkylamine loading amounts in MIL-101(Cr).

There are also other strategies to design MOFs for carbon capture than using the above exemplified methods. For example, in the recent work of Bien et al. [104] nucleophilic metal-hydroxide (M−OH) functional groups were appended to the MOF. The nucleophilic Zn−OH sites in CFA-1 displayed remarkable performance under DAC conditions with an adsorption capacity of 2.20 mmol g$^{-1}$ and adsorption heat of − 71 kJ mol$^{-1}$ indicating $CO_2$ chemisorption mechanism, wherein Zn−OH converts to Zn−$O_2$COH with aid of inter-cluster hydrogen-bonding interactions that were confirmed by DRIFTS experiments and DFT calculations. The adsorbent was subjected to column breakthrough experiments for both dry and 100% relative humidity at 0.4 mbar $CO_2$. Notably, under dry conditions, $CO_2$ capacity of 2.7–3.2 mmol g$^{-1}$ was observed in three consecutive cycles but in humid conditions adsorption did not seem to occur at all, limiting the use of sorbent considerably. Furthermore, Bien et al. [268] presented a series of heterobimetallic Co, Ni, or Cu analogues of CFA-1. The Cu-exchanged MOF analogue experienced degradation with PSM while the Ni-OH analogue exceeded the parent Zn-MOF by displaying greater capacity of 2.7 mmol g$^{-1}$ (0.4 mbar) and high adsorption heat of − 84 kJ mol$^{-1}$. Again, based on DRIFTS experiments, and DFT calculations the Ni−$O_2$COH species did not seem to participate in the inter-cluster hydrogen bonding, unlike in the parent Zn–OH system. Both Zn−OH and Ni−OH variants were subjected to column breakthrough experiments using again both dry and humid conditions (0.25 mbar $CO_2$, 8–13 % relative humidity) resulting in unchanged capacity for Zn−OH in dry conditions, whereas the capacity of Ni−OH variant decreased slightly. However, under humid conditions and after consecutive cycling experiments Ni−OH system appeared to be the more stable one. Overall, it was suggested that MOFs comprising nucleophilic M−OH groups could hold great potential for $CO_2$ capture at low pressures, while some challenges associated with somewhat poor water compatibility and stability of the M-OH-based adsorbents still need to be overcome.

### 2.6. Confinement of water within MOFs pores

As discussed earlier, water molecules inside the pore structure of MOF can have adverse effects on the desired adsorption process but its presence can also have beneficial effects on $CO_2$ adsorption. In this chapter, we briefly highlight some studies that we believe are benchmarks for describing methods wherein by pre-confining solvents in the cavities of the MOFs will enhance the adsorption of $CO_2$. In 2012, Soubeyrand-Lenoir et al. [269] presented a detailed study for improving carbon capturing properties of UiO-66(Zr), MIL100 (Fe), and HKUST-1, by pre-adsorbing water into the pore structure. Under varied relative humidity (3, 10, 20, 40 %), water vapor had no relevant positive effects on $CO_2$ uptake in case of UiO-66. While MIL-100(Fe) demonstrated more promising results in comparison to dry conditions, as significant 3- and 5-fold $CO_2$ uptake increments were observed at 20 % and 40 % RH conditions, respectively. This was attributed to the fact that pre-adsorbed water in the mesoporous MIL-100(Fe) forms microporous pockets that will be filled with $CO_2$ molecules at lower pressures. On HKUST-1, low water content showed an increase in $CO_2$ uptake but conversely, at higher humidity, the adsorption capacity decreased most likely due to the gradual deterioration of the framework via hydrolysis and saturation of OMSsS by water.

The promoting effect of water on $CO_2$ uptake is evidenced also in more water-stable MOFs that were decorated with bridging hydroxo groups ($\mu_2$-OH), like in case of NOTT-400 ([$Sc_2(OH)_2$(BPTC)] made of biphenyl-3,3′,5,5′-tetracarboxylic acid ($H_4$BPTC) [270], NOTT-401 ([Sc (OH)(TDA)] made of 2,5-thiophenedicarboxylic acid ($H_2$TDC) [271, 272], InOF-1 [$In_2(OH)_2$(BPTC)] [273], MIL-53(Al) ([Al(OH)(BDC)] [274,275], Mg-CUK-1 [$Mg_3(OH)_2$(2,4-PDC)$_2$] made of 2,4-pyridinecarboxylic acid (2,4-$H_2$PCD) [276], CAU-10 [$AlO_4(OH)_2$BDC] [277], and PCN-250 made of 3,3′,5,5′-azobenzenetetracarboxylic acid ($H_4$ABTC) [278], to mention few. Overall, MOF dependently $CO_2$ capacity could initially rise, depending on the MOF, substantially in the presence of water but only up to a certain level before it is eventually reduced back to zero. For instance, in the case of the NOT-400 [270], sorption at 20 % RH resulted to a 2.5-fold increase in $CO_2$ uptake but at higher humidity (35 % and 60 %) uptake was no longer observed at all, which could indicate blocking of the pores by water molecules. In a similar fashion with NOTT-401 [272], higher $CO_2$ uptake was achieved reaching 3.2-fold at 5 %, 1.6-fold at 10 % and reducing virtually to zero adsorption at higher than 30 % humidity. Likewise, for indium-containing InOF-1 MOF [273], its capacity doubled at 20 % but above 40 % humidity capture capacity decreased, suggesting again pore blocking by water molecules. Similar trend was observed with CAU-10 [277], Mg-CUK-1 [276], and MIL-53(Al)-TDC containing [$Al_2(\mu_2$-OH)] units [274,275,279]. It was concluded that $\mu_2$-OH interacts with water molecules via strong hydrogen bonds thereby inducing so-called confinement effect [280,281] that causes reduction of the micropores,

**Table 3**

Summary of $CO_2$ adsorption for post-synthetically modified MOFs.

| MOF | Capacity (mmol g$^{-1}$) | | | -Q$_{st}$ (kJ mol$^{-1}$) | Temp. (°C) | Ref. |
|---|---|---|---|---|---|---|
| | 0.39 (mbar) | 150 (mbar) | 1 (bar) | | | |
| en-Mg$_2$(dobdc) | 1.51 | | | | 25 | [227] |
| Mg$_2$(dobdc)(N$_2$H$_4$)$_{1.8}$ | 3.89 | 5.18 | 5.51 | 90 | 25 | [229] |
| tepa-Mg$_2$(dobpc) | | 6.06\8.31$^H$ | | | 25 | [232] |
| en-Mg$_2$(dondc) | | 1.99 | 2.63 | 7–50 | 25 | [123] |
| ppz-Mg$_2$(dondc) | | 2.04 | 3.15 | 20–47 | 25 | [123] |
| mmen-Mg$_2$(dondc) | | 3.20 | 4.13 | 13–83 | 25 | [123] |
| mmen-Mg$_2$(dobpdc) | 2.0 | 3.13 | 3.86 | 71 | 25 | [101] |
| en-Mg$_2$(dobpdc) | 2.83 | 3.62 | 4.57 | 49–51 | 25 | [235] |
| dmen-Mg$_2$(dobpdc) | | 3.77$^a$ | 4.34$^a$ | 71–75 | 40 | [236] |
| men-Mg$_2$(dobpdc) | ~0.41\2.19$^{**}$ | 3.6$^a$ | 4.5 | 65–77 | 25 | [238,246] |
| den-Mg$_2$(dobpdc) | | 2.15$^a$ | 3.15 | 65–77 | 25 | [238] |
| ipen-Mg$_2$(dobpdc) | ~0.06\0.93$^{**}$ | 3.47$^a$ | 4.05$^a$ | 76–85 | 40 | [239,246] |
| een-Mg$_2$(dobpdc) | | 4.04$^a$ | 5.05$^a$ | 70–74 | 40 | [239] |
| nmen-Mg$_2$(dobpdc) | ~0.76\1.77$^{**}$ | 2.92$^a$ | 3.99$^a$ | 60–72 | 40 | [239,246] |
| pn-Mg$_2$(dobpdc) | ~1.76\2.77$^{**}$ | 4.01$^a$ | 4.49$^a$ | | 40 | [103,246] |
| mpn-Mg$_2$(dobpdc) | | 3.82$^a$ | 4.14$^a$ | | 40 | [103] |
| dmpn-Mg$_2$(dobpdc) | | 2.91$^a$ | 3.73$^a$ | | 40 | [103] |
| T02-Mg$_2$(dobpdc) | | 2.17$^a$ | | 31–39 | 40 | [242] |
| T2-Mg$_2$(dobpdc) | | 2.53$^a$ | | 77–109 | 40 | [242] |
| T20-Mg$_2$(dobpdc) | | 1.43$^a$ | | 77–109 | 40 | [242] |
| T200-Mg$_2$(dobpdc) | | 1.46$^a$ | | 77–109 | 40 | [242] |
| 2-ampd-Mg$_2$(dobpdc) | 3.47$^{a,*}$ | | | 73 | 40 | [243] |
| Mg$_2$(dobpdc)(3–4–3) | ~3.40$^{d,*}$ | | | 99 | 90 | [244] |
| e-2-OH-Mg$_2$(dobpdc) | | ~2.10$^b$ | | 81 | 50 | [245] |
| nPr-2-OH-Mg$_2$(dobpdc) | | ~1.90$^b$ | | | 50 | [245] |
| iPr-2-OH-Mg$_2$(dobpdc) | | ~1.75$^b$ | | | 50 | [245] |
| cy-2-OH-Mg$_2$(dobpdc) | | ~1.50$^b$ | | | 50 | [245] |
| nBu-2-OH-Mg$_2$(dobpdc) | | ~1.70$^c$ | | | 75 | [245] |
| iPent-2-OH-Mg$_2$(dobpdc) | | ~1.40$^c$ | | | 75 | [245] |
| epn-Mg$_2$(dobpdc) | ~1.76\2.88$^{**}$ | | | | 25 | [246] |
| | | | | | | |
| *Table 3*. Continued. | | | | | | |
| Nmpn-Mg$_2$(dobpdc) | ~1.76\2.50$^{**}$ | | | | 25 | [246] |
| 1-pn- Mg$_2$(dobpdc) | | | 4.19$^a$ | | 40 | [247] |
| 1-bn- Mg$_2$(dobpdc) | | | 1.87$^a$ | 46–62 | 40 | [247] |
| 1-pen- Mg$_2$(dobpdc) | | | 1.57$^a$ | | 40 | [247] |
| 1-hn- Mg$_2$(dobpdc) | | | 0.57$^a$ | | 40 | [247] |
| 1-on- Mg$_2$(dobpdc) | | | 0.72$^a$ | | 40 | [247] |
| en-MIL-100(Cr) | | | 2.4 | 80 | 25 | [248] |
| mmen-MIL-100(Cr) | | | 1.7 | 80 | 25 | [248] |
| MIL-101(Cr)-TREN | 0.35 | | | | 25 | [26] |
| MIL-101(Cr)-PEI-300 | | 4.1 | | | 25 | [249] |
| P$_3$/azoMOF | | | ~2.9 | 64 | 25 | [250] |
| R-PM24 @MOF | | 1.4 | 3.6 | 50 | 25 | [251] |
| PANI@MIL-101(Cr) | | | 1.62 * *** | 26 | 20 | [252] |
| PVAm (0.7)@MIL-101 | | 1.5 | 3.3 | 49 | 25 | [253] |
| Cr-MIL-101-SO$_3$H-TAEA | 1.12 | 2.28$^a$ | | 87 | 25 | [257] |
| CuBTTri-mmen | | 2.38 | | 96 | 25 | [260] |
| tepa-NH$_2$-MIL-101 | | | 3.1 | | 25 | [262] |
| MIL-100-PPD | | | 1.3 | | 25 | [254] |
| MIL-101-PPD | | | 1.7 | | 25 | [254] |
| ed-MIL-101(Cr) | | | 1.93 | | 25 | [255] |
| TAEA-MIL-101(Cr) | | | 2.19 | | 25 | [255] |
| TEDA-MIL-101(Cr) | | | 1.65 | | 25 | [255] |
| DETA-MIL-101(Fe) | | | 1.82 | 74.2 | 25 | [263] |
| PEI-MIL101 (Cr, Mg) | | | 3.04 | | 25 | [264] |
| ed-MIL-101(Cr)-NH$_2$ | | | 3.4 | | 25 | [258] |
| PEI-UiO-66 | | | 3.3 | | 25 | [265] |
| PEI-UiO-66-NH$_2$ | | 2.3 | 3.1 | 68 | 25 | [266] |
| ed-HKUST | | | 2.4 | | 25 | [261] |
| DETA-MOF-177 | | | 2.83 | | 25 | [267] |
| TEPA-MOF-177 | | | 3.82 | | 25 | [267] |
| PEI-MOF-177 | | | 2.84 | | 25 | [267] |
| CFA-1(Zn-OH) | 2.2 | | | 71 | 25 | [104] |
| CFA-1(Ni-OH) | 2.7 | | | 84 | 25 | [268] |

$^a$ at 40, $^b$ 50, $^c$ 75, $^d$ and at 90 °C, $^H$ humid condition, * at 40 mbar, ** at 1 mbar, *** at 1.2 bar.

which further allow the better packing of $CO_2$ molecules [282,283]. Thus, in the microporous MOF that contains hydroxo (μ$_2$-OH) functional groups, it is advantageous to pre-adsorb small amounts of water, as their presence in the pores could increase the adsorption of $CO_2$. Nonetheless, more work in experimental and computational research is required to accurately elucidate the adsorption mechanism under humid conditions in these adsorbents. In general, as discussed above, water presence can also adversely effects on adsorption, because of pore blocking properties, or competitive adsorption to OMSs and amine sites.

## 2.7. Improved hydrophobicity of MOF adsorbents by coating techniques

As reviewed above hydrophobicity of a MOF can be improved by modifying its internal structure but physical surface structure of the MOF particles can be modified as well. Typical methods used for surface modification are, such as surface coating, post-synthetic thermal annealing, and post-synthetic chemical modification of the surface, as already briefly mentioned in previous chapters. In 2014, Zhang et al. [284] presented a comprehensive polydimethylsiloxane (PDMS) coating technique for amplifying the water stability of the designed MOFs (Fig. 22). Three structurally different MOFs, namely MOF-5, HKUST-1, and ZnBT were coated by PDMS. Surprisingly, hydrophobic PDMS coating induced positive outcomes in humid conditions as adsorption efficiency remained relatively unchanged compared to pristine MOFs. Also, the surface area, crystalline nature and pore texture of the MOF remained reasonably unchanged. Qian et al. [285] deposited a hydrophobic organosilicone layer on the exterior surface of HKUST-1, MIL-125, and ZIF-67 via a facile solution-immersion process without using any heat treatment. The hydrophobic organosilicone layer provided durable protection against exposure to water, and the MOF maintained its porosity for 5 days. Yang et al. [286] successfully established a two-step post-synthetic polymerization strategy to improve the stability of structurally different MOFs, including, HKUST-1, ZIF-67(Co), ZIF-8(Zn), UiO-66(Zr), Cu-TDPAT, Mg-MOF-74 and MIL-100(Fe). This novel technique based on using free base like dopamine as a binder. However, dopamine hydrochloride was used as a precursor to eliminate need of an aqueous alkaline environment for the coating process. The actual process is two-step (Fig. 23), wherein first polydopamine (PDA) was coated on the surface of the MOFs, under a mild oxygen atmosphere, yielding MOF@PDA. In the second step, the new external surface was covalently modified with hydrophobic 1 H, 1 H,2 H,2 H-perfluorodecanethiol (HSF), which eventually improved the water stability of the adsorbent significantly even under harsh acidic and alkaline conditions. In view of the foregoing, this facile strategy could be universally applied to incorporate hydrophobicity into MOFs and to taper their water permeability.

An alternative method for hydrophobic coating is the surface pyrolysis described by Park et al. They synthesized an exceedingly moisture-resistant, black-colored MOF-5 via heat treatment [287]. Although the surface area of the thermally modified MOF-5 was only half of the pristine adsorbent (1740 vs. 3450 $m^2$ $g^{-1}$, respectively), the crystallinity, and the remaining porosity were found to be unchanged for two weeks upon exposure to moist ambient air. Hence showing clearly better hydrostability compared to MOF-5. Moreover, Gadipelli et al. [288] tested the effects of post-synthetic thermal annealing on MOF-5 at temperatures lower than its typical thermal decomposition temperature

at around 500 °C. The MOF-5 samples annealed at 380 (also 6 h) and 400 °C for three hours showed higher $CO_2$ uptakes of 1.5, 2, and 1.1 mmol $g^{-1}$ in comparison to the pristine MOF-5 having 0.8 mmol $g^{-1}$ capacity. Furthermore, in terms of air/water stability, the sample annealed at 400 °C for 3 h maintained its porosity when exposed under ambient air for a maximum 15 days, in contrast to an unmodified adsorbent that showed complete collapse of pore structure under the same conditions.

Sun et al. [289] presented new perspective to preserve structural properties of porous materials under humid $CO_2$, and harsh acid/base conditions by chemically coating the exterior of MOF crystals (Fig. 24). The vinyl-functionalized crystalline zeolite imidazole framework ZIF-8-V was employed for the molecular coating. Its external surface was hydrophobically treated with per-fluoroalkyl groups using a thiol-ene Click reaction. The new surface modified ZIF-8 remained structurally unchanged, when exposed to 100% humidity for over 720 h (at 45 °C), while the pristine ZIF-8 eventually degraded completely under the same conditions already considerably earlier (240 h).

The study of Deria et al. [290] can be highlighted (Fig. 25) as a functionalization method for improving water-resistance of MOFs by modifying the metal nodes inside the pore structure by introducing functional groups as charge compensating units. In the study, Zr-based MOFs were post-synthetically modified using method called solvent-assisted ligand incorporation (SALI) wherein perfluoroalkane carboxylates of different chain lengths (C1 - C9) were incorporated to NU-1000 [(Zr$_6$($\mu_3$-O)$_4$($\mu_3$-OH)$_4$(-OH)$_4$]$_2$(TBAPy)$_6$] consisting of 1,3,6,8-tetrakis($p$-benzoic acid)pyrene)] (H$_4$TBAPy). Particularly with per-fluorodecanoic acid, NU-1000 preserved both its crystallinity and porosity under 20 cycles of water vapor adsorption and desorption [291], albeit in most cases, porosity was significantly reduced, and the hydrophobically treated Zr$_6$-oxo centers did not necessarily cooperated directly with the $CO_2$ uptake as desired. Although fluorinated carboxylates somewhat improved the tolerance of Zr$_6$-oxo centers towards water molecules. Recently, Amato et al. [292] reported MOFs that outperform their Zr-based analogues (MIL-140(Zr) and UiO-66(Zr)). Since the fluorinated MOFs have shown remarkable results with respect to physisorption based capture capacity in DAC, the Amato et al. introduced tetrafluoroterephthalic acid (H$_2$TFBDC) as a linker and prepared Ce-MOFs with MIL-140 and UiO-66 topologies. The adsorption heats were found to be about $-$ 39 kJ mol$^{-1}$ indicating physisorption and the evaluated $CO_2/N_2$ selectivities were determined to be particularly high among the reported MOFs (>1900).

## 3. Engineering aspects in $CO_2$ capture by MOFs

Successful implementation of adsorption-based gas separation into a real-life application relies on the recognition of the most suitable adsorbent to match for the practical process conditions. This requires mutual contributions both from the MOF chemistry and engineering communities to constitute a fundamental understanding of their work. It is mandatory that the engineer community is familiar with the basic knowledge of the different adsorbents, and their functionalities while designing optimal process conditions but also keeping in mind the limitations of the adsorbents. Similarly, the chemist or material scientist should be aware of the process requirements and, with those in mind, try to design an adsorbent in a way that its best possible efficiency can be achieved within the technical boundaries set by the process. In this context, to bridge the gap between adsorbents and their engineering aspects, we herein outline the major approaches in the literature for real gas separation characteristics, namely, adsorption heat, gas selectivity, multicomponent gas adsorption, and MOFs post-processing cycles, regeneration, and cost.

### 3.1. Isosteric heat of adsorption

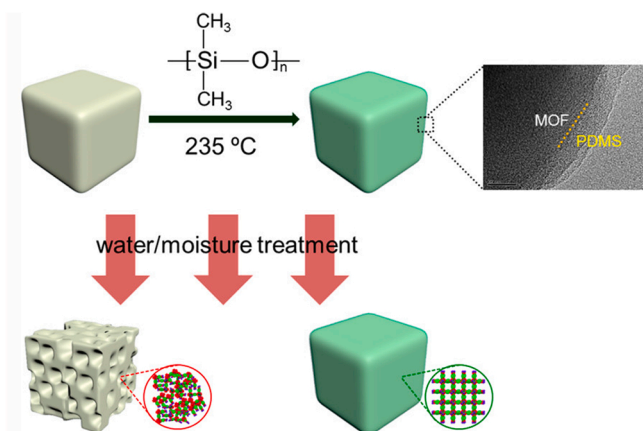Isosteric adsorption heat relates to the strength of adsorption of a



**Fig. 22.** Illustration of PDMS-Coating on the MOFs Surface. Adapted from Ref. [284].
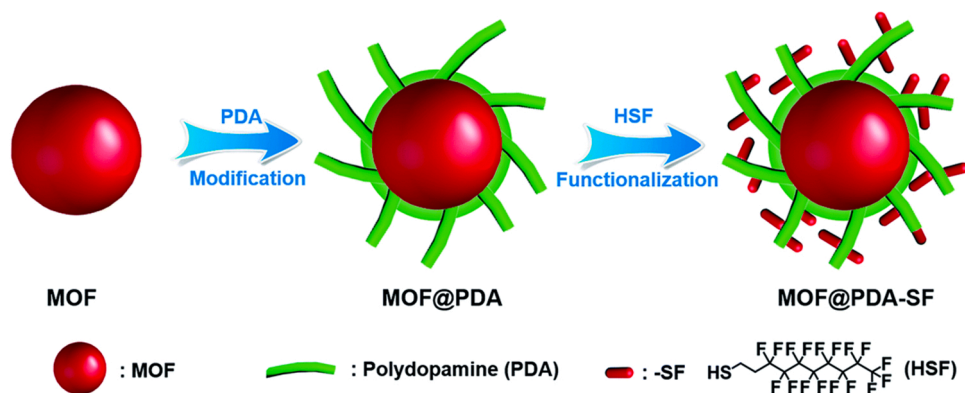
**Fig. 23.** The modification process used for preparing hydrophobic MOF@PDA-SF composites.
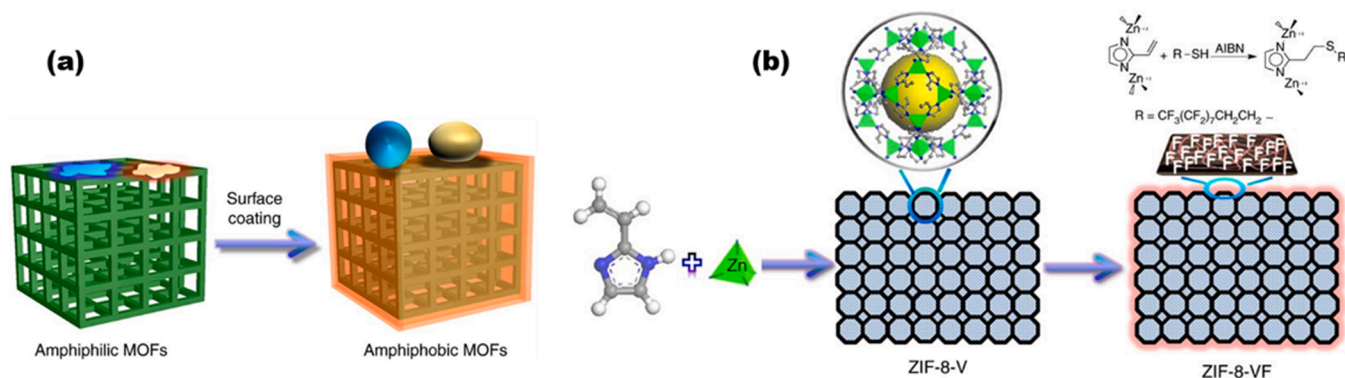Adapted from Ref. [286].



**Fig. 24.** (a) Amphiphobic surface engineering for MOFs, and (b) schematic illustration to impart amphiphobicity on ZIF-8-V.
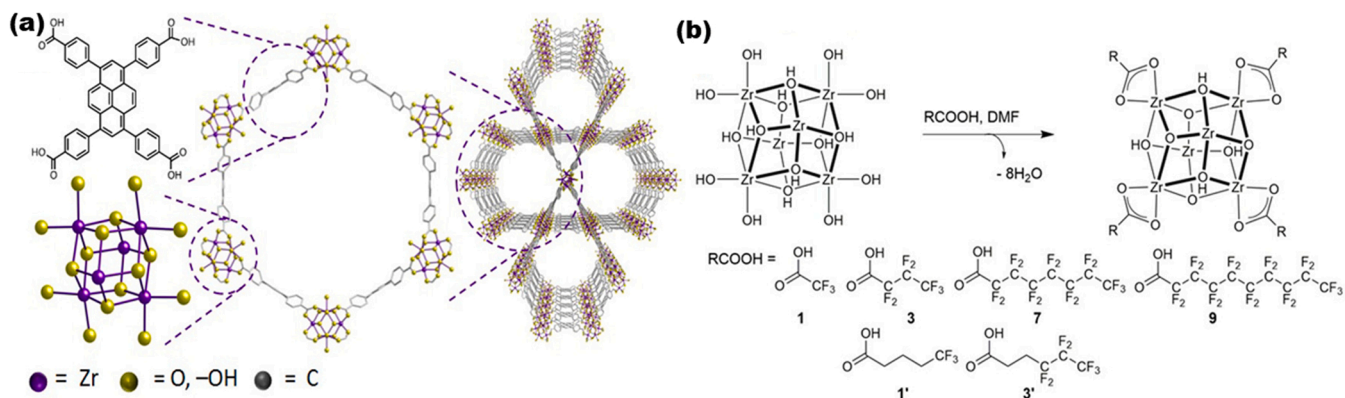Adapted from Ref. [289].



**Fig. 25.** Crystal structure of (a) NU-1000, and (b) illustration of solvent-assisted ligand incorporation (SALI).
Adapted from Ref. [290].

given adsorbate on a given adsorbent. Thus, the energetic interaction strength between the adsorbents and adsorbates is significant in assessing the adsorptive selectivity and the design of regeneration processes [293]. Broadly, the isosteric heat ($Q_{st}$) can be determined by the well-known Clausius–Clapeyron equation when the following conditions are fulfilled: a) the gas adsorbed obeys the characteristics of an ideal gas, and b) the volume of the gas adsorbed is insignificant [294]. Based on the single-component isotherm curves at divergent temperatures, $Q_{st}$ can be calculated according to the following Clapeyron Eq. (6): [295].

$$\ln p = -\frac{Q}{RT} + C \qquad (6)$$

Where, P is pressure correspondent to the same $CO_2$ uptake under different temperatures, R is the universal gas constant, T is temperature, and C is a constant. Thus, the $Q_{st}$ at each adsorption point is determined based upon the slope of the plot ln P as a function of (1/T). Also, the other common way to determine the $Q_{st}$ is to fit the temperature dependent isotherms to virial-type Eqs. (7) and (8):

$$\ln P = \ln N + \frac{1}{T} \sum_{i=0}^{m} a_i N^i + \sum_{i=0}^{n} b_i N^i \qquad (7)$$

$$Q_{st} = -R \sum_{i=0}^{m} a_i N^i \qquad (8)$$

where P is the pressure (bar), N is the adsorbed quantity (mmol g$^{-1}$), T is the temperature (K), R is the gas constant (8.314 J K$^{-1}$ mol$^{-1}$), $a_i$ and $b_i$ represent the virial coefficients, and m and n exemplify the number of coefficients needed for the appropriate fitting of the isotherms. From the above, researchers have utilized $Q_{st}$ as an important parameter to discover the beneficial changes in the sorbate–adsorbent interaction, and its effect on gas selectivity in functionalized frameworks [296–298]. For instance, Park et al. [299] demonstrated improved adsorption heat, selectivity, and $CO_2$ capacity of SNU-100 MOF by impregnating different metal ions, namely Li$^+$, Mg$^{2+}$, Ca$^{2+}$, Co$^{2+}$, and Ni$^{2+}$ into the pores. The formed electrostatic interactions between $CO_2$ and the impregnated metal ions, impacted to the adsorption heats which increased from $-29.3$ of pristine SNU-100 to between $-37.4$ and $-34.5$ kJ mol$^{-1}$ depending on the metal ion used for impregnation. Similarly, the adsorption selectivity elevated from 25 to the range of 31–40.

## 3.2. Ideal adsorbed solution theory (IAST)

The successful implementation of $CO_2$ capture processes equally demands the study of both a) single component and b) mixture sorption equilibrium data [298,300,301]. Acceptedly, single-component isotherms can be simply obtained by volumetric adsorption experiments. Nevertheless, mixture adsorption equilibrium studies represent a complicated process owing to the participation of different variables in the process [112,302]. In this regard, to resolve these complexities, the IAST method is utilized to describe multicomponent adsorption isotherms under the following three major considerations: a) adsorbate molecules in the mixture have equal accessibility to the whole surface area of the adsorbent, b) the adsorbent surface is homogeneous, and c) the adsorbed phase is an ideal solution in which intermolecular interactions are comparable in strength [303,304]. Such a methodology that explains the multicomponent adsorption isotherms from single-component adsorption isotherms starts from Raoults' law type of relationship between the adsorbed phase and fluid. Utilizing the mathematical fitting outlined by Myers & Prausnitz, the IAST permits the selectivity of an ideal multicomponent mixture to be estimated.[303] In regard to a binary mixture, the selectivity can be obtained by the following Eq. (9):

$$S_{ads} = \frac{q_1 \backslash q_2}{p_1 \backslash p_2} \qquad (9)$$

For instance, based on the IAST calculations, McDonald et al. [260] demonstrated significant improvement on selectivity (327 at 25 °C) for mmen-CuBTTri, with a mixture of $CO_2/N_2$ at 150 and 750 mbar $CO_2$, respectively. Similarly, using IAST Hu et al. [305] represented $CO_2/N_2$ selectivity factor of 346 for MIL-101-DETA at 23 °C. IAST has been broadly employed regarding MOFs to investigate the selectivity for separation of mixtures of industrial concerns, like the gas mixtures of $N_2/CO_2$, $CH_4/CO_2$ and $CH_4/N_2$ [306–308]. Recently, Billemont et al. [309] utilized IAST to study adsorption of $CO_2$ from gas mixture like biogas and natural gas using mesoporous MIL-100(Fe) as adsorbent. Overall, IAST emerged with an appropriate model for these promising adsorption processes and based on that MIL-100(Fe) seemed to be potential adsorbent for $CO_2/N_2$ separation.

## 3.3. Single-component adsorption experiment

A single component adsorption experiment is often the first screening tool to determine the $CO_2$ adsorption capacity. Gas sorption

analyzers are categorized in two ways: volumetric (also known as manometric) and gravimetric. Gravimetric $CO_2$ adsorption capacity describes the weight fraction requisite of MOF for an application, whereas the volumetric uptake reveals information about the bed volume of adsorbent, dimensions of required equipment and capturing unit. Data is often reported based on gravimetric analysis, which is the amount of gas adsorbed (in mass or volume, STP or moles) per unit weight of adsorbent. By multiplying this data with the adsorbent density, volumetric capacity can be obtained (cc cc$^{-1}$ or v/v). Particularly for MOFs, crystal density is often employed for this type of conversion. Notwithstanding, it is the highest theoretical value, as in comparison to single crystal, MOF bulk powders are typically loosely packed [310]. For instance, opt-UiO-66(Zr)-(OH)$_2$ exhibits higher crystal density of 1.36 g cm$^{-3}$ than Mg-MOF-74 (0.91 g cm$^{-3}$). Thus, higher volumetric capacity is determined for opt-UiO-66(Zr)-(OH)$_2$ than Mg-MOF-74 (172 and 165 cm$^3$ (STP) cm$^{-3}$, respectively) at 1 bar and 25 °C. However, in terms of gravimetric capacity under the same conditions Mg-MOF-74 demonstrates higher $CO_2$ capacity than opt-UiO-66(Zr)-(OH)$_2$ (8 and 5.63 mmol g$^{-1}$, respectively). Few examples of volumetric capacities of known MOF$_S$ includes SIFSIX-2-Cu-I (1.24 g cm$^{-3}$, 151 cm$^3$ (STP) cm$^{-3}$), UTSA-16 (1.66 g cm$^{-3}$, 160 cm$^3$ (STP) cm$^{-3}$), mmen-Mg$_2$(-dobpdc) (1.16 g cm$^{-3}$, 107 cm$^3$ (STP) cm$^{-3}$), and Mg$_2$(dobdc)-(N$_2$H$_4$) (1.18 g cm$^{-3}$, 145 cm$^3$ (STP) cm$^{-3}$) [112]. Thus, the actual volumetric capacity is overestimated and can differ if the interstitial void of the particles and crystal defects are included. Thus, to prevent any incorrect interpretation of the experimental results, it is necessary to mention all the important details, including pressure steps, system response time, sample weight, and representative data demonstrating the suitability of the theoretical model to the experimental response curves [311]. Since the single component adsorption experiment does not consider competitive adsorption among various components, it is therefore, unable to measure the behavior of binary\ternary adsorption. Thus, under real working conditions, dynamic column breakthrough data is suggested, as discussed in 3.5.

## 3.4. Working capacity

Working capacity is one of the most critical parameters to determine the overall performance of adsorbent, as it takes material regeneration into consideration. Recovery is determined as the fraction between the quantity of product formed over the quantity of product in the feed stream. It is essential to pay attention to fact that the working capacity and the adsorption capacity are different quantity parameters. Working capacity (WC) relates to the difference between the quantities adsorbed at the adsorption and desorption conditions, thus $CO_2$ uptake capacity ($q_{ads}$) under adsorption minus $CO_2$ uptake capacity ($q_{des}$) under desorption conditions, Eq. (10).

$$WC_q = q_{ads} - q_{des} \qquad (10)$$

Working capacity can be determined based on the type of the process, for instance being pressure swing (PSA), vacuum swing (VSA) or temperature swing adsorption (TSA). Increasing the temperature of the column above that of the feed temperature is known as temperature swing adsorption (TSA) and reducing the pressure to a value below that of the feed is known as pressure swing adsorption (PSA). If the desorption is under vacuum, the process is also called vacuum swing adsorption (VSA). In connection with PSA/VSA, the nature of the process is often regarded under isothermal conditions. A single sorption isotherm at a specific temperature $T_1$, is considered to suffice for calculating the working capacity by merely subtracting the equilibrium uptake at the partial pressure of gas under adsorption conditions (high P), and the uptake at the partial pressure under desorption conditions (low P). However, in the case of TSA, isotherms collected at different temperatures are required, where the working capacity is calculated by subtracting the equilibrium uptake at the partial pressure of gas under

adsorption conditions (low T) from the uptake at the partial pressure under desorption conditions (high T) [231,310].

## 3.5. Dynamic breakthrough experiments

The comprehensive insight of the mixed gas equilibrium adsorption data is crucial for selecting the best adsorbent material, process design, and for substantiating theoretical models of mixture adsorption [112]. This engineering method can be utilized to analyze MOFs in the context of mixture-component adsorption performance and display a screen between idealistic and practicable adsorptions in the industrial applications. Thus, dynamic breakthrough experiments are conducted under conditions like those of a large-scale separation. Since the commercial equipment for breakthrough experiments is not generally available, many breakthrough experiments are conducted using in-house setups. With in-house systems, the measurement accuracy and operational control might vary, and this can lead to erroneous results and interpretations. Therefore, the establishment and running of an experimental breakthrough setup, though straightforward in theory, needs careful consideration and execution practice.

Hu et al. [312] presented a straightforward and comprehensive breakthrough setup for the gas separation. As illustrated in (Fig. 26), the fundamental part of the setup is the stainless-steel adsorption column, wherein an adsorbent is typically loaded in either as powdered or compacted form. The adsorbent bed is introduced to a gaseous stream (generally a binary or ternary mixture), and the mixture composition is continually regulated with an in-line analytical instrument (typically a mass spectrometer). The pressure drop is recorded before and after the adsorbent bed. Additionally, the exit velocity of the breakthrough column is recorded for mass balance accuracy, using argon at a constant flow rate as the internal reference. Thus, the authors presented the comprehensive procedures for conducting the breakthrough experiments so that the change in the gas velocity at the exit, and the pressure drop across the breakthrough column have been considered, which are often overlooked in the literature.

## 3.6. Gas diffusion

The gas diffusion parameter holds paramount importance in evaluating sorption kinetics in the MOF-based $CO_2$ capture. The mass transfer coefficient relates the mass transfer rate in separation processes and reveals to the particular preconditions in the design and construction of separation process equipment [313]. Diffusion studies can be categorized into two major classes, those being microscopic and macroscopic [112,314]. Microscopic methods include pulse-field gradient (PFG)-NMR [315], infra-red microscopy (IRM), and interference



**Fig. 26.** Breakthrough setup for $CO_2$ adsorption study.
Adapted from Ref. [312].

microscopy (IFM) [316]. The above methods render comprehensive details about the diffusional characteristics at the atomic level, indicating the existence of inhomogeneities, in particular surface barriers that have an impact on the behavior of adsorbates. Unfavorably, methods such as those demand samples with larger particle sizes, likely single crystals, that are commonly not available, as powdered adsorbents dominate in real-life applications. Macroscopic methods include frequency response, chromatographic methods, and zero length column methods (ZLC) [317]. Gas diffusion parameters obtained from macroscopic methods can be evaluated on the basis of the overall gas adsorption behavior of realistic powders like samples and thereby give information that can be useful for the process development [318].

## 3.7. MOF post-processing cycles and regenerability

As adsorbent materials exhibit a finite uptake capacity of $CO_2$, thereby continual interaction with ambient air or flue gas conditions will subsequently lead to a thermodynamic equilibrium between the two phases (solid and gas), wherein the adsorption and desorption rates are equivalent [313]. In view of this, it is important that adsorbents are regenerated, and semi-continuous process is developed where the adsorption and regeneration processes are grouped together.

It should also be noted that the post-processing of MOF materials is a crucial step to enable their use in an application. In lab-scale experiments, adsorbents are often supported by fine metal meshes in a fixed bed, prepared on quartz wool, or attached to a substrate. However, utilizing the powdery MOFs in an industrial application can lead to several issues, such as pressure drop, reduced or blocked flow, and abrasion due to powder migration in the system [319]. Thus, they require sufficient post-processing before being secured on a fixed bed. In this manner, the cross-column pressure drop can also be attenuated to increase the column breakthrough dynamics [312].

Darunte et al. [320] explored the possibility of utilizing an amine functionalized mmen-$M_2$(dobpdc) (M = Mg and Mn) as secured on a structured monolith contactor under simulated flue gas (Fig. 27). Similarly, Lawson et al. [321] presented polyethylenimine and tetraethylenepentamine impregnated MOF-monoliths that were made with a 3D printing technique using pre- and post-functionalization approaches (Fig. 28a). Recently, Lawson et al. [322] demonstrated HKUST-1 monolith formulation based on the gel-print-grow strategy (Fig. 28b).

As mentioned above, regeneration can be accomplished by different processes or sometimes a combination of one or more methods, such as increasing the temperature, lowering the partial pressure of the adsorbates, reduction in the concentration, or inert gas purging. The objective is to place the adsorbent in a state where its uptake capacity for the adsorbent is lower than in the adsorption step, thus activating the desorption mechanism. In some cases, it is favorable to associate both temperature and pressure/vacuum swing to accomplish more desirable regeneration and, consequently, improved working capacity. After the regeneration of the bed, a new cycle can be initiated. [112].

## 3.8. Cost of MOFs

Currently, the production cost of MOFs is the key limiting factor for the commercialization of MOF-based adsorbents. The market price of any MOF from commercial suppliers is still exorbitant compared to that of the "conventional" adsorbents like activated carbon, silica, and zeolites. This is largely attributable to the lack of scale-up production methods developed for MOFs. Material costs are dependent mainly on four components that are required in MOF synthesis; solvents (used for reaction media and washing), metal source(s), organic ligand(s), and acid/base catalyst. As an example, material costs for some typical MOFs are shown in Fig. 29. For instance, in the case of MOF-5, producing 1 kg of activated MOF-5 demands 81.30 L of DMF, 1.03 kg of terephthalic acid, and 3.45 kg of zinc acetate dihydrate (with a reaction yield of 63 %). These components cost about 414, 34, and 79 USD, respectively. The
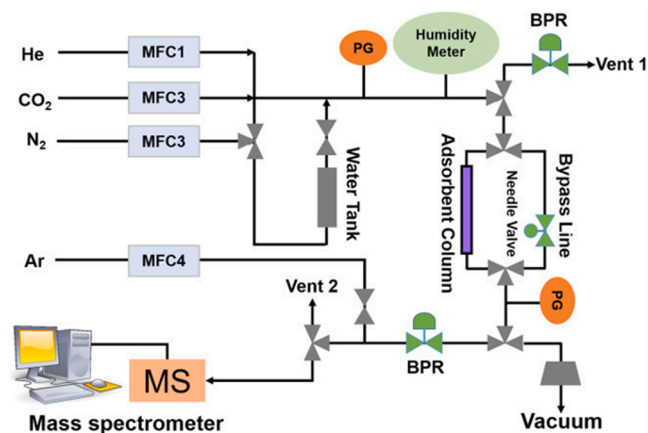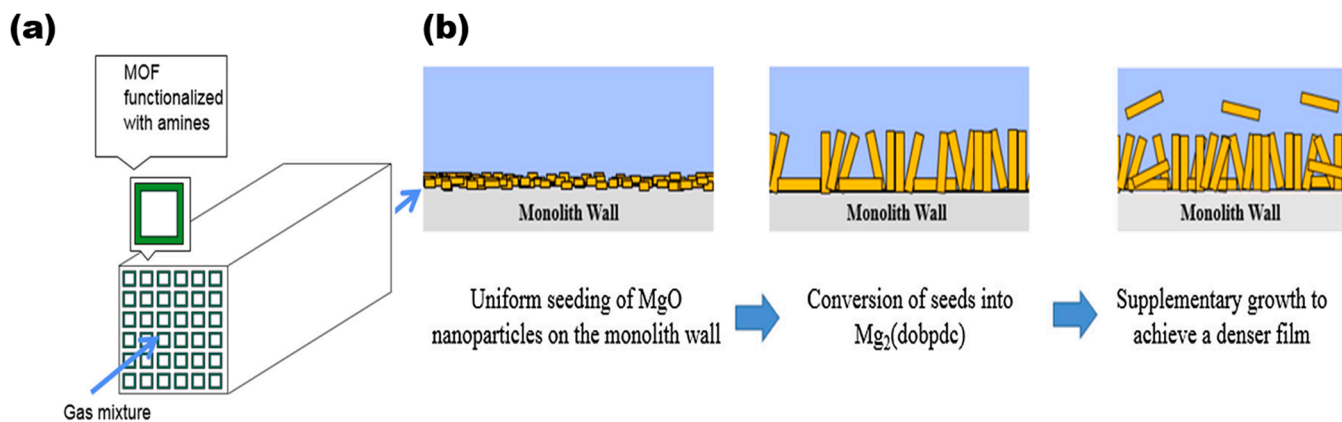
**Fig. 27.** (a) Monolith -supported MOF system (b) approach to create MOF films
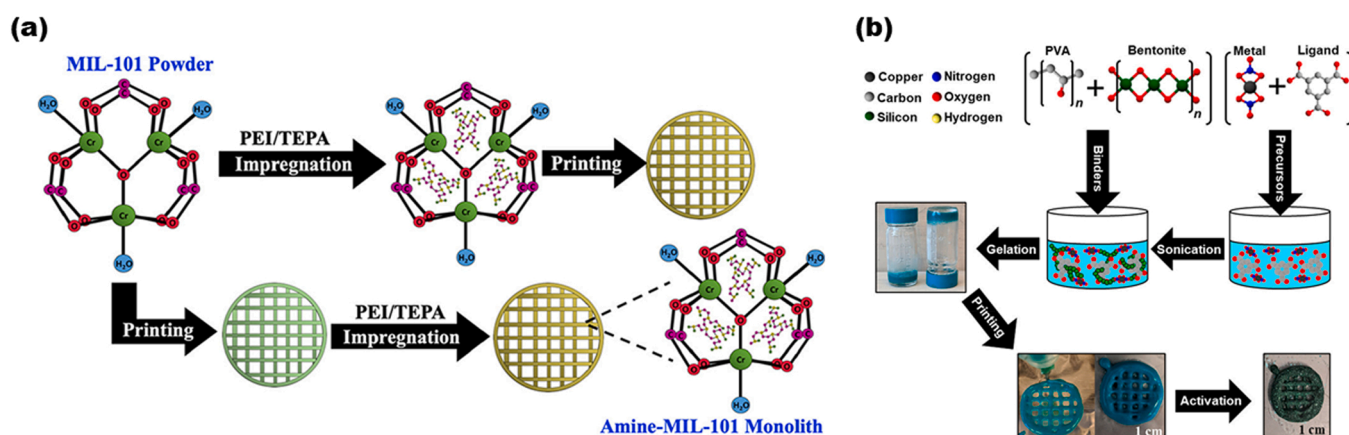Adapted from Ref. [320].



**Fig. 28.** (a) Manufacturing processes for pre- and post-impregnated MIL-101 monoliths, and (b) illustration of HKUST-1 monolith formulation by gel-print-grow technique.
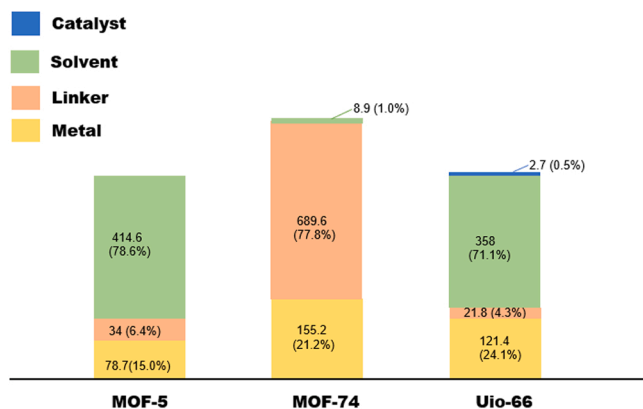Adapted from Refs. [321,322].



**Fig. 29.** Material costs of MOF-5, Ni-MOF-74, and UiO-66, given in US $ [319].

overall product cost is ~527 USD kg$^{-1}$, of which about 79 % arises from the solvent [323]. For activated Ni-MOF-74, the total material cost is reported to be ~887 USD kg$^{-1}$, of which approximately 78 % originates from the ligand [324]. In the case of the UiO-66 total material cost is ~504 USD kg$^{-1}$ wherein solvent accounts for 72 % of the cost [325]. In this regard, substantial efforts need to be made to optimize synthesis methods, including solvent recycling, using water as a (co-)solvent, or using solvent-free mechanochemical synthesis, as well as primarily utilizing economically inexpensive starting materials. Having said that, MOFs commercialization still requires further intensive research efforts to substantially decrease manufacturing costs and, by that enable the MOF technologies to evolve and prosper on gas sorption-based technologies.

## 4. Conclusions

Undoubtedly, chemists, materials scientists, and engineers have shown a deep interest in the utilization of MOF for carbon capture to minimize the impact of atmospheric $CO_2$ on the global temperature rise. The growing number of publications highlights the significant progress that has been already made on $CO_2$ related applications as reflected by the vast diversity of MOFs known to us, and the good properties they reveal for them to operate already somewhat close to real-life conditions. However, when it comes to their applicability to technical applications, it is important to point out that there are still certain challenges that need to be addressed and require further extensive research efforts.

Firstly, a very limited number of MOFs have been investigated under lower $CO_2$ concentrations, and mostly single-component $CO_2$ sorption isotherms are reported instead of real mixtures. For MOFs to be utilized in practical applications, it is important to collect a considerable range of dynamic breakthrough experiment data to establish the constructive relationship between material structure, surface chemical property, and $CO_2$ capture efficiency. Secondly, the next challenge circles around the MOFs synthesis on a large scale (first at Kg quantities) with reasonable

cost, sufficient phase purity and correct morphology (pellets, monoliths), as well as chemically robust nature, so that they can withstand tens of thousands of loading/unloading cycles. More research efforts are needed to further enhance $CO_2$ capture capacity and selectivity, particularly under humid conditions.

From a structural point of view, modification of the metal centers on the frameworks, remains a promising strategy and central research direction towards $CO_2$ capture. However, considering Mg-MOF-74, the best performing MOF under relatively higher pressures and concentrations, is not compatible with DAC owing to its unsatisfactory $CO_2$ selectivity at lower concentrations. Therefore, physisorption by MOFs is only applicable at relatively higher pressures and concentrations and not in low $CO_2$ partial pressures. Nevertheless, this is not the case with hybrid ultramicroporous (HUM) mesh-like adsorbents that exhibit physisorption mechanisms.

To support this, Kumar et al.[150] presented a screening of four different classes of porous adsorbents namely SIFSIX-3-Ni, HKUST-1, Mg-MOF-74/Mg-dobdc, zeolite-13X, and TEPA-SBA-15. Predictably, the only chemisorbing TEPA-SBA-15 exhibited superior DAC performance and $CO_2/H_2O$ selectivity in comparison with the other physisorbents. However, even though SIFSIX-3-Ni demonstrated also good efficiency in DAC conditions it still showed poor $CO_2/H_2O$ selectivity, which was also the case for all the other physisorbents. Amongst similar MOFs, the NbOFFIVE-1-Ni has shown the best DAC performance in comparison to a series of similar isostructural materials. In terms of regeneration, HUMs displayed optimal regeneration energy at a relatively low temperature range 90–100 °C under purging with inert gas or vacuum but at humid conditions significant drop in $CO_2$ uptake, and lower working capacity were observed due to the competitive water adsorption. Thus, it is evident that this class of MOFs is limited only to dry atmospheric conditions and are not good enough to compete with chemisorbents without further development.

These shortcomings can be resolved by functionalization of MOF pores with amines that react with $CO_2$ via chemisorption and convert it into carbamic acid, carbamate, or bicarbonate species. The stronger interaction between amine and $CO_2$ offers superior $CO_2/H_2O$ selectivity in comparison to physisorbents. In this context, diamine functionalized $Mg_2(dobpdc)$ has so far displayed superior $CO_2$ uptake capacity combined with good stability under humid conditions. Further optimization is still required for shaping this MOF into industrially suitable forms (granules, pellets, beads, films, or monoliths). Massive scale-up of production (Mt per year) but with reasonable costs (<$10 per kg)[326] also needs technical solutions, as well as stability since adsorbent needs to withstand thousands of sorption cycles under practical flue gas conditions and especially in DAC. To fulfill these requirements, DAC technologies must overcome several technical and economic challenges. Although DAC has undergone considerable technical advances in the recent years, the field is still in its infancy. As demonstrated earlier, for efficiently working adsorbent in DAC, the high enough $CO_2$ capacity with high enough adsorption heat to capture $CO_2$ selectively via chemisorption are the essential parameters to develop but also meeting the low enough energy requirement for the desorption process. Future studies should also focus on parameters such as degradation and cycle time of adsorbents. In practical DAC process, both loading\unloading times should be measured instead inert gas purge or gravimetric $CO_2$ uptake experiment. Thus, adsorbent regeneration strategies and capacity measurements based on laboratory scale often encounters new obstacles when they are translated to real-life DAC. More research in the case of DAC adsorbents is needed to evaluate their true potential for commercial carbon capture [38,326–329]. Overall, utilizing MOFs in carbon capture involves many barriers and challenges which are so far unsolved and require both chemists and process engineers to come forward for constructive collaboration in the field of carbon capture. We anticipate that further extensive research efforts and investigations are needed for MOFs to boost them to future applications, and we certainly believe that this progress is possible, as there are diverse possibilities to

formulate, synthesize, and modify MOF-based adsorbents to fulfil the high expectations of an ultimately effective and energy-efficient adsorbents suitable task-specifically for different areas of carbon capture, like for flue gases emissions and DAC.

## Declaration of Competing Interest

The authors declare that they have no known competing financial interests or personal relationships that could have appeared to influence the work reported in this paper.

## Data Availability

No data was used for the research described in the article.

## Acknowledgements

## References

[1] N.J.L. Lenssen, G.A. Schmidt, J.E. Hansen, M.J. Menne, A. Persin, R. Ruedy, D. Zyss, Improvements in the GISTEMP uncertainty model, J. Geophys. Res.: Atmos. 124 (2019) 6307–6326, https://doi.org/10.1029/2018JD029522.

[2] T.R. Anderson, E. Hawkins, P.D. Jones, $CO_2$, the greenhouse effect and global warming: from the pioneering work of Arrhenius and callendar to today's earth system models, Endeavour 40 (2016) 178–187, https://doi.org/10.1016/j.endeavour.2016.07.002.

[3] Q. Wang, J. Luo, Z. Zhong, A. Borgna, $CO_2$ capture by solid adsorbents and their applications: current status and new trends, Energy Environ. Sci. 4 (2011) 42–55, https://doi.org/10.1039/c0ee00064g.

[4] E.S. Sanz-Pérez, C.R. Murdock, S.A. Didas, C.W. Jones, Direct capture of $CO_2$ from ambient air, Chem. Rev. 116 (2016) 11840–11876, https://doi.org/10.1021/acs.chemrev.6b00173.

[5] IPCC, The IPCC and 6th Assessment Cycle, 2021.

[6] IPCC, Climate change 2014 synthesis report. contribution of working groups I, II, and III to the fifth assessment report of the Intergovernmental Panel on Climate Change, 2014.

[7] Y. Kim, E. Worrell, $CO_2$ emission trends in the cement industry: an international comparison, Mitig. Adapt. Strateg. Glob. Change 7 (2002) 115–133, https://doi.org/10.1023/A:1022857829028.

[8] M. Mikkelsen, M. Jørgensen, F.C. Krebs, The teraton challenge. a review of fixation and transformation of carbon dioxide, Energy Environ. Sci. 3 (2010) 43–81, https://doi.org/10.1039/b912904a.

[9] X. Shi, H. Xiao, H. Azarabadi, J. Song, X. Wu, X. Chen, K.S. Lackner, Sorbents for the direct capture of $CO_2$ from ambient air, Angew. Chem. - Int. Ed. 59 (2020) 6984–7006, https://doi.org/10.1002/anie.201906756.

[10] J.G. Vitillo, M. Savonnet, G. Ricchiardi, S. Bordiga, Tailoring metal-organic frameworks for $CO_2$ capture: The amino effect, ChemSusChem 4 (2011) 1281–1290, https://doi.org/10.1002/cssc.201000458.

[11] M. Ding, R.W. Flaig, H.L. Jiang, O.M. Yaghi, Carbon capture and conversion using metal-organic frameworks and MOF-based materials, Chem. Soc. Rev. 48 (2019) 2783–2828, https://doi.org/10.1039/c8cs00829a.

[12] Y. Zhang, X. Lu, X. Ji, Carbon dioxide capture, in: Deep Eutectic Solvents, Wiley, 2019, pp. 297–319, https://doi.org/10.1002/9783527818488.ch15.

[13] IPCC, 2018/24/PR IPCC PRESS RELEASE 8 October 2018, Ipcc. (2018) 13–16.

[14] IEA, Energy Technology Perspectives 2020, Paris, 2020.

[15] IEA, Energy Technology Perspectives 2016, Paris, 2016.

[16] IEA, Energy Technology Perspectives 2017, Paris, 2017.

[17] Z. Sun, Y. Liao, S. Zhao, X. Zhang, Q. Liu, X. Shi, Research progress in metal–organic frameworks (MOFs) in CO 2 capture from post-combustion coal-fired flue gas: characteristics, preparation, modification and applications, J. Mater. Chem. A 10 (2022) 5174–5211, https://doi.org/10.1039/d1ta07856a.

[18] Y. Fu, Y.B. Jiang, D. Dunphy, H. Xiong, E. Coker, S. Chou, H. Zhang, J. M. Vanegas, J.G. Croissant, J.L. Cecchi, S.B. Rempe, C.J. Brinker, Ultra-thin enzymatic liquid membrane for $CO_2$ separation and capture, Nat. Commun. 9 (2018) 1–12, https://doi.org/10.1038/s41467-018-03285-x.

[19] C. Castel, R. Bounaceur, E. Favre, Membrane processes for direct carbon dioxide capture from air: possibilities and limitations, Front. Chem. Eng. 3 (2021) 1–15, https://doi.org/10.3389/fceng.2021.668867.

[20] A.C. Forse, P.J. Milner, New chemistry for enhanced carbon capture: beyond ammonium carbamates, Chem. Sci. 12 (2021) 508–516, https://doi.org/10.1039/d0sc06059c.

[21] E.E. Ünveren, B.Ö. Monkul, Ş. Sarıoğlan, N. Karademir, E. Alper, Solid amine sorbents for $CO_2$ capture by chemical adsorption:a review, Petroleum 3 (2017) 37–50, https://doi.org/10.1016/j.petlm.2016.11.001.

[22] A.M. Varghese, G.N. Karanikolos, $CO_2$ capture adsorbents functionalized by amine – bearing polymers: a review, Int. J. Greenh. Gas Control 96 (2020), 103005, https://doi.org/10.1016/j.ijggc.2020.103005.

[23] P. Zhao, G. Zhang, H. Yan, Y. Zhao, The latest development on amine functionalized solid adsorbents for post-combustion $CO_2$ capture: analysis review, Chin. J. Chem. Eng. 35 (2021) 17–43, https://doi.org/10.1016/j.cjche.2020.11.028.

[24] Y. Lin, C. Kong, Q. Zhang, L. Chen, Metal-organic frameworks for carbon dioxide capture and methane storage, Adv. Energy Mater. 7 (2017) 1601296, https://doi.org/10.1002/aenm.201601296.

[25] C.A. Trickett, A. Helal, B.A. Al-Maythalony, Z.H. Yamani, K.E. Cordova, O. M. Yaghi, The chemistry of metal-organic frameworks for $CO_2$ capture, regeneration and conversion, Nat. Rev. Mater. 2 (2017) 1–16, https://doi.org/10.1038/natrevmats.2017.45.

[26] L.A. Darunte, A.D. Oetomo, K.S. Walton, D.S. Sholl, C.W. Jones, Direct air capture of $CO_2$ using amine functionalized MIL-101(Cr), ACS Sustain. Chem. Eng. 4 (2016) 5761–5768, https://doi.org/10.1021/acssuschemeng.6b01692.

[27] R. Socolow, M. Desmond, R. Aines, J. Blackstock, O. Bolland, T. Kaarsberg, N. Lewis, M. Mazzotti, A. Pfeffer, K. Sawyer, J. Siirola, B. Smit, J. Wilcox, Direct air capture of $CO_2$ with chemicals A technology assessment for the APS panel on public affairs, Technol. Singap. World Sci. (2011) 1–119.

[28] M. Fasihi, O. Efimova, C. Breyer, Techno-economic assessment of $CO_2$ direct air capture plants, J. Clean. Prod. 224 (2019) 957–980, https://doi.org/10.1016/j.jclepro.2019.03.086.

[29] Composition of Pure Air in Atmospheric Chemistry, The IUPAC Compendium of Chemical Terminology. 2167 (2008) 2172. ⟨https://doi.org/10.1351/goldbook.c01214⟩.

[30] D.W. Keith, G. Holmes, D. Angelo St., K. Heidel, A process for capturing $CO_2$ from the atmosphere, Joule 2 (2018) 1573–1594, https://doi.org/10.1016/j.joule.2018.05.006.

[31] J. Wilcox, P.C. Psarras, S. Liguori, Assessment of reasonable opportunities for direct air capture, Environ. Res. Lett. 12 (2017), 065001, https://doi.org/10.1088/1748-9326/aa6de5.

[32] R.S. Liu, S. Xu, G.P. Hao, A.H. Lu, Recent advances of porous solids for ultradilute $CO_2$ capture, Chem. Res. Chin. Univ. 38 (2022) 18–30, https://doi.org/10.1007/s40242-021-1394-x.

[33] A. Goeppert, M. Czaun, G.K. Surya Prakash, G.A. Olah, Air as the renewable carbon source of the future: An overview of $CO_2$ capture from the atmosphere, Energy Environ. Sci. 5 (2012) 7833–7853, https://doi.org/10.1039/c2ee21586a.

[34] K.S. Lackner, Capture of carbon dioxide from ambient air, Eur. Phys. J.: Spec. Top. 176 (2009) 93–106, https://doi.org/10.1140/epjst/e2009-01150-3.

[35] M. Mahmoudkhani, D.W. Keith, Low-energy sodium hydroxide recovery for $CO_2$ capture from atmospheric air-Thermodynamic analysis, Int. J. Greenh. Gas Control 3 (2009) 376–384, https://doi.org/10.1016/j.ijggc.2009.02.003.

[36] J.K. Stolaroff, D.W. Keith, G.V. Lowry, Carbon dioxide capture from atmospheric air using sodium hydroxide spray, Environ. Sci. Technol. 42 (2008) 2728–2735, https://doi.org/10.1021/es702607w.

[37] G. Holmes, D.W. Keith, An air-liquid contactor for large-scale capture of $CO_2$ from air, Philos. Trans. R. Soc. A: Math. Phys. Eng. Sci. 370 (2012) 4380–4403, https://doi.org/10.1098/rsta.2012.0137.

[38] N. McQueen, K.V. Gomes, C. McCormick, K. Blumanthal, M. Pisciotta, J. Wilcox, A review of direct air capture (DAC): scaling up commercial technologies and innovating for the future, Prog. Energy 3 (2021), 032001, https://doi.org/10.1088/2516-1083/abf1ce.

[39] P. Bollini, S.A. Didas, C.W. Jones, Amine-oxide hybrid materials for acid gas separations, J. Mater. Chem. 21 (2011) 15100–15120, https://doi.org/10.1039/c1jm12522b.

[40] P. Folger, Carbon capture and sequestration (CCS), Carbon Capture Greenh. Gases 325 (2010) 1–28, https://doi.org/10.1007/978-3-642-28036-8_100191.

[41] C.K. Boynton, A.K. Colling, Solid amine $CO_2$ removal system for submarine application, SAE Tech. Papers 92 (1983) 601–614, https://doi.org/10.4271/831131.

[42] A.M. Boehm, F.A. Ouellette, Chamber testing of $CO_2$ removal systems using solid amines, SAE Tech. Papers 104 (1995) 512–519, https://doi.org/10.4271/951488.

[43] O. Leal, C. Bolívar, C. Ovalles, J.J. García, Y. Espidel, Reversible adsorption of carbon dioxide on amine surface-bonded silica gel, Inorg. Chim. Acta 240 (1995) 183–189, https://doi.org/10.1016/0020-1693(95)04534-1.

[44] S. Satyapal, T. Filburn, J. Trela, J. Strange, Performance and properties of a solid amine sorbent for carbon dioxide removal in space life support applications, Energy Fuels 15 (2001) 250–255, https://doi.org/10.1021/ef0002391.

[45] X. Xu, C. Song, J.M. Andresen, B.G. Miller, A.W. Scaroni, Novel polyethylenimine-modified mesoporous molecular sieve of MCM-41 type as high-capacity adsorbent for $CO_2$ capture, Energy Fuels 16 (2002) 1463–1469, https://doi.org/10.1021/ef020058u.

[46] H.Y. Huang, R.T. Yang, D. Chinn, C.L. Munson, Amine-grafted MCM-48 and silica xerogel as superior sorbents for acidic gas removal from natural gas, Ind. Eng. Chem. Res. 42 (2003) 2427–2433, https://doi.org/10.1021/ie020440u.

[47] A.C.C. Chang, S.S.C. Chuang, M. Gray, Y. Soong, In-situ infrared study of $CO_2$ adsorption on SBA-15 grafted with γ-(Aminopropyl)triethoxysilane, Energy Fuels 17 (2003) 468–473, https://doi.org/10.1021/ef020176h.

[48] N. Hiyoshi, K. Yogo, T. Yashima, Adsorption of carbon dioxide on amine modified SBA-15 in the presence of water vapor, Chem. Lett. 33 (2004) 510–511, https://doi.org/10.1246/cl.2004.510.

[49] N. Hiyoshi, K. Yogo, T. Yashima, Adsorption characteristics of carbon dioxide on organically functionalized SBA-15, Microporous Mesoporous Mater. 84 (2005) 357–365, https://doi.org/10.1016/j.micromeso.2005.06.010.

[50] P.J.E. Harlick, A. Sayari, Applications of pore-expanded mesoporous silica. 5. triamine grafted material with exceptional $CO_2$ dynamic and equilibrium adsorption performance, Ind. Eng. Chem. Res. 46 (2007) 446–458, https://doi.org/10.1021/ie060774.

[51] C. Chen, J. Kim, W. Ahn, $CO_2$ capture by amine-functionalized nanoporous materials: a review, Korean J. Chem. Eng. 31 (2014) 1919–1934, https://doi.org/10.1007/s11814-014-0257-2.

[52] S. Choi, J.H. Drese, P.M. Eisenberger, C.W. Jones, Application of amine-tethered solid sorbents for direct $CO_2$ capture from the ambient air, Environ. Sci. Technol. 45 (2011) 2420–2427, https://doi.org/10.1021/es102797w.

[53] X. (Eric) Hu, L. Liu, X. Luo, G. Xiao, E. Shiko, R. Zhang, X. Fan, Y. Zhou, Y. Liu, Z. Zeng, C. Li, A review of N-functionalized solid adsorbents for post-combustion $CO_2$ capture, Appl. Energy 260 (2020), 114244, https://doi.org/10.1016/j.apenergy.2019.114244.

[54] L.A. Darunte, K.S. Walton, D.S. Sholl, C.W. Jones, $CO_2$ capture via adsorption in amine-functionalized sorbents, Curr. Opin. Chem. Eng. 12 (2016) 82–90, https://doi.org/10.1016/j.coche.2016.03.002.

[55] H.A. Patel, J. Byun, C.T. Yavuz, Carbon dioxide capture adsorbents: chemistry and methods, ChemSusChem 10 (2017) 1303–1317, https://doi.org/10.1002/cssc.201601545.

[56] A. Popa, S. Borcanescu, I. Holclajtner-Antunović, D. Bajuk-Bogdanović, S. Uskoković-Marković, Preparation and characterisation of amino-functionalized pore-expanded mesoporous silica for carbon dioxide capture, J. Porous Mater. 28 (2021) 143–156, https://doi.org/10.1007/s10934-020-00974-1.

[57] J.A. Cecilia, E. Vilarrasa-García, R. Morales-Ospino, M. Bastos-Neto, D.C. S. Azevedo, E. Rodríguez-Castellón, Insights into $CO_2$ adsorption in amino-functionalized SBA-15 synthesized at different aging temperature, Adsorption 26 (2020) 225–240, https://doi.org/10.1007/s10450-019-00118-1.

[58] P. Muchan, C. Saiwan, M. Nithitanakul, Investigation of adsorption/desorption performance by aminopropyltriethoxysilane grafted onto different mesoporous silica for post-combustion $CO_2$ capture, Clean. Energy 4 (2020) 120–131, https://doi.org/10.1093/ce/zkaa003.

[59] C. Zhou, S. Yu, K. Ma, B. Liang, S. Tang, C. Liu, H. Yue, Amine-functionalized mesoporous monolithic adsorbents for post-combustion carbon dioxide capture, Chem. Eng. J. 413 (2021), 127675, https://doi.org/10.1016/j.cej.2020.127675.

[60] Z. Lin, J. Wei, L. Geng, D. Mei, L. Liao, Adsorption of carbon dioxide by a novel amine impregnated ZSM-5/KIT-6 composite, RSC Adv. 7 (2017) 54422–54430, https://doi.org/10.1039/c7ra11235a.

[61] R. Kishor, A.K. Ghoshal, Amine-modified mesoporous silica for $CO_2$ adsorption: the role of structural parameters, Ind. Eng. Chem. Res. 56 (2017) 6078–6087, https://doi.org/10.1021/acs.iecr.7b00890.

[62] H. Tang, Q. Xu, M. Wang, J. Jiang, Rapid screening of metal-organic frameworks for propane/propylene separation by synergizing molecular simulation and machine learning, ACS Appl. Mater. Interfaces 13 (2021) 53454–53467, https://doi.org/10.1021/acsami.1c13786.

[63] H. Furukawa, Y.B. Go, N. Ko, Y.K. Park, F.J. Uribe-Romo, J. Kim, M. O'Keeffe, O. M. Yaghi, Isoreticular expansion of metal-organic frameworks with triangular and square building units and the lowest calculated density for porous crystals, Inorg. Chem. 50 (2011) 9147–9152, https://doi.org/10.1021/ic201376t.

[64] H. Furukawa, N. Ko, Y.B. Go, N. Aratani, S.B. Choi, E. Choi, A.Ö. Yazaydin, R. Q. Snurr, M. O'Keeffe, J. Kim, O.M. Yaghi, Ultrahigh porosity in metal-organic frameworks, Science 329 (2010) 424–428, https://doi.org/10.1126/science.1192160.

[65] O.K. Farha, I. Eryazici, N.C. Jeong, B.G. Hauser, C.E. Wilmer, A.A. Sarjeant, R. Q. Snurr, S.T. Nguyen, A.Ö. Yazaydin, J.T. Hupp, Metal-organic framework materials with ultrahigh surface areas: is the sky the limit? J. Am. Chem. Soc. 134 (2012) 15016–15021, https://doi.org/10.1021/ja3055639.

[66] R. Grünker, V. Bon, P. Müller, U. Stoeck, S. Krause, U. Mueller, I. Senkovska, S. Kaskel, A new metal-organic framework with ultra-high surface area, Chem. Commun. 50 (2014) 3450–3452, https://doi.org/10.1039/c4cc00113c.

[67] K. Koh, A.G. Wong-Foy, A.J. Matzger, A porous coordination copolymer with over 5000 m$^2$/g BET surface area, J. Am. Chem. Soc. 131 (2009) 4184–4185, https://doi.org/10.1021/ja809985t.

[68] J.L.C. Rowsell, O.M. Yaghi, Strategies for hydrogen storage in metal-organic frameworks, Angew. Chem. - Int. Ed. 44 (2005) 4670–4679, https://doi.org/10.1002/anie.200462786.

[69] J.L. Wang, C. Wang, W. Lin, Metal-organic frameworks for light harvesting and photocatalysis, ACS Catal. 2 (2012) 2630–2640, https://doi.org/10.1021/cs3005874.

[70] J. Gascon, A. Corma, F. Kapteijn, F.X. Llabrés, I. Xamena, Metal organic framework catalysis: quo vadis? ACS Catal. 4 (2014) 361–378, https://doi.org/10.1021/cs400959k.

[71] A. Corma, H. García, F.X. Llabrés, I. Xamena, Engineering metal organic frameworks for heterogeneous catalysis, Chem. Rev. 110 (2010) 4606–4655, https://doi.org/10.1021/cr9003924.

[72] R.C. Huxford, J. Della Rocca, W. Lin, Metal-organic frameworks as potential drug carriers, Curr. Opin. Chem. Biol. 14 (2010) 262–268, https://doi.org/10.1016/j.cbpa.2009.12.012.

[73] P. Horcajada, T. Chalati, C. Serre, B. Gillet, C. Sebrie, T. Baati, J.F. Eubank, D. Heurtaux, P. Clayette, C. Kreuz, J.S. Chang, Y.K. Hwang, V. Marsaud, P. N. Bories, L. Cynober, S. Gil, G. Férey, P. Couvreur, R. Gref, Porous metal-organic-framework nanoscale carriers as a potential platform for drug deliveryand imaging, Nat. Mater. 9 (2010) 172–178, https://doi.org/10.1038/nmat2608.

[74] J. Della Rocca, D. Liu, W. Lin, Nanoscale metal–organic frameworks for biomedical imaging and drug delivery, Acc. Chem. Res. 44 (2011) 957–968, https://doi.org/10.1021/ar200028a.

[75] I. Imaz, M. Rubio-Martínez, J. An, I. Solé-Font, N.L. Rosi, D. Maspoch, Metal-biomolecule frameworks (MBioFs), Chem. Commun. 47 (2011) 7287–7302, https://doi.org/10.1039/c1cc11202c.

[76] M.C. So, G.P. Wiederrecht, J.E. Mondloch, J.T. Hupp, O.K. Farha, Metal-organic framework materials for light-harvesting and energy transfer, Chem. Commun. 51 (2015) 3501–3510, https://doi.org/10.1039/c4cc09596k.

[77] D.E. Williams, N.B. Shustova, Metal-organic frameworks as a versatile tool to study and model energy transfer processes, Chem. Eur. J. 21 (2015) 15474–15479, https://doi.org/10.1002/chem.201502334.

[78] X. Zhao, X. Bu, T. Wu, S.T. Zheng, L. Wang, P. Feng, Selective anion exchange with nanogated isoreticular positive metal-organic frameworks, Nat. Commun. 4 (2013) 1–9, https://doi.org/10.1038/ncomms3344.

[79] A. Morozan, F. Jaouen, Metal organic frameworks for electrochemical applications, Energy Environ. Sci. 5 (2012) 9269–9290, https://doi.org/10.1039/c2ee22989g.

[80] J.E. Mondloch, M.J. Katz, W.C. Isley, P. Ghosh, P. Liao, W. Bury, G.W. Wagner, M.G. Hall, J.B. Decoste, G.W. Peterson, R.Q. Snurr, C.J. Cramer, J.T. Hupp, O.K. Farha, Destruction of chemical warfare agents using metal-organic frameworks, Nat. Mater. 14 (2015) 512–516, https://doi.org/10.1038/nmat4238.

[81] S.Y. Moon, Y. Liu, J.T. Hupp, O.K. Farha, Instantaneous hydrolysis of nerve-agent simulants with a six-connected zirconium-based metal-organic framework, Angew. Chem. - Int. Ed. 54 (2015) 6795–6799, https://doi.org/10.1002/anie.201502155.

[82] J.B. Decoste, G.W. Peterson, Metal-organic frameworks for air purification of toxic chemicals, Chem. Rev. 114 (2014) 5695–5727, https://doi.org/10.1021/cr4006473.

[83] A.J. Howarth, Y. Liu, J.T. Hupp, O.K. Farha, Metal-organic frameworks for applications in remediation of oxyanion/cation-contaminated water, CrystEngComm 17 (2015) 7245–7253, https://doi.org/10.1039/c5ce01428j.

[84] J. Zhang, J.M. Shreeve, 3D Nitrogen-rich metal-organic frameworks: opportunities for safer energetics, Dalton Trans. 45 (2016) 2363–2368, https://doi.org/10.1039/c5dt04456a.

[85] S.S. Nagarkar, A.V. Desai, S.K. Ghosh, Stimulus-responsive metal-organic frameworks, Chem. Asian J. 9 (2014) 2358–2376, https://doi.org/10.1002/asia.201402004.

[86] K. Sumida, D.L. Rogow, J.A. Mason, T.M. McDonald, E.D. Bloch, Z.R. Herm, T.-H. Bae, J.R. Long, Carbon dioxide capture in metal–organic frameworks, Chem. Rev. 112 (2012) 724–781, https://doi.org/10.1021/cr2003272.

[87] A.R. Millward, O.M. Yaghi, Metal-organic frameworks with exceptionally high capacity for storage of carbon dioxide at room temperature, J. Am. Chem. Soc. 127 (2005) 17998–17999, https://doi.org/10.1021/ja0570032.

[88] Z. Li, P. Liu, C. Ou, X. Dong, Porous metal-organic frameworks for carbon dioxide adsorption and separation at low pressure, ACS Sustain. Chem. Eng. 8 (2020) 15378–15404, https://doi.org/10.1021/acssuschemeng.0c05155.

[89] A. Schoedel, S. Rajeh, Why design matters: from decorated metal oxide clusters to functional metal–organic frameworks, Top. Curr. Chem. 378 (2020) 19, https://doi.org/10.1007/s41061-020-0281-0.

[90] M. Eddaoudi, D.B. Moler, H. Li, B. Chen, T.M. Reineke, M. O'Keeffe, O.M. Yaghi, Modular chemistry: secondary building units as a basis for the design of highly porous and robust metal-organic carboxylate frameworks, Acc. Chem. Res. 34 (2001) 319–330, https://doi.org/10.1021/ar000034b.

[91] M.J. Kalmutzki, N. Hanikel, O.M. Yaghi, Secondary building units as the turning point in the development of the reticular chemistry of MOFs, Sci. Adv. 4 (2018), eaat9180, https://doi.org/10.1126/sciadv.aat9180.

[92] Y. Liu, Z.U. Wang, H.-C. Zhou, Recent advances in carbon dioxide capture with metal-organic frameworks, Greenh. Gases: Sci. Technol. 2 (2012) 239–259, https://doi.org/10.1002/ghg.1296.

[93] C. Wang, D. Liu, W. Lin, Metal-organic frameworks as a tunable platform for designing functional molecular materials, J. Am. Chem. Soc. 135 (2013) 13222–13234, https://doi.org/10.1021/ja308229p.

[94] T. Islamoglu, S. Goswami, Z. Li, A.J. Howarth, O.K. Farha, J.T. Hupp, Postsynthetic tuning of metal-organic frameworks for targeted applications, Acc. Chem. Res 50 (2017) 805–813, https://doi.org/10.1021/acs.accounts.6b00577.

[95] M. Bosch, S. Yuan, W. Rutledge, H.C. Zhou, Stepwise synthesis of metal-organic frameworks, Acc. Chem. Res. 50 (2017) 857–865, https://doi.org/10.1021/acs.accounts.6b00457.

[96] J. Liu, P.K. Thallapally, B.P. Mc Grail, D.R. Brown, J. Liu, Progress in adsorption-based CO$_2$ capture by metal–organic frameworks, Chem. Soc. Rev. 41 (2012) 2308–2322, https://doi.org/10.1039/c1cs15221a.

[97] Y. Zhang, X. Cui, H. Xing, Recent advances in the capture and abatement of toxic gases and vapors by metal–organic frameworks, Mater. Chem. Front. 5 (2021) 5970–6013, https://doi.org/10.1039/d1qm00516b.

[98] S.E.M. Elhenawy, M. Khraisheh, F. Almomani, G. Walker, Metal-organic frameworks as a platform for CO$_2$ capture and chemical processes: adsorption, membrane separation, catalytic-conversion, and electrochemical reduction of CO$_2$, Catalysts 10 (2020) 1–33, https://doi.org/10.3390/catal10111293.

[99] S.R. Caskey, A.G. Wong-Foy, A.J. Matzger, Dramatic tuning of carbon dioxide uptake via metal substitution in a coordination polymer with cylindrical pores, J. Am. Chem. Soc. 130 (2008) 10870–10871, https://doi.org/10.1021/ja8036096.

[100] B. Arstad, H. Fjellvåg, K.O. Kongshaug, O. Swang, R. Blom, Amine functionalised metal organic frameworks (MOFs) as adsorbents for carbon dioxide, Adsorption 14 (2008) 755–762, https://doi.org/10.1007/s10450-008-9137-6.

[101] T.M. McDonald, W.R. Lee, J.A. Mason, B.M. Wiers, C.S. Hong, J.R. Long, Capture of carbon dioxide from air and flue gas in the alkylamine-appended metal-organic framework mmen-Mg $_2$(dobpdc), J. Am. Chem. Soc. 134 (2012) 7056–7065, https://doi.org/10.1021/ja300034j.

[102] P. Nugent, E.G. Giannopoulou, S.D. Burd, O. Elemento, E.G. Giannopoulou, K. Forrest, T. Pham, S. Ma, B. Space, L. Wojtas, M. Eddaoudi, M.J. Zaworotko, Porous materials with optimal adsorption thermodynamics and kinetics for co$_2$ separation, Nature 495 (2013) 80–84, https://doi.org/10.1038/nature11893.

[103] P.J. Milner, R.L. Siegelman, A.C. Forse, M.I. Gonzalez, T. Runčevski, J.D. Martell, J.A. Reimer, J.R. Long, A Diaminopropane-Appended Metal-Organic, Framework enabling efficient CO$_2$ capture from coal flue gas via a mixed adsorption mechanism, J. Am. Chem. Soc. 139 (2017) 13541–13553, https://doi.org/10.1021/jacs.7b07612.

[104] C.E. Bien, K.K. Chen, S.C. Chien, B.R. Reiner, L.C. Lin, C.R. Wade, W.S.W. Ho, Bioinspired metal-organic framework for trace CO$_2$ capture, J. Am. Chem. Soc. 140 (2018) 12662–12666, https://doi.org/10.1021/jacs.8b06109.

[105] Z.S. Wang, M. Li, Y.L. Peng, Z. Zhang, W. Chen, X.C. Huang, An ultrastable metal azolate framework with binding pockets for optimal carbon dioxide capture, Angew. Chem. - Int. Ed. 58 (2019) 16071–16076, https://doi.org/10.1002/anie.201909046.

[106] Z. Zhang, Q. Ding, J. Cui, X. Cui, H. Xing, High and selective capture of low-concentration CO$_2$ with an anion-functionalized ultramicroporous metal-organic framework, Sci. China Mater. 64 (2021) 691–697, https://doi.org/10.1007/s40843-020-1471-0.

[107] S.S.-Y. Chui, S.M.-F. Lo, J.P.H. Charmant, A.G. Orpen, I.D. Williams, A chemically functionalizable nanoporous material [Cu$_3$(TMA)$_2$(H$_2$O)$_3$]$_n$, Science 283 (1999) 1148–1150, https://doi.org/10.1126/science.283.5405.1148.

[108] P.D.C. Dietzel, R. Blom, H. Fjellvåg, Base-induced formation of two magnesium metal-organic framework compounds with a bifunctional tetratopic ligand, Eur. J. Inorg. Chem. 2008 (2008) 3624–3632, https://doi.org/10.1002/ejic.200701284.

[109] T. Loiseau, C. Serre, C. Huguenard, G. Fink, F. Taulelle, M. Henry, T. Bataille, G. Férey, A rationale for the large breathing of the porous aluminum terephthalate (MIL-53) upon hydration, Chem. Eur. J. 10 (2004) 1373–1382, https://doi.org/10.1002/chem.200305413.

[110] C.R. Groom, I.J. Bruno, M.P. Lightfoot, S.C. Ward, The cambridge structural database, Acta Crystallogr. B Struct. Sci. Cryst. Eng. Mater. 72 (2016) 171–179, https://doi.org/10.1107/S2052520616003954.

[111] C.F. Macrae, I.J. Bruno, J.A. Chisholm, P.R. Edgington, P. McCabe, E. Pidcock, L. Rodriguez-Monge, R. Taylor, J. van de Streek, P.A. Wood, Mercury CSD 2.0 - new features for the visualization and investigation of crystal structures, J. Appl. Crystallogr. 41 (2008) 466–470, https://doi.org/10.1107/S0021889807067908.

[112] Z. Hu, Y. Wang, B.B. Shah, D. Zhao, CO$_2$ capture in metal-organic framework adsorbents: an engineering perspective, Adv. Sustain. Syst. 3 (2019) 1800080, https://doi.org/10.1002/adsu.201800080.

[113] J. Yu, L.H. Xie, J.R. Li, Y. Ma, J.M. Seminario, P.B. Balbuena, CO$_2$ capture and separations using MOFs: Computational and experimental studies, Chem. Rev. 117 (2017) 9674–9754, https://doi.org/10.1021/acs.chemrev.6b00626.

[114] J.H. Choe, H. Kim, C.S. Hong, MOF-74 type variants for CO$_2$ capture, Mater. Chem. Front. 5 (2021) 5172–5185, https://doi.org/10.1039/d1qm00205h.

[115] R. Custelcean, Direct air capture of CO$_2$: via crystal engineering, Chem. Sci. 12 (2021) 12518–12528, https://doi.org/10.1039/d1sc04097a.

[116] W.L. Queen, M.R. Hudson, E.D. Bloch, J.A. Mason, M.I. Gonzalez, J.S. Lee, D. Gygi, J.D. Howe, K. Lee, T.A. Darwish, M. James, V.K. Peterson, S.J. Teat, B. Smit, J.B. Neaton, J.R. Long, C.M. Brown, Comprehensive study of carbon dioxide adsorption in the metal-organic frameworks M$_2$(dobdc) (M = Mg, Mn, Fe, Co, Ni, Cu, Zn), Chem. Sci. 5 (2014) 4569–4581, https://doi.org/10.1039/c4sc02064b.

[117] X. Wu, Z. Bao, B. Yuan, J. Wang, Y. Sun, H. Luo, S. Deng, Microwave synthesis and characterization of MOF-74 (M = Ni, Mg) for gas separation, Microporous Mesoporous Mater. 180 (2013) 114–122, https://doi.org/10.1016/j.micromeso.2013.06.023.

[118] L. Valenzano, B. Civalleri, S. Chavan, G.T. Palomino, C.O. Areán, S. Bordiga, Computational and experimental studies on the adsorption of CO, N$_2$, and CO$_2$ on Mg-MOF-74, J. Phys. Chem. C 114 (2010) 11185–11191, https://doi.org/10.1021/jp102574f.

[119] A.Ö. Yazaydin, R.Q. Snurr, T.H. Park, K. Koh, J. Liu, M.D. LeVan, A.I. Benin, P. Jakubczak, M. Lanuza, D.B. Galloway, J.J. Low, R.R. Willis, Screening of metal-organic frameworks for carbon dioxide capture from flue gas using a combined experimental and modeling approach, J. Am. Chem. Soc. 131 (2009) 18198–18199, https://doi.org/10.1021/ja9057234.

[120] P.J. Milner, J.D. Martell, R.L. Siegelman, D. Gygi, S.C. Weston, J.R. Long, Overcoming double-step CO$_2$ adsorption and minimizing water co-adsorption in bulky diamine-appended variants of Mg$_2$(dobpdc), Chem. Sci. 9 (2017) 160–174, https://doi.org/10.1039/c7sc04266c.

[121] G.Y. Yoo, W.R. Lee, H. Jo, J. Park, J.H. Song, K.S. Lim, D. Moon, H. Jung, J. Lim, S.S. Han, Y. Jung, C.S. Hong, Adsorption of carbon dioxide on unsaturated metal sites in M$_2$(dobpdc) frameworks with exceptional structural stability and relation between lewis acidity and adsorption enthalpy, Chem. Eur. J. 22 (2016) 7444–7451, https://doi.org/10.1002/chem.201600189.

[122] K.S. Lim, W.R. Lee, H.G. Lee, D.W. Kang, J.H. Song, J. Hilgar, J.D. Rinehart, D. Moon, C.S. Hong, Control of interchain antiferromagnetic coupling in porous Co(II)-based metal-organic frameworks by tuning the aromatic linker length: how

far does magnetic interaction propagate? Inorg. Chem. 56 (2017) 7443–7448, https://doi.org/10.1021/acs.inorgchem.7b00899.

[123] J.S. Yeon, W.R. Lee, N.W. Kim, H. Jo, H. Lee, J.H. Song, K.S. Lim, D.W. Kang, J. G. Seo, D. Moon, B. Wiers, C.S. Hong, Homodiamine-functionalized metal-organic frameworks with a MOF-74-type extended structure for superior selectivity of $CO_2$ over $N_2$, J. Mater. Chem. A Mater. 3 (2015) 19177–19185, https://doi.org/10.1039/c5ta02357b.

[124] H.H. Wang, L. Hou, Y.Z. Li, C.Y. Jiang, Y.Y. Wang, Z. Zhu, Porous MOF with highly efficient selectivity and chemical conversion for $CO_2$, ACS Appl. Mater. Interfaces 9 (2017) 17969–17976, https://doi.org/10.1021/acsami.7b03835.

[125] T. Zurrer, K. Wong, J. Horlyck, E.C. Lovell, J. Wright, N.M. Bedford, Z. Han, K. Liang, J. Scott, R. Amal, Mixed-metal MOF-74 templated catalysts for efficient carbon dioxide capture and methanation, Adv. Funct. Mater. 31 (2021) 1–12, https://doi.org/10.1002/adfm.202007624.

[126] S. Abednatanzi, P. Gohari Derakhshandeh, H. Depauw, F.X. Coudert, H. Vrielinck, P. Van Der Voort, K. Leus, Mixed-metal metal–organic frameworks, Chem. Soc. Rev. 48 (2019) 2535–2565, https://doi.org/10.1039/c8cs00337h.

[127] M.Y. Masoomi, A. Morsali, A. Dhakshinamoorthy, H. Garcia, Mixed-metal MOFs: unique opportunities in metal–organic framework (MOF) functionality and design, Angew. Chem. - Int. Ed. 58 (2019) 15188–15205, https://doi.org/10.1002/anie.201902229.

[128] D. Kim, A. Coskun, Template-directed approach towards the realization of ordered heterogeneity in bimetallic metal–organic frameworks, Angew. Chem. - Int. Ed. 56 (2017) 5071–5076, https://doi.org/10.1002/anie.201702501.

[129] H. Kim, H.Y. Lee, D.W. Kang, M. Kang, J.H. Choe, W.R. Lee, C.S. Hong, Control of the metal composition in bimetallic Mg/Zn(dobpdc) constructed from a one-dimensional Zn-based template, Inorg. Chem. 58 (2019) 14107–14111, https://doi.org/10.1021/acs.inorgchem.9b02126.

[130] V.A. Bolotov, K.A. Kovalenko, D.G. Samsonenko, X. Han, X. Zhang, G.L. Smith, L. J. McCormick, S.J. Teat, S. Yang, M.J. Lennox, A. Henley, E. Besley, V.P. Fedin, D. N. Dybtsev, M. Schröder, Enhancement of $CO_2$ uptake and selectivity in a metal-organic framework by the incorporation of thiophene functionality, Inorg. Chem. 57 (2018) 5074–5082, https://doi.org/10.1021/acs.inorgchem.8b00138.

[131] A.C. Kizzie, A.G. Wong-Foy, A.J. Matzger, Effect of humidity on the performance of microporous coordination polymers as adsorbents for $CO_2$ capture, Langmuir 27 (2011) 6368–6373, https://doi.org/10.1021/la200547k.

[132] S. Keskin, T.M. van Heest, D.S. Sholl, Can metal-organic framework materials play a useful role in large-scale carbon dioxide separations, ChemSusChem 3 (2010) 879–891, https://doi.org/10.1002/cssc.201000114.

[133] Y. Jiao, C.R. Morelock, N.C. Burtch, W.P. Mounfield, J.T. Hungerford, K. S. Walton, Tuning the kinetic water stability and adsorption interactions of Mg-MOF-74 by partial substitution with Co or Ni, Ind. Eng. Chem. Res. 54 (2015) 12408–12414, https://doi.org/10.1021/acs.iecr.5b03843.

[134] J.B. Decoste, G.W. Peterson, B.J. Schindler, K.L. Killops, M.A. Browe, J.J. Mahle, The effect of water adsorption on the structure of the carboxylate containing metal-organic frameworks Cu-BTC, Mg-MOF-74, and UiO-66, J. Mater. Chem. A 1 (2013) 11922–11932. ⟨https://doi.org/10.1039/c3ta12497e⟩.

[135] R.A. Maia, B. Louis, W. Gao, Q. Wang, $CO_2$ adsorption mechanisms on MOFs: a case study of open metal sites, ultra-microporosity and flexible framework, React. Chem. Eng. 6 (2021) 1118–1133, https://doi.org/10.1039/d1re00090j.

[136] D. Bernin, N. Hedin, Perspectives on NMR studies of $CO_2$ adsorption, Curr. Opin. Colloid Interface Sci. 33 (2018) 53–62, https://doi.org/10.1016/j.cocis.2018.02.003.

[137] E. Fuentes-Fernandez, S. Jensen, K. Tan, S. Zuluaga, H. Wang, J. Li, T. Thonhauser, Y. Chabal, Controlling chemical reactions in confined environments: water dissociation in MOF-74, Appl. Sci. 8 (2018) 270, https://doi.org/10.3390/app8020270.

[138] S. Xiang, Y. He, Z. Zhang, H. Wu, W. Zhou, R. Krishna, B. Chen, Microporous metal-organic framework with potential for carbon dioxide capture at ambient conditions, Nat. Commun. 3 (2012) 954, https://doi.org/10.1038/ncomms1956.

[139] A. Masala, J.G. Vitillo, G. Mondino, C.A. Grande, R. Blom, M. Manzoli, M. Marshall, S. Bordiga, $CO_2$ capture in dry and wet conditions in UTSA-16 metal-organic framework, ACS Appl. Mater. Interfaces 9 (2017) 455–463, https://doi.org/10.1021/acsami.6b13216.

[140] S. Gaikwad, S.-J. Kim, S. Han, Novel metal–organic framework of UTSA-16 (Zn) synthesized by a microwave method: outstanding performance for $CO_2$ capture with improved stability to acid gases, J. Ind. Eng. Chem. 87 (2020) 250–263, https://doi.org/10.1016/j.jiec.2020.04.015.

[141] Y. Zheng, X. Xu, X. Zhang, L. Qin, Y. Lu, G. Zhang, Design of metal-organic frameworks with high low pressure adsorption performance of $CO_2$, IOP Conf. Ser. Earth Environ. Sci. 170 (2018) 032073, https://doi.org/10.1088/1755-1315/170/3/032073.

[142] M. Ding, X. Cai, H.L. Jiang, Improving MOF stability: approaches and applications, Chem. Sci. 10 (2019) 10209–10230, https://doi.org/10.1039/c9sc03916c.

[143] Z. Hu, S. Faucher, Y. Zhuo, Y. Sun, S. Wang, D. Zhao, Combination of optimization and metalated-ligand exchange: an effective approach to functionalize UiO-66(Zr) MOFs for $CO_2$ separation, Chem. - A Eur. J. 21 (2015) 17246–17255, https://doi.org/10.1002/chem.201503078.

[144] O. Shekhah, Y. Belmabkhout, Z. Chen, V. Guillerm, A. Cairns, K. Adil, M. Eddaoudi, Made-to-order metal-organic frameworks for trace carbon dioxide removal and air capture, Nat. Commun. 5 (2014) 1–7, https://doi.org/10.1038/ncomms5228.

[145] P.M. Bhatt, Y. Belmabkhout, A. Cadiau, K. Adil, O. Shekhah, A. Shkurenko, L. J. Barbour, M. Eddaoudi, A. Fine-Tuned, Fluorinated MOF addresses the needs for

trace $CO_2$ removal and air capture using physisorption, J. Am. Chem. Soc. 138 (2016) 9301–9307, https://doi.org/10.1021/jacs.6b05345.

[146] A. Kumar, C. Hua, D.G. Madden, D. O'Nolan, K.J. Chen, L.A.J. Keane, J.J. Perry, M.J. Zaworotko, Hybrid ultramicroporous materials (HUMs) with enhanced stability and trace carbon capture performance, Chem. Commun. 53 (2017) 5946–5949, https://doi.org/10.1039/c7cc02289a.

[147] M. Jiang, B. Li, X. Cui, Q. Yang, Z. Bao, Y. Yang, H. Wu, W. Zhou, B. Chen, H. Xing, Controlling pore shape and size of interpenetrated anion-pillared ultramicroporous materials enables molecular sieving of $CO_2$ combined with ultrahigh uptake capacity, ACS Appl. Mater. Interfaces 10 (2018) 16628–16635, https://doi.org/10.1021/acsami.8b03358.

[148] S. Mukherjee, N. Sikdar, D. O'Nolan, D.M. Franz, V. Gascón, A. Kumar, N. Kumar, H.S. Scott, D.G. Madden, P.E. Kruger, B. Space, M.J. Zaworotko, Trace $CO_2$ capture by an ultramicroporous physisorbent with low water affinity, Sci. Adv. 5 (2019) 1–8, https://doi.org/10.1126/sciadv.aax9171.

[149] W. Liang, P.M. Bhatt, A. Shkurenko, K. Adil, G. Mouchaham, H. Aggarwal, A. Mallick, A. Jamal, Y. Belmabkhout, M. Eddaoudi, A tailor-made interpenetrated MOF with exceptional carbon-capture performance from flue gas, Chem 5 (2019) 950–963, https://doi.org/10.1016/j.chempr.2019.02.007.

[150] A. Kumar, D.G. Madden, M. Lusi, K.J. Chen, E.A. Daniels, T. Curtin, J.J. Perry, M. J. Zaworotko, Direct air capture of $CO_2$ by physisorbent materials, Angew. Chem. - Int. Ed. 54 (2015) 14372–14377, https://doi.org/10.1002/anie.201506952.

[151] M. Märcz, R.E. Johnsen, P.D.C. Dietzel, H. Fjellvåg, The iron member of the CPO-27 coordination polymer series: synthesis, characterization, and intriguing redox properties, Microporous Mesoporous Mater. 157 (2012) 62–74, https://doi.org/10.1016/j.micromeso.2011.12.035.

[152] C. Chen, N. Feng, Q. Guo, Z. Li, X. Li, J. Ding, L. Wang, H. Wan, G. Guan, Surface engineering of a chromium metal-organic framework with bifunctional ionic liquids for selective $CO_2$ adsorption: synergistic effect between multiple active sites, J. Colloid Interface Sci. 521 (2018) 91–101, https://doi.org/10.1016/j.jcis.2018.03.029.

[153] D. Britt, H. Furukawa, B. Wang, T.G. Glover, O.M. Yaghi, Highly efficient separation of carbon dioxide by a metal-organic framework replete with open metal sites, Proc. Natl. Acad. Sci. U.S.A. 106 (2009) 20637–20640, https://doi.org/10.1073/pnas.0909719106.

[154] Z. Bao, L. Yu, Q. Ren, X. Lu, S. Deng, Adsorption of $CO_2$ and $CH_4$ on a magnesium-based metal organic framework, J. Colloid Interface Sci. 353 (2011) 549–556, https://doi.org/10.1016/j.jcis.2010.09.065.

[155] D.G. Madden, H.S. Scott, A. Kumar, K. Chen, R. Sanii, A. Bajpai, M. Lusi, T. Curtin, J.J. Perry, M.J. Zaworotko, Flue-gas and direct-air capture of $CO_2$ by porous metal–organic materials, Philos. Trans. R. Soc. A: Math. Phys. Eng. Sci. 375 (2017) 20160025, https://doi.org/10.1098/rsta.2016.0025.

[156] M.E. Braun, C.D. Steffek, J. Kim, P.G. Rasmussen, O.M. Yaghi, 1,4-Benzenedicarboxylate derivatives as links in the design of paddle-wheel units and metal-organic frameworks, Chem. Commun. 2 (2001) 2532–2533, https://doi.org/10.1039/B108031H.

[157] M. Eddaoudi, J. Kim, N. Rosi, D. Vodak, J. Wachter, M. O'Keeffe, O.M. Yaghi, Systematic design of pore size and functionality in isoreticular MOFs and their application in methane storage, Science 295 (2002) 469–472, https://doi.org/10.1126/science.1067208.

[158] S. Ullah, M.A. Bustam, M.A. Assiri, A.G. Al-Sehemi, F.A. Abdul Kareem, A. Mukhtar, M. Ayoub, G. Gonfa, Synthesis and characterization of iso-reticular metal-organic framework-3 (IRMOF-3) for $CO_2$/$CH_4$ adsorption: impact of post-synthetic aminomethyl propanol (AMP) functionalization, J. Nat. Gas Sci. Eng. 72 (2019), 103014, https://doi.org/10.1016/j.jngse.2019.103014.

[159] S. Ding, Q. Dong, J. Hu, W. Xiao, X. Liu, L. Liao, N. Zhang, Enhanced selective adsorption of $CO_2$ on nitrogen-doped porous carbon monoliths derived from IRMOF-3, Chem. Commun. 52 (2016) 9757–9760, https://doi.org/10.1039/C6CC04416F.

[160] G. Férey, C. Mellot-Draznieks, C. Serre, F. Millange, J. Dutour, S. Surblé, I. Margiolaki, A Chromium terephthalate-based solid with unusually large pore volumes and surface area, Science 309 (2005) 2040–2042. ⟨https://doi.org/10.1126/science.1116275⟩.

[161] Y. Lin, C. Kong, L. Chen, Direct synthesis of amine-functionalized MIL-101(Cr) nanoparticles and application for $CO_2$ capture, RSC Adv. 2 (2012) 6417–6419, https://doi.org/10.1039/c2ra20641b.

[162] A. Khutia, H.U. Rammelberg, T. Schmidt, S. Henninger, C. Janiak, Water sorption cycle measurements on functionalized MIL-101Cr for aplication, Chem. Mater. 25 (2013) 790–798, https://doi.org/10.1021/cm304055k.

[163] X. Li, Y. Mao, K. Leng, G. Ye, Y. Sun, W. Xu, Synthesis of amino-functionalized MIL-101 (Cr) with large surface area, Mater. Lett. 197 (2017) 192–195, https://doi.org/10.1016/j.matlet.2017.03.034.

[164] D. Jiang, L.L. Keenan, A.D. Burrows, K.J. Edler, Synthesis and post-synthetic modification of MIL-101(Cr)-$NH_2$ via a tandem diazotisation process, Chem. Commun. 48 (2012) 12053, https://doi.org/10.1039/c2cc36344e.

[165] P. Serra-Crespo, E.V. Ramos-Fernandez, J. Gascon, F. Kapteijn, Synthesis and characterization of an amino functionalized MIL-101(Al): separation and catalytic properties, Chem. Mater. 23 (2011) 2565–2572, https://doi.org/10.1021/cm103644b.

[166] Y. Fu, D. Sun, Y. Chen, R. Huang, Z. Ding, X. Fu, Z. Li, An amine-functionalized titanium metal-organic framework photocatalyst with visible-light-induced activity for $CO_2$ reduction, Angew. Chem. Int. Ed. 51 (2012) 3364–3367, https://doi.org/10.1002/anie.201108357.

[167] F. Zhang, X. Zou, X. Gao, S. Fan, F. Sun, H. Ren, G. Zhu, Hydrogen selective $NH_2$-MIL-53(Al) MOF membranes with high permeability, Adv. Funct. Mater. 22 (2012) 3583–3590, https://doi.org/10.1002/adfm.201200084.

[168] S. Couck, J.F.M. Denayer, G.V. Baron, T. Rémy, J. Gascon, F. Kapteijn, An amine-functionalized MIL-53 metal-organic framework with large separation power for $CO_2$ and $CH_4$, J. Am. Chem. Soc. 131 (2009) 6326–6327, https://doi.org/10.1021/ja900555r.

[169] X. Si, C. Jiao, F. Li, J. Zhang, S. Wang, S. Liu, Z. Li, L. Sun, F. Xu, Z. Gabelica, C. Schick, High and selective $CO_2$ uptake, $H_2$ storage and methanol sensing on the amine-decorated 12-connected MOF CAU-1, Energy Environ. Sci. 4 (2011) 4522–4527, https://doi.org/10.1039/c1ee01380g.

[170] G.E. Cmarik, M. Kim, S.M. Cohen, K.S. Walton, Tuning the adsorption properties of UiO-66 via ligand functionalization, Langmuir 28 (2012) 15606–15613, https://doi.org/10.1021/la3035352.

[171] K. Peikert, F. Hoffmann, M. Fröba, Amino substituted Cu3(btc)2: a new metal–organic framework with a versatile functionality, Chem. Commun. 48 (2012) 11196–11198, https://doi.org/10.1039/c2cc36220a.

[172] G. Ortiz, G. Chaplais, J.-L. Paillaud, H. Nouali, J. Patarin, J. Raya, C. Marichal, New insights into the hydrogen bond network in Al-MIL-53 and Ga-MIL-53, J. Phys. Chem. C 118 (2014) 22021–22029, https://doi.org/10.1021/jp505893s.

[173] M.W. Logan, S. Ayad, J.D. Adamson, T. Dilbeck, K. Hanson, F.J. Uribe-Romo, Systematic variation of the optical bandgap in titanium based isoreticular metal-organic frameworks for photocatalytic reduction of $CO_2$ under blue light, J. Mater. Chem. A 5 (2017) 11854–11863, https://doi.org/10.1039/c7ta00437k.

[174] S. SinghDhankhar, N. Sharma, S. Kumar, T.J. DhilipKumar, C.M. Nagaraja, Rational design of a bifunctional, two-fold interpenetrated $Zn^{II}$ -metal–organic framework for selective adsorption of $CO_2$ and efficient aqueous phase sensing of 2,4,6–trinitrophenol, Chem. Eur. J. 23 (2017) 16204–16212, https://doi.org/10.1002/chem.201703384.

[175] R. Das, S.S. Dhankhar, C.M. Nagaraja, Construction of a bifunctional Zn(ii)-organic framework containing a basic amine functionality for selective capture and room temperature fixation of $CO_2$, Inorg. Chem. Front. 7 (2019) 72–81, https://doi.org/10.1039/c9qi01058k.

[176] R. Das, D. Muthukumar, R.S. Pillai, C.M. Nagaraja, Rational design of a $Zn^{II}$ MOF with multiple functional sites for highly efficient fixation of $CO_2$ under mild conditions: combined experimental and theoretical investigation, Chem. - A Eur. J. 26 (2020) 17445–17454, https://doi.org/10.1002/chem.202002688.

[177] L. Liang, C. Liu, F. Jiang, Q. Chen, L. Zhang, H. Xue, H.-L. Jiang, J. Qian, D. Yuan, M. Hong, Carbon dioxide capture and conversion by an acid-base resistant metal-organic framework, Nat. Commun. 8 (2017) 1233, https://doi.org/10.1038/s41467-017-01166-3.

[178] Z. Lu, F. Meng, L. Du, W. Jiang, H. Cao, J. Duan, H. Huang, H. He, A free tetrazolyl decorated metal-organic framework exhibiting high and selective $CO_2$ adsorption, Inorg. Chem. 57 (2018) 14018–14022, https://doi.org/10.1021/acs.inorgchem.8b02031.

[179] Z. Lu, J. Zhang, Z. Duan, L. Du, C. Hang, Pore space partition via secondary metal ions entrapped by pyrimidine hooks: influences on structural flexibility and carbon dioxide capture, J. Mater. Chem. A 5 (2017) 17287–17292, https://doi.org/10.1039/C7TA02852K.

[180] S. Jeong, D. Kim, S. Shin, D. Moon, S.J. Cho, M.S. Lah, Combinational synthetic approaches for isoreticular and polymorphic metal-organic frameworks with tuned pore geometries and surface properties, Chem. Mater. 26 (2014) 1711–1719, https://doi.org/10.1021/cm404239s.

[181] P.Z. Li, X.J. Wang, J. Liu, J.S. Lim, R. Zou, Y. Zhao, A Triazole-Containing Metal-Organic, Framework as a highly effective and substrate size-dependent catalyst for $CO_2$ conversion, J. Am. Chem. Soc. 138 (2016) 2142–2145, https://doi.org/10.1021/jacs.5b13335.

[182] J. An, S.J. Geib, N.L. Rosi, High and selective $CO_2$ uptake in a cobalt adeninate metal−organic framework exhibiting pyrimidine- and amino-decorated pores, J. Am. Chem. Soc. 132 (2010) 38–39, https://doi.org/10.1021/ja909169x.

[183] Y. Chen, J. Jiang, A bio-metal-organic framework for highly selective $CO_2$ capture: a molecular simulation study, ChemSusChem 3 (2010) 982–988, https://doi.org/10.1002/cssc.201000080.

[184] C. Chen, Q. Jiang, H. Xu, Z. Lin, Highly efficient synthesis of a moisture-stable nitrogen-abundant metal-organic framework (MOF) for large-scale $CO_2$ capture, Ind. Eng. Chem. Res. 58 (2019) 1773–1777, https://doi.org/10.1021/acs.iecr.8b05239.

[185] D.K. Maity, A. Dey, S. Ghosh, A. Halder, P.P. Ray, D. Ghoshal, Set of multifunctional azo functionalized semiconducting Cd(II)-MOFs showing photoswitching property and selective $CO_2$ adsorption, Inorg. Chem. 57 (2018) 251–263, https://doi.org/10.1021/acs.inorgchem.7b02435.

[186] B. Bhattacharya, R. Dey, P. Pachfule, R. Banerjee, D. Ghoshal, Four 3D Cd(II)-based metal organic hybrids with different N,N′-donor spacers: syntheses, characterizations, and selective gas adsorption properties, Cryst. Growth Des. 13 (2013) 731–739, https://doi.org/10.1021/cg3014464.

[187] L.W. Lee, T.T. Luo, S.H. Lo, G.H. Lee, S.M. Peng, Y.H. Liu, S.L. Lee, K.L. Lu, Pillared-bilayer zinc(ii)-organic laminae: pore modification and selective gas adsorption, CrystEngComm 17 (2015) 6320–6327, https://doi.org/10.1039/c5ce00923e.

[188] C.M. Nagaraja, R. Haldar, T.K. Maji, C.N.R. Rao, Chiral porous metal-organic frameworks of Co(II) and Ni(II): Synthesis, structure, magnetic properties, and $CO_2$ uptake, Cryst. Growth Des. 12 (2012) 975–981, https://doi.org/10.1021/cg201447c.

[189] N. Sharma, S.S. Dhankhar, S. Kumar, T.J.D. Kumar, C.M. Nagaraja, Rational design of a 3D $Mn^{II}$ -metal-organic framework based on a nonmetallated porphyrin linker for selective capture of $CO_2$ and one-pot synthesis of styrene carbonates, Chem. Eur. J. 24 (2018) 16662–16669, https://doi.org/10.1002/chem.201803842.

[190] C. Song, J. Hu, Y. Ling, Y. Feng, R. Krishna, D.L. Chen, Y. He, The accessibility of nitrogen sites makes a difference in selective $CO_2$ adsorption of a family of isostructural metal-organic frameworks, J. Mater. Chem. A 3 (2015) 19417–19426, https://doi.org/10.1039/c5ta05481h.

[191] S. Chand, A. Pal, R. Saha, P. Das, R. Sahoo, P.K. Chattaraj, M.C. Das, Two closely related Zn(II)-MOFs for their large difference in $CO_2$ uptake capacities and selective $CO_2$ sorption, Inorg. Chem. 59 (2020) 7056–7066, https://doi.org/10.1021/acs.inorgchem.0c00551.

[192] N. Gcwensa, C.L. Oliver, Large differences in carbon dioxide and water sorption capabilities in a system of closely related isoreticular Cd(II)-based mixed-ligand metal-organic frameworks, Inorg. Chem. 59 (2020) 13211–13222, https://doi.org/10.1021/acs.inorgchem.0c01533.

[193] O.T. Qazvini, S.G. Telfer, A robust metal-organic framework for post-combustion carbon dioxide capture, J. Mater. Chem. A 8 (2020) 12028–12034, https://doi.org/10.1039/d0ta04121a.

[194] J.R. Li, J. Yu, W. Lu, L.B. Sun, J. Sculley, P.B. Balbuena, H.C. Zhou, Porous materials with pre-designed single-molecule traps for $CO_2$ selective adsorption, Nat. Commun. 4 (2013) 1–8, https://doi.org/10.1038/ncomms2552.

[195] X. Song, M. Zhang, J. Duan, J. Bai, Constructing and finely tuning the $CO_2$ traps of stable and various-pore-containing MOFs towards highly selective $CO_2$ capture, Chem. Commun. 55 (2019) 3477–3480, https://doi.org/10.1039/c8cc10116g.

[196] R. Vaidhyanathan, S.S. Iremonger, K.W. Dawson, G.K.H. Shimizu, An amine-functionalized metal organic framework for preferential $CO_2$ adsorption at low pressures, Chem. Commun. (2009) 5230–5232, https://doi.org/10.1039/b911481e.

[197] B. Li, Z. Zhang, Y. Li, K. Yao, Y. Zhu, Z. Deng, F. Yang, X. Zhou, G. Li, H. Wu, N. Nijem, Y.J. Chabal, Z. Lai, Y. Han, Z. Shi, S. Feng, J. Li, Enhanced binding affinity, remarkable selectivity, and high capacity of $CO_2$ by dual functionalization of a rht-type metal-organic framework, Angew. Chem. - Int. Ed. 51 (2012) 1412–1415, https://doi.org/10.1002/anie.201105966.

[198] P.Q. Liao, D.D. Zhou, A.X. Zhu, L. Jiang, R.B. Lin, J.P. Zhang, X.M. Chen, Strong and dynamic $CO_2$ sorption in a flexible porous framework possessing guest chelating claws, J. Am. Chem. Soc. 134 (2012) 17380–17383, https://doi.org/10.1021/ja3073512.

[199] L. Pei-Qin, C. Xiao-Ming, Post-synthetic coordination modification of robust pillared-rod metal-azolate frameworks for diversified applications, Bull. Jpn Soc. Coord. Chem. 77 (2021) 3–10, https://doi.org/10.4019/bjscc.77.3.

[200] T. He, X.J. Kong, J.R. Li, Chemically stable metal-organic frameworks: rational construction and application expansion, Acc. Chem. Res. 54 (2021) 3083–3094, https://doi.org/10.1021/acs.accounts.1c00280.

[201] S. Nandi, P. De Luna, T.D. Daff, J. Rother, M. Liu, W. Buchanan, A.I. Hawari, T. K. Woo, R. Vaidhyanathan, A single-ligand ultra-microporous MOF for precombustion $CO_2$ capture and hydrogen purification, Sci. Adv. 1 (2015) 1–10, https://doi.org/10.1126/sciadv.1500421.

[202] Z. Lu, F. Meng, L. Du, W. Jiang, H. Cao, J. Duan, H. Huang, H. He, A free tetrazolyl decorated metal–organic framework exhibiting high and selective $CO_2$ adsorption, Inorg. Chem. 57 (2018) 14018–14022, https://doi.org/10.1021/acs.inorgchem.8b02031.

[203] S. Nandi, U. Werner-Zwanziger, R. Vaidhyanathan, A triazine-resorcinol based porous polymer with polar pores and exceptional surface hydrophobicity showing $CO_2$ uptake under humid conditions, J. Mater. Chem. A 3 (2015) 21116–21122, https://doi.org/10.1039/c5ta04241k.

[204] X. Luo, L. Sun, J. Zhao, D.S. Li, D. Wang, G. Li, Q. Huo, Y. Liu, Three metal-organic frameworks based on binodal inorganic building units and hetero-O, N donor ligand: solvothermal syntheses, structures, and gas sorption properties, Cryst. Growth Des. 15 (2015) 4901–4907, https://doi.org/10.1021/acs.cgd.5b00791.

[205] Y. Ye, H. Zhang, L. Chen, S. Chen, Q. Lin, F. Wei, Z. Zhang, S. Xiang, Metal-organic framework with rich accessible nitrogen sites for highly efficient $CO_2$ capture and separation, Inorg. Chem. 58 (2019) 7754–7759, https://doi.org/10.1021/acs.inorgchem.9b00182.

[206] D. Kim, J. Park, Y.S. Kim, M.S. Lah, Temperature dependent $CO_2$ behavior in microporous 1-D channels of a metal-organic framework with multiple interaction sites, Sci. Rep. 7 (2017) 6–12, https://doi.org/10.1038/srep41447.

[207] Q. Li, M.H. Yu, J. Xu, A.L. Li, T.L. Hu, X.H. Bu, Two new metal-organic frameworks based on tetrazole-heterocyclic ligands accompanied by in situ ligand formation, Dalton Trans. 46 (2017) 3223–3228, https://doi.org/10.1039/c7dt00005g.

[208] Y.H. Tang, F. Wang, J.X. Liu, J. Zhang, Diverse tetrahedral tetrazolate frameworks with N-rich surface, Chem. Commun. 52 (2016) 5625–5628, https://doi.org/10.1039/c6cc00589f.

[209] S.J. Bao, R. Krishna, Y.B. He, J.S. Qin, Z.M. Su, S.L. Li, W. Xie, D.Y. Du, W.W. He, S.R. Zhang, Y.Q. Lan, A stable metal-organic framework with suitable pore sizes and rich uncoordinated nitrogen atoms on the internal surface of micropores for highly efficient $CO_2$ capture, J. Mater. Chem. A 3 (2015) 7361–7367, https://doi.org/10.1039/c5ta00256g.

[210] G. Orcajo, G. Calleja, J.A. Botas, L. Wojtas, M.H. Alkordi, M. Sánchez-Sánchez, Rationally designed nitrogen-rich metal–organic cube material: an efficient $CO_2$ adsorbent and $H_2$ confiner, Cryst. Growth Des. 14 (2014) 739–746, https://doi.org/10.1021/cg401613w.

[211] J.S. Qin, D.Y. Du, W.L. Li, J.P. Zhang, S.L. Li, Z.M. Su, X.L. Wang, Q. Xu, K. Z. Shao, Y.Q. Lan, N-rich zeolite-like metal–organic framework with sodalite topology: high $CO_2$ uptake, selective gas adsorption and efficient drug delivery, Chem. Sci. 3 (2012) 2114–2118, https://doi.org/10.1039/c2sc00017b.

[212] P. Cui, Y.G. Ma, H.H. Li, B. Zhao, J.R. Li, P. Cheng, P.B. Balbuena, H.C. Zhou, Multipoint interactions enhanced $CO_2$ uptake: a zeolite-like zinc-tetrazole

framework with 24-nuclear zinc cages, J. Am. Chem. Soc. 134 (2012) 18892–18895, https://doi.org/10.1021/ja3063138.

[213] D. Song, B. Li, Y. Li, X. Li, F. Yang, G. Zeng, Y. Peng, Z. Zhang, G. Li, Z. Shi, S. Feng, An N-rich metal-organic framework with an rht topology: high $CO_2$ and $C_2$ hydrocarbons uptake and selective capture from $CH_4$, Chem. Commun. 50 (2014) 5031–5033, https://doi.org/10.1039/c4cc00375f.

[214] R. Vaidhyanathan, S.S. Iremonger, G.K.H. Shimizu, P.G. Boyd, S. Alavi, T.K. Woo, Direct observation and quantification of $CO_2$ binding within an amine-functionalized nanoporous solid, Science 330 (2010) 650–653, https://doi.org/10.1126/science.1194237.

[215] R. Vaidhyanathan, S.S. Iremonger, G.K.H. Shimizu, P.G. Boyd, S. Alavi, T.K. Woo, Competition and cooperativity in carbon dioxide sorption by amine-functionalized metal-organic frameworks, Angew. Chem. - Int. Ed. 51 (2012) 1826–1829, https://doi.org/10.1002/anie.201105109.

[216] R.B. Lin, D. Chen, Y.Y. Lin, J.P. Zhang, X.M. Chen, A zeolite-like zinc triazolate framework with high gas adsorption and separation performance, Inorg. Chem. 51 (2012) 9950–9955, https://doi.org/10.1021/ic301463z.

[217] Z. Shi, Y. Tao, J. Wu, C. Zhang, H. He, L. Long, Y. Lee, T. Li, Y.B. Zhang, Robust metal-triazolate frameworks for $CO_2$ capture from flue gas, J. Am. Chem. Soc. 142 (2020) 2750–2754, https://doi.org/10.1021/jacs.9b12879.

[218] A.M. Fracaroli, H. Furukawa, M. Suzuki, M. Dodd, S. Okajima, F. Gándara, J. A. Reimer, O.M. Yaghi, Metal–organic frameworks with precisely designed interior for carbon dioxide capture in the presence of water, J. Am. Chem. Soc. 136 (2014) 8863–8866, https://doi.org/10.1021/ja503296c.

[219] R.W. Flaig, T.M. Osborn Popp, A.M. Fracaroli, E.A. Kapustin, M.J. Kalmutzki, R. M. Altamimi, F. Fathieh, J.A. Reimer, O.M. Yaghi, The chemistry of $CO_2$ capture in an amine-functionalized metal-organic framework under dry and humid conditions, J. Am. Chem. Soc. 139 (2017) 12125–12128, https://doi.org/10.1021/jacs.7b06382.

[220] N.T.T. Nguyen, H. Furukawa, F. Gándara, H.T. Nguyen, K.E. Cordova, O.M. Yaghi, Selective capture of carbon dioxide under humid conditions by hydrophobic chabazite-type zeolitic imidazolate frameworks, Angew. Chem. - Int. Ed. 53 (2014) 10645–10648, https://doi.org/10.1002/anie.201403980.

[221] J.-B. Lin, T.T.T. Nguyen, R. Vaidhyanathan, J. Burner, J.M. Taylor, H. Durekova, F. Akhtar, R.K. Mah, O. Ghaffari-Nik, S. Marx, N. Fylstra, S.S. Iremonger, K. W. Dawson, P. Sarkar, P. Hovington, A. Rajendran, T.K. Woo, G.K.H. Shimizu, A scalable metal-organic framework as a durable physisorbent for carbon dioxide capture, Science 374 (2021) 1464–1469, https://doi.org/10.1126/science.abi7281.

[222] B. Ray, S.R. Churipard, S.C. Peter, An overview of the materials and methodologies for $CO_2$ capture under humid conditions, J. Mater. Chem. A 9 (2021) 26498–26527, https://doi.org/10.1039/D1TA08862A.

[223] S. Nandi, S. Collins, D. Chakraborty, R. Vaidhyanathan, Strategically designed azolyl-carboxylate MOFs for potential humid $CO_2$ capture, J. Mater. Chem. A 5 (2017) 535–543, https://doi.org/10.1039/c6ta07145g.

[224] L. Xie, M. Xu, X. Liu, M. Zhao, J. Li, Hydrophobic metal–organic frameworks: assessment, construction, and diverse applications, Adv. Sci. 7 (2020) 1901758, https://doi.org/10.1002/advs.201901758.

[225] C. Mottillo, T. Friščić, Carbon dioxide sensitivity of zeolitic imidazolate frameworks, Angew. Chem. Int. Ed. (2014) 7471–7474. ⟨https://doi.org/10.1002/anie.201402082⟩.

[226] A.C. Kizzie, A.G. Wong-Foy, A.J. Matzger, Effect of humidity on the performance of microporous coordination polymers as adsorbents for $CO_2$ capture, Langmuir 27 (2011) 6368–6373, https://doi.org/10.1021/la200547k.

[227] S. Choi, T. Watanabe, T.H. Bae, D.S. Sholl, C.W. Jones, Modification of the Mg/DOBDC MOF with amines to enhance $CO_2$ adsorption from ultradilute gases, J. Phys. Chem. Lett. 3 (2012) 1136–1141, https://doi.org/10.1021/jz300328j.

[228] M.C. Bernini, A.A. García Blanco, J. Villarroel-Rocha, D. Fairen-Jimenez, K. Sapag, A.J. Ramirez-Pastor, G.E. Narda, Tuning the target composition of amine-grafted CPO-27-Mg for capture of $CO_2$ under post-combustion and air filtering conditions: a combined experimental and computational study, Dalton Trans. 44 (2015) 18970–18982, https://doi.org/10.1039/c5dt03137k.

[229] P.Q. Liao, X.W. Chen, S.Y. Liu, X.Y. Li, Y.T. Xu, M. Tang, Z. Rui, H. Ji, J.P. Zhang, X.M. Chen, Putting an ultrahigh concentration of amine groups into a metal-organic framework for $CO_2$ capture at low pressures, Chem. Sci. 7 (2016) 6528–6533, https://doi.org/10.1039/c6sc00836d.

[230] S. Choi, J.H. Drese, C.W. Jones, Adsorbent materials for carbon dioxide capture from large anthropogenic point sources, ChemSusChem 2 (2009) 796–854, https://doi.org/10.1002/cssc.200900036.

[231] T.M. McDonald, J.A. Mason, X. Kong, E.D. Bloch, D. Gygi, A. Dani, V. Crocellà, F. Giordanino, S.O. Odoh, W.S. Drisdell, B. Vlaisavljevich, A.L. Dzubak, R. Poloni, S.K. Schnell, N. Planas, K. Lee, T. Pascal, L.F. Wan, D. Prendergast, J.B. Neaton, B. Smit, J.B. Kortright, L. Gagliardi, S. Bordiga, J.A. Reimer, J.R. Long, Cooperative insertion of $CO_2$ in diamine-appended metal-organic frameworks, Nature 519 (2015) 303–308, https://doi.org/10.1038/nature14327.

[232] Y. Cao, F. Song, Y. Zhao, Q. Zhong, Capture of carbon dioxide from flue gas on TEPA-grafted metal-organic framework $Mg_2$(dobdc), J. Environ. Sci. 25 (2013) 2081–2087, https://doi.org/10.1016/S1001-0742(12)60267-8.

[233] N. Planas, A.L. Dzubak, R. Poloni, L.C. Lin, A. McManus, T.M. McDonald, J. B. Neaton, J.R. Long, B. Smit, L. Gagliardi, The mechanism of carbon dioxide adsorption in an alkylamine-functionalized metal-organic framework, J. Am. Chem. Soc. 135 (2013) 7402–7405, https://doi.org/10.1021/ja4004766.

[234] J. Liu, Y. Wei, Y. Zhao, Trace carbon dioxide capture by metal–organic frameworks, ACS Sustain. Chem. Eng. 7 (2019) 82–93, https://doi.org/10.1021/acssuschemeng.8b05590.

[235] W.R. Lee, S.Y. Hwang, D.W. Ryu, K.S. Lim, S.S. Han, D. Moon, J. Choi, C.S. Hong, Diamine-functionalized metal-organic framework: exceptionally high $CO_2$ capacities from ambient air and flue gas, ultrafast $CO_2$ uptake rate, and adsorption mechanism, Energy Environ. Sci. 7 (2014) 744–751, https://doi.org/10.1039/c3ee42328j.

[236] W.R. Lee, H. Jo, L.M. Yang, H. Lee, D.W. Ryu, K.S. Lim, J.H. Song, D.Y. Min, S. S. Han, J.G. Seo, Y.K. Park, D. Moon, C.S. Hong, Exceptional $CO_2$ working capacity in a heterodiamine-grafted metal-organic framework, Chem. Sci. 6 (2015) 3697–3705, https://doi.org/10.1039/c5sc01191d.

[237] W.S. Drisdell, R. Poloni, T.M. McDonald, T.A. Pascal, L.F. Wan, C. Das Pemmaraju, B. Vlaisavljevich, S.O. Odoh, J.B. Neaton, J.R. Long, D. Prendergast, J.B. Kortright, Probing the mechanism of $CO_2$ capture in diamine-appended metal-organic frameworks using measured and simulated X-ray spectroscopy, Phys. Chem. Chem. Phys. 17 (2015) 21448–21457, https://doi.org/10.1039/c5cp02951a.

[238] H. Jo, W.R. Lee, N.W. Kim, H. Jung, K.S. Lim, J.E. Kim, D.W. Kang, H. Lee, V. Hiremath, J.G. Seo, H. Jin, D. Moon, S.S. Han, C.S. Hong, Fine-tuning of the carbon dioxide capture capability of diamine-grafted metal–organic framework adsorbents through amine functionalization, ChemSusChem 10 (2017) 541–550, https://doi.org/10.1002/cssc.201601203.

[239] W.R. Lee, J.E. Kim, S.J. Lee, M. Kang, D.W. Kang, H.Y. Lee, V. Hiremath, J.G. Seo, H. Jin, D. Moon, M. Cho, Y. Jung, C.S. Hong, Diamine-functionalization of a metal–organic framework adsorbent for superb carbon dioxide adsorption and desorption properties, ChemSusChem 11 (2018) 1694–1707, https://doi.org/10.1002/cssc.201800363.

[240] M. Kang, J.E. Kim, D.W. Kang, H.Y. Lee, D. Moon, C.S. Hong, A diamine-grafted metal–organic framework with outstanding $CO_2$ capture properties and a facile coating approach for imparting exceptional moisture stability, J. Mater. Chem. A 7 (2019) 8177–8183, https://doi.org/10.1039/c8ta07965j.

[241] R.L. Siegelman, T.M. McDonald, M.I. Gonzalez, J.D. Martell, P.J. Milner, J. A. Mason, A.H. Berger, A.S. Bhown, J.R. Long, Controlling cooperative $CO_2$ adsorption in diamine-appended $Mg_2$(dobpdc) metal-organic frameworks, J. Am. Chem. Soc. 139 (2017) 10526–10538, https://doi.org/10.1021/jacs.7b05858.

[242] J.H. Choe, D.W. Kang, M. Kang, H. Kim, J.R. Park, D.W. Kim, C.S. Hong, Revealing an unusual temperature-dependent $CO_2$ adsorption trend and selective $CO_2$ uptake over water vapors in a polyamine-appended metal-organic framework, Mater. Chem. Front. 3 (2019) 2759–2767, https://doi.org/10.1039/c9qm00581a.

[243] R.L. Siegelman, P.J. Milner, A.C. Forse, J.H. Lee, K.A. Colwell, J.B. Neaton, J. A. Reimer, S.C. Weston, J.R. Long, Water enables efficient $CO_2$ capture from natural gas flue emissions in an oxidation-resistant diamine-appended metal-organic framework, J. Am. Chem. Soc. 141 (2019) 13171–13186, https://doi.org/10.1021/jacs.9b05567.

[244] E.J. Kim, R.L. Siegelman, H.Z.H. Jiang, A.C. Forse, J.-H. Lee, J.D. Martell, P. J. Milner, J.M. Falkowski, J.B. Neaton, J.A. Reimer, S.C. Weston, J.R. Long, Cooperative carbon capture and steam regeneration with tetraamine-appended metal–organic frameworks, Science 369 (2020) 392–396, https://doi.org/10.1126/science.abb3976.

[245] V.Y. Mao, P.J. Milner, J.H. Lee, A.C. Forse, E.J. Kim, R.L. Siegelman, C. M. McGuirk, L.B. Porter-Zasada, J.B. Neaton, J.A. Reimer, J.R. Long, Cooperative carbon dioxide adsorption in alcoholamine- and alkoxyalkylamine-functionalized metal–organic frameworks, Angew. Chem. - Int. Ed. 59 (2020) 19468–19477, https://doi.org/10.1002/anie.201915561.

[246] J. Park, J.R. Park, J.H. Choe, S. Kim, M. Kang, D.W. Kang, J.Y. Kim, Y.W. Jeong, C.S. Hong, Metal-organic framework adsorbent for practical capture of trace carbon dioxide, ACS Appl. Mater. Interfaces 12 (2020) 50534–50540, https://doi.org/10.1021/acsami.0c16224.

[247] S.E. Ju, J.H. Choe, M. Kang, D.W. Kang, H. Kim, J.H. Lee, C.S. Hong, Understanding correlation between $CO_2$ insertion mechanism and chain length of diamine in metal-organic framework adsorbents, ChemSusChem 14 (2021) 2426–2433, https://doi.org/10.1002/cssc.202100582.

[248] C.P. Cabello, G. Berlier, G. Magnacca, P. Rumori, G.T. Palomino, Enhanced $CO_2$ adsorption capacity of amine-functionalized MIL-100(Cr) metal-organic frameworks, CrystEngComm 17 (2015) 430–437, https://doi.org/10.1039/c4ce01265h.

[249] Y. Lin, H. Lin, H. Wang, Y. Suo, B. Li, C. Kong, L. Chen, Enhanced selective $CO_2$ adsorption on polyamine/MIL-101(Cr) composites, J. Mater. Chem. A 2 (2014) 14658–14665, https://doi.org/10.1039/c4ta01174k.

[250] Y. Jiang, X. Shi, P. Tan, S. Qi, C. Gu, T. Yang, S. Peng, X. Liu, L. Sun, Controllable $CO_2$ capture in metal–organic frameworks: making targeted active sites respond to light, Ind. Eng. Chem. Res 59 (2020) 21894–21900, https://doi.org/10.1021/acs.iecr.0c04126.

[251] D. Kyu, T. Yoon, Y. Bae, S. Hwa, Metal-organic framework MIL-101 loaded with polymethacrylamide with or without further reduction: effective and selective $CO_2$ adsorption with amino or amide functionality, Chem. Eng. J. 380 (2020), 122496, https://doi.org/10.1016/j.cej.2019.122496.

[252] A.B. Sokhrab, D.G. Samsonenko, E. Maksimovskiy, E.O. Fedorovskaya, A. Sapchenko, V.P. Fedin, Polyaniline-intercalated MIL-101: selective $CO_2$ sorption and supercapacitor properties, New J. Chem. 40 (2016) 5306–5312, https://doi.org/10.1039/c5nj03477a.

[253] S. Shin, D.K. Yoo, Y. Bae, S.H. Jhung, Polyvinylamine-loaded metal–organic framework MIL-101 for effective and selective $CO_2$ adsorption under atmospheric or lower pressure, Chem. Eng. J. 389 (2020), 123429, https://doi.org/10.1016/j.cej.2019.123429.

[254] M. Babaei, S. Salehi, M. Anbia, M. Kazemipour, Improving $CO_2$ adsorption capacity and $CO_2$/$CH_4$ selectivity with amine functionalization of MIL-100 and

MIL-101, J. Chem. Eng. Data 63 (2018) 1657–1662, https://doi.org/10.1021/acs.jced.8b00014.

[255] R. Zhong, X. Yu, W. Meng, J. Liu, C. Zhi, R. Zou, Amine-grafted MIL-101(Cr) via double-solvent incorporation for synergistic enhancement of $CO_2$ uptake and selectivity, ACS Sustain. Chem. Eng. 6 (2018) 16493–16502, https://doi.org/10.1021/acssuschemeng.8b03597.

[256] H. Li, K. Wang, Z. Hu, Y.P. Chen, W. Verdegaal, D. Zhao, H.C. Zhou, Harnessing solvent effects to integrate alkylamine into metal-organic frameworks for exceptionally high $CO_2$ uptake, J. Mater. Chem. A 7 (2019) 7867–7874, https://doi.org/10.1039/c8ta11300a.

[257] H. Li, K. Wang, D. Feng, Y. Chen, W. Verdegaal, H. Zhou, Incorporation of alkylamine into metal–organic frameworks through a Brønsted acid–base reaction for $CO_2$ capture, ChemSusChem 9 (2016) 2832–2840, https://doi.org/10.1002/cssc.201600768.

[258] T.K. Vo, W.S. Kim, J. Kim, Ethylenediamine-incorporated MIL-101(Cr)-NH₂ metal-organic frameworks for enhanced $CO_2$ adsorption, Korean J. Chem. Eng. 37 (2020) 1206–1211, https://doi.org/10.1007/s11814-020-0548-8.

[259] Y. Li, H.-T. Wang, Y.-L. Zhao, J. Lv, X. Zhang, Q. Chen, J.-R. Li, Regulation of hydrophobicity and water adsorption of MIL-101(Cr) through post-synthetic modification, Inorg. Chem. Commun. 130 (2021), 108741, https://doi.org/10.1016/j.inoche.2021.108741.

[260] T.M. McDonald, D.M. D'Alessandro, R. Krishna, J.R. Long, Enhanced carbon dioxide capture upon incorporation of N,N′- dimethylethylenediamine in the metal-organic framework CuBTTri, Chem. Sci. 2 (2011) 2022–2028, https://doi.org/10.1039/c1sc00354b.

[261] N. Vrtovec, M. Mazaj, G. Buscarino, A. Terracina, S. Agnello, I. Arčon, J. Kovač, N. Zabukovec Logar, Structural and $CO_2$ capture properties of ethylenediamine-modified HKUST-1 metal-organic framework, Cryst. Growth Des. 20 (2020) 5455–5465, https://doi.org/10.1021/acs.cgd.0c00667.

[262] X. Huang, J. Lu, W. Wang, X. Wei, J. Ding, Experimental and computational investigation of $CO_2$ capture on amine grafted metal-organic framework NH₂-MIL-101, Appl. Surf. Sci. 371 (2016) 307–313, https://doi.org/10.1016/j.apsusc.2016.02.154.

[263] S. Mutyala, S.M. Yakout, S.S. Ibrahim, M. Jonnalagadda, H. Mitta, Enhancement of $CO_2$ capture and separation of $CO_2/N_2$ using post-synthetic modified MIL-100 (Fe), New J. Chem. 43 (2019) 9725–9731, https://doi.org/10.1039/c9nj02258a.

[264] S. Gaikwad, S.J. Kim, S. Han, $CO_2$ capture using amine-functionalized bimetallic MIL-101 MOFs and their stability on exposure to humid air and acid gases, Microporous Mesoporous Mater. 277 (2019) 253–260, https://doi.org/10.1016/j.micromeso.2018.11.001.

[265] S. Xian, Y. Wu, J. Wu, X. Wang, J. Xiao, Enhanced dynamic $CO_2$ adsorption capacity and $CO_2/CH_4$ selectivity on polyethylenimine-impregnated UiO-66, Ind. Eng. Chem. Res. 54 (2015) 11151–11158, https://doi.org/10.1021/acs.iecr.5b03517.

[266] J. Zhu, L. Wu, Z. Bu, S. Jie, B.G. Li, Polyethyleneimine-modified UiO-66-NH₂(Zr) metal-organic frameworks: preparation and enhanced $CO_2$ selective adsorption, ACS Omega 4 (2019) 3188–3197, https://doi.org/10.1021/acsomega.8b02319.

[267] S. Gaikwad, Y. Kim, R. Gaikwad, S. Han, Enhanced $CO_2$ capture capacity of amine-functionalized MOF-177 metal organic framework, J. Environ. Chem. Eng. 9 (2021), 105523, https://doi.org/10.1016/j.jece.2021.105523.

[268] C.E. Bien, Q. Liu, C.R. Wade, Assessing the role of metal identity on $CO_2$ adsorption in MOFs containing M-OH functional groups, Chem. Mater. 32 (2020) 489–497, https://doi.org/10.1021/acs.chemmater.9b04228.

[269] E. Soubeyrand-Lenoir, C. Vagner, J.W. Yoon, P. Bazin, F. Ragon, Y.K. Hwang, C. Serre, J.S. Chang, P.L. Llewellyn, How water fosters a remarkable 5-fold increase in low-pressure $CO_2$ uptake within mesoporous MIL-100(Fe), J. Am. Chem. Soc. 134 (2012) 10174–10181, https://doi.org/10.1021/ja302787x.

[270] J.R. Álvarez, R.A. Peralta, J. Balmaseda, E. González-Zamora, I.A. Ibarra, Water adsorption properties of a Sc(III) porous coordination polymer for $CO_2$ capture applications, Inorg. Chem. Front. 2 (2015) 1080–1084, https://doi.org/10.1039/c5qi00176e.

[271] H.A. Lara-García, M.R. Gonzalez, J.H. González-Estefan, P. Sánchez-Camacho, E. Lima, I.A. Ibarra, Removal of $CO_2$ from $CH_4$ and $CO_2$ capture in the presence of $H_2O$ vapour in NOTT-401, Inorg. Chem. Front. 2 (2015) 442–447, https://doi.org/10.1039/c5qi00049a.

[272] E. Sánchez-González, J.R. Álvarez, R.A. Peralta, A. Campos-Reales-Pineda, A. Tejeda-Cruz, E. Lima, J. Balmaseda, E. González-Zamora, I.A. Ibarra, Water adsorption properties of NOTT-401 and $CO_2$ capture under humid conditions, ACS Omega 1 (2016) 305–310, https://doi.org/10.1021/acsomega.6b00102.

[273] R.A. Peralta, B. Alcántar-Vázquez, M. Sánchez-Serratos, E. González-Zamora, I.A. Ibarra, Carbon dioxide capture in the presence of water vapour in InOF-1, Inorg. Chem. Front. 2 (2015) 898–903, https://doi.org/10.1039/c5qi00077g.

[274] M. Sánchez-Serratos, P.A. Bayliss, R.A. Peralta, E. González-Zamora, E. Lima, I.A. Ibarra, $CO_2$ capture in the presence of water vapour in MIL-53(Al), New J. Chem. 40 (2016) 68–72, https://doi.org/10.1039/c5nj02312b.

[275] G.A. González-Martí, T. Jurado-Vázquez, D. Solís-Ibarra, B. Vargas, E. Sánchez-González, A. Martínez, R. Vargas, E. González-Zamora, I.A. Ibarra, Confinement of $H_2O$ and EtOH to enhance $CO_2$ capture in MIL-53(Al)-TDC, Dalton Trans. 47 (2018) 9459–9465, https://doi.org/10.1039/c8dt01369a.

[276] M. Sagastuy-Breña, P.G.M. Mileo, E. Sánchez-González, J.E. Reynolds, T. Jurado-Vázquez, J. Balmaseda, E. González-Zamora, S. Devautour-Vinot, S.M. Humphrey, G. Maurin, I.A. Ibarra, Humidity-induced $CO_2$ capture enhancement in Mg-CUK-1, Dalton Trans. 47 (2018) 15827–15834, https://doi.org/10.1039/c8dt03365j.

[277] V.B. López-Cervantes, E. Sánchez-González, T. Jurado-Vázquez, A. Tejeda-Cruz, E. González-Zamora, I.A. Ibarra, $CO_2$ adsorption under humid conditions: Self-

[278] Y. Chen, Z. Qiao, J. Huang, H. Wu, J. Xiao, Q. Xia, H. Xi, J. Hu, J. Zhou, Z. Li, Unusual moisture-enhanced $CO_2$ capture within microporous PCN-250 frameworks, ACS Appl. Mater. Interfaces 10 (2018) 38638–38647, https://doi.org/10.1021/acsami.8b14400.

[279] A. Zárate, R.A. Peralta, P.A. Bayliss, R. Howie, M. Sánchez-Serratos, P. Carmona-Monroy, D. Solis-Ibarra, E. González-Zamora, I.A. Ibarra, $CO_2$ capture under humid conditions in NH₂-MIL-53(Al): The influence of the amine functional group, RSC Adv. 6 (2016) 9978–9983, https://doi.org/10.1039/c5ra26517g.

[280] N.L. Ho, F. Porcheron, R.J.M. Pellenq, Experimental and molecular simulation investigation of enhanced $CO_2$ solubility in hybrid adsorbents, Langmuir 26 (2010) 13287–13296, https://doi.org/10.1021/la1015934.

[281] L.N. Ho, J. Perez Pellitero, F. Porcheron, R.J.M. Pellenq, Enhanced $CO_2$ solubility in hybrid MCM-41: molecular simulations and experiments, Langmuir 27 (2011) 8187–8197, https://doi.org/10.1021/la2012765.

[282] E. González-Zamora, I.A. Ibarra, $CO_2$ capture under humid conditions in metal-organic frameworks, Mater. Chem. Front. 1 (2017) 1471–1484, https://doi.org/10.1039/c6qm00301j.

[283] J.M. Kolle, M. Fayaz, A. Sayari, Understanding the effect of water on $CO_2$ adsorption, Chem. Rev. 121 (2021) 7280–7345, https://doi.org/10.1021/acs.chemrev.0c00762.

[284] W. Zhang, Y. Hu, J. Ge, H.L. Jiang, S.H. Yu, A facile and general coating approach to moisture/water-resistant metal-organic frameworks with intact porosity, J. Am. Chem. Soc. 136 (2014) 16978–16981, https://doi.org/10.1021/ja509960n.

[285] X. Qian, F. Sun, J. Sun, H. Wu, F. Xiao, X. Wu, G. Zhu, Imparting surface hydrophobicity to metal-organic frameworks using a facile solution-immersion process to enhance water stability for $CO_2$ capture, Nanoscale 9 (2017) 2003–2008, https://doi.org/10.1039/c6nr07801j.

[286] S. Yang, L. Peng, D.T. Sun, M. Asgari, E. Oveisi, O. Trukhina, S. Bulut, A. Jamali, W.L. Queen, A new post-synthetic polymerization strategy makes metal-organic frameworks more stable, Chem. Sci. 10 (2019) 4542–4549, https://doi.org/10.1039/c9sc00135b.

[287] S.J. Yang, C.R. Park, Preparation of highly moisture-resistant black-colored metal organic frameworks, Adv. Mater. 24 (2012) 4010–4013, https://doi.org/10.1002/adma.201200790.

[288] S. Gadipelli, Z. Guo, Postsynthesis annealing of MOF-5 remarkably enhances the framework structural stability and $CO_2$ uptake, Chem. Mater. 26 (2014) 6333–6338, https://doi.org/10.1021/cm502399q.

[289] Q. Sun, H. He, W.Y. Gao, B. Aguila, L. Wojtas, Z. Dai, J. Li, Y.S. Chen, F.S. Xiao, S. Ma, Imparting amphiphobicity on single-crystalline porous materials, Nat. Commun. 7 (2016) 1–7, https://doi.org/10.1038/ncomms13300.

[290] P. Deria, J.E. Mondloch, E. Tylianakis, P. Ghosh, W. Bury, R.Q. Snurr, J.T. Hupp, O.K. Farha, Perfluoroalkane functionalization of NU-1000 via solvent-assisted ligand incorporation: synthesis and $CO_2$ adsorption studies, J. Am. Chem. Soc. 135 (2013) 16801–16804, https://doi.org/10.1021/ja408959g.

[291] P. Deria, Y.G. Chung, R.Q. Snurr, J.T. Hupp, O.K. Farha, Water stabilization of Zr₆-based metal-organic frameworks via solvent-assisted ligand incorporation, Chem. Sci. 6 (2015) 5172–5176, https://doi.org/10.1039/c5sc01784j.

[292] R. D'Amato, A. Donnadio, M. Carta, C. Sangregorio, D. Tiana, R. Vivani, M. Taddei, F. Costantino, Water-based synthesis and enhanced $CO_2$ capture performance of perfluorinated cerium-based metal–organic frameworks with UiO-66 and MIL-140 topology, ACS Sustain Chem. Eng. 7 (2019) 394–402, https://doi.org/10.1021/acssuschemeng.8b03765.

[293] S. Sircar, R. Mohr, C. Ristic, M.B. Rao, Isosteric heat of adsorption: theory and experiment S. J. Phys. Chem. B 103 (1999) 6539–6546, https://doi.org/10.1021/jp9903817.

[294] M.S. Ray, Adsorptive and membrane-type separations: a bibliographical update (1998), Adsorpt. Sci. Technol. 53 (1999) 1107–1122, https://doi.org/10.1177/026361749901700307.

[295] M. Dincă, A. Dailly, Y. Liu, C.M. Brown, D.A. Neumann, J.R. Long, Hydrogen storage in a microporous metal - organic framework with exposed $Mn^{2+}$ coordination sites, J. Am. Chem. Soc. 128 (2006) 16876–16883, https://doi.org/10.1021/ja0656853.

[296] J. An, N.L. Rosi, Tuning MOF $CO_2$ adsorption properties via cation exchange, J. Am. Chem. Soc. 132 (2010) 5578–5579, https://doi.org/10.1021/ja1012992.

[297] T. Li, N.L. Rosi, Screening and evaluating aminated cationic functional moieties for potential $CO_2$ capture applications using an anionic MOF scaffold, Chem. Commun. 49 (2013) 11385–11387, https://doi.org/10.1039/c3cc47031h.

[298] J. Gandara-Loe, L. Pastor-Perez, L.F. Bobadilla, J.A. Odriozola, T.R. Reina, Understanding the opportunities of metal-organic frameworks (MOFs) for $CO_2$ capture and gas-phase $CO_2$ conversion processes: a comprehensive overview, React. Chem. Eng. 6 (2021) 787–814, https://doi.org/10.1039/d1re00034a.

[299] H.J. Park, M.P. Suh, Enhanced isosteric heat, selectivity, and uptake capacity of $CO_2$ adsorption in a metal-organic framework by impregnated metal ions, Chem. Sci. 4 (2013) 685–690, https://doi.org/10.1039/c2sc21253f.

[300] A. Raksajati, M.T. Ho, D.E. Wiley, Reducing the cost of $CO_2$ capture from flue gases using phase change solvent absorption, Energy Procedia 63 (2014) 2280–2288, https://doi.org/10.1016/j.egypro.2014.11.247.

[301] A. Raksajati, M.T. Ho, D.E. Wiley, Understanding the impact of process design on the cost of $CO_2$ capture for precipitating solvent absorption, Ind. Eng. Chem. Res. 55 (2016) 1980–1994, https://doi.org/10.1021/acs.iecr.5b03633.

[302] Q. Yang, S. Vaesen, F. Ragon, A.D. Wiersum, D. Wu, A. Lago, T. Devic, C. Martineau, F. Taulelle, P.L. Llewellyn, H. Jobic, C. Zhong, C. Serre, G. De Weireld, G. Maurin, A water stable metal-organic framework with optimal

features for CO$_2$ capture, Angew. Chem. - Int. Ed. 52 (2013) 10316–10320, https://doi.org/10.1002/anie.201302682.

[303] A.L. Myers, J.M. Prausnitz, Thermodynamics of mixed-gas adsorption, AIChE J. 11 (1965) 121–127, https://doi.org/10.1002/aic.690110125.

[304] K.S. Walton, D.S. Sholl, Predicting multicomponent adsorption: 50 years of the ideal adsorbed solution theory, AIChE J. 59 (2015) 215–228, https://doi.org/10.1002/aic.

[305] Y. Hu, W.M. Verdegaal, S.H. Yu, H.L. Jiang, Alkylamine-tethered stable metal-organic framework for CO$_2$ capture from flue gas, ChemSusChem 7 (2014) 734–737, https://doi.org/10.1002/cssc.201301163.

[306] Y.-S. Bae, O.K. Farha, A.M. Spokoyny, C.A. Mirkin, J.T. Hupp, R.Q. Snurr, Carborane-based metal–organic frameworks as highly selective sorbents for CO$_2$ over methane, Chem. Commun. (2008) 4135–4137, https://doi.org/10.1039/b805785k.

[307] B. Liu, B. Smit, Comparative molecular simulation study of CO$_2$/N$_2$ and CH$_4$/N$_2$ separation in zeolites and metal-organic frameworks, Langmuir 25 (2009) 5918–5926, https://doi.org/10.1021/la900823d.

[308] F.X. Coudert, C. Mellot-Draznieks, A.H. Fuchs, A. Boutin, Prediction of breathing and gate-opening transitions upon binary mixture adsorption in metal-organic frameworks, J. Am. Chem. Soc. 131 (2009) 11329–11331, https://doi.org/10.1021/ja904123f.

[309] P. Billemont, N. Heymans, P. Normand, G. De Weireld, IAST predictions vs co-adsorption measurements for CO$_2$ capture and separation on MIL-100 (Fe), Adsorption 23 (2017) 225–237, https://doi.org/10.1007/s10450-016-9825-6.

[310] M. Taddei, C. Petit, Engineering metal–organic frameworks for adsorption-based gas separations: from process to atomic scale, Mol. Syst. Des. Eng. 6 (2021) 841–875, https://doi.org/10.1039/D1ME00085C.

[311] J.Y. Wang, E. Mangano, S. Brandani, D.M. Ruthven, A review of common practices in gravimetric and volumetric adsorption kinetic experiments, Adsorption 27 (2021) 295–318, https://doi.org/10.1007/s10450-020-00276-7.

[312] Z. Hu, Y. Wang, S. Farooq, D. Zhao, A highly stable metal-organic framework with optimum aperture size for CO$_2$ capture, AIChE J. 63 (2017) 4103–4114, https://doi.org/10.1002/aic.15837.

[313] D.M. Ruthven, S. Farooq, K.S. Knaebel, Pressure swing Adsorption, VCH, 1994.

[314] J. Kärger, D.M. Ruthven, Diffusion in nanoporous materials: fundamental principles, insights and challenges, New J. Chem. 40 (2016) 4027–4048, https://doi.org/10.1039/C5NJ02836A.

[315] A.C. Forse, C. Merlet, C.P. Grey, J.M. Griffin, NMR studies of adsorption and diffusion in porous carbonaceous materials, Prog. Nucl. Magn. Reson Spectrosc. 124–125 (2021) 57–84, https://doi.org/10.1016/j.pnmrs.2021.03.003.

[316] D.M. Ruthven, J. Kärger, S. Brandani, E. Mangano, Sorption kinetics: measurement of surface resistance, Adsorption 27 (2021) 787–799, https://doi.org/10.1007/s10450-020-00257-w.

[317] S. Brandani, E. Mangano, The zero length column technique to measure adsorption equilibrium and kinetics: lessons learnt from 30 years of experience, Adsorption 27 (2021) 319–351, https://doi.org/10.1007/s10450-020-00273-w.

[318] J. Gandara-Loe, L. Pastor-Perez, L.F. Bobadilla, J.A. Odriozola, T.R. Reina, Understanding the opportunities of metal-organic frameworks (MOFs) for CO$_2$ capture and gas-phase CO$_2$ conversion processes: a comprehensive overview, React, Chem. Eng. 6 (2021) 787–814, https://doi.org/10.1039/d1re00034a.

[319] U. Ryu, S. Jee, P. Chandra, J. Shin, C. Ko, M. Yoon, K. Sung, K. Min, Recent advances in process engineering and upcoming applications of metal – organic frameworks, Coord. Chem. Rev. 426 (2021), 213544, https://doi.org/10.1016/j.ccr.2020.213544.

[320] L.A. Darunte, Y. Terada, C.R. Murdock, K.S. Walton, D.S. Sholl, C.W. Jones, Monolith-supported amine-functionalized Mg$_2$(dobpdc) adsorbents for CO$_2$ capture, ACS Appl. Mater. Interfaces 9 (2017) 17042–17050, https://doi.org/10.1021/acsami.7b02035.

[321] S. Lawson, C. Griffin, K. Rapp, A.A. Rownaghi, F. Rezaei, Amine-functionalized MIL-101 monoliths for CO$_2$ removal from enclosed environments, Energy Fuels 33 (2019) 2399–2407, https://doi.org/10.1021/acs.energyfuels.8b04508.

[322] S. Lawson, A. Alwakwak, A.A. Rownaghi, F. Rezaei, Gel–print–grow: a new way of 3D printing metal–organic frameworks, ACS Appl. Mater. Interfaces 12 (2020) 56108–56117, https://doi.org/10.1021/acsami.0c18720.

[323] D.J. Tranchemontagne, J.R. Hunt, O.M. Yaghi, Room temperature synthesis of metal-organic frameworks: MOF-5, MOF-74, MOF-177, MOF-199, and IRMOF-0, Tetrahedron 64 (2008) 8553–8557, https://doi.org/10.1016/j.tet.2008.06.036.

[324] S. Cadot, L. Veyre, D. Luneau, D. Farrusseng, E. Alessandra Quadrelli, A water-based and high space-time yield synthetic route to MOF Ni$_2$(dhtp) and its linker 2,5-dihydroxyterephthalic acid, J. Mater. Chem. A 2 (2014) 17757–17763, https://doi.org/10.1039/C4TA03066D.

[325] Z. Hu, D. Zhao, De facto methodologies toward the synthesis and scale-up production of UiO-66-type metal–organic frameworks and membrane materials, Dalton Trans. 44 (2015) 19018–19040, https://doi.org/10.1039/C5DT03359D.

[326] H. Azarabadi, K.S. Lackner, A sorbent-focused techno-economic analysis of direct air capture, Appl. Energy 250 (2019) 959–975, https://doi.org/10.1016/j.apenergy.2019.04.012.

[327] R. Das, T. Ezhil, A.S. Palakkal, D. Muthukumar, R.S. Pillai, C.M. Nagaraja, Efficient chemical fixation of CO$_2$ from direct air under environment-friendly co-catalyst and solvent-free ambient conditions, J. Mater. Chem. A 9 (2021) 23127–23139, https://doi.org/10.1039/D1TA05138E.

[328] M. Erans, E.S. Sanz-Pérez, D.P. Hanak, Z. Clulow, D.M. Reiner, G.A. Mutch, Direct air capture: process technology, techno-economic and socio-political challenges, Energy Environ. Sci. 15 (2022) 1360–1405, https://doi.org/10.1039/d1ee03523a.

[329] X. Zhu, W. Xie, J. Wu, Y. Miao, C. Xiang, C. Chen, B. Ge, Z. Gan, F. Yang, M. Zhang, D. O'Hare, J. Li, T. Ge, R. Wang, Recent advances in direct air capture by adsorption, Chem. Soc. Rev. 51 (2022) 6574–6651, https://doi.org/10.1039/D1CS00970B.